ORIGIN OF DIAMONDS IN CHROMITITES OF THE LUOBUSA OPHIOLITE, SOUTHERN TIBET, CHINA

By

Xu-Feng Hu

Submitted in partial fulfilment of the requirements
for the degree of Master of Science

At

Dalhousie University
Halifax, Nova Scotia
January, 1999

TABLE OF CONTENTS

LIST OF FIGURES

LIST OF TABLES

ABSTRACT

Diamonds and an extensive assemblage of associated minerals were discovered in podiform chromitites of the Luobusa ophiolite, southern Tibet, China. Thus far, 25 diamonds have been recovered from the mineral separates of samples collected in 1996.

All the diamonds are colourless and transparent. Most of them are euhedral crystals, showing sharp-edged octahedral morphology. Others are broken fragments. Euhedral crystals are 150 × 150 μm to 400 × 400 μm in size, whereas broken fragments range from 200 × 250 μm to 900 × 1000 μm. Both Raman spectra and X-ray diffraction techniques have been used to confirm the identification of the diamonds. One diamond fragment contains three discrete silicate mineral inclusions. One of the inclusions was analysed with the electron microprobe, and has an unusual composition, high in MgO (30.7 wt%) and SiO_2 (64.1 wt%). Its formula best fits that of clinoenstatite. SEI images show that the inclusion possesses an octahedral morphology typical of that imposed on many syngenetic inclusions by contemporaneous growth of the surrounding diamond.

Minerals associated with the diamonds include chromite, forsterite, enstatite, Cr-diopside, PGE minerals, graphite, SiC (moissanite), gehlenite, Si-Fe and Cr-C alloys, zircon, sphene, rutile, apatite, corundum, sillimanite, plagioclase, K-feldspar, amphibole, biotite, phlogopite, chlorite, serpentine, sulphides, carbonates, celestite, uvarovite, almandine, wollastonite, quartz, and Fe-Ni and Au-Ag alloys. All the minerals were recovered from mineral separates and confirmed by either electron microprobe or X-ray diffraction studies. Most of the chromites are rich in magnesian and chromium, with Cr#s [100 Cr/(Cr + Al)] ranging from 77 to 84 and Mg#s [100 Mg/(Mg + Fe)] between 62 and 76, suggesting crystallisation from a boninitic melt. Olivines have Fo contents ranging from 91 to 98%, with NiO contents varying from 0.3 to 1.35 wt%, correspondingly. Enstatites contain 88-95% En end-member, with Cr_2O_3 contents varying from 0.15 to 0.90 wt%. SiC crystals are 0.1 to 1.1 mm in size, and transparent (if not deeply coloured) with a strong brilliant adamantine luster. Colours range from colourless to grey-blue to pale green to yellow to yellow-blue to bluish-green to blue-black. Many SiC grains are colour-zoned with graduations between zones. The Cr-C alloy is steel gray and displays a well-developed acicular form. It has a Cr/C ratio of 1:1. The Si-Fe grains up to 1 mm in size, are black, very shiny, and fractured. The Fe/Si ratio averages 2.76/7, very similar to ferrosilicite (Fe_3Si_7) inclusions in SiC from the Yakutia kimberlite. The hydrous minerals are Ti rich and distinct in composition from those of secondary origin in Oman chromitites.

The sampling and separation procedures were designed to minimize any possibility of natural or anthropogenic contamination of the samples. The well-developed crystal morphology of diamond, SiC (moissanite) and Cr-C alloys signifies that they crystallized from melts/fluids, and they are interpreted as original phases in the Luobusa chromitites. The well-preserved character of the diamonds indicates they have not undergone any resorption after formation. Based on the available data, two models are proposed for the formation of the Luobusa diamonds: they may have formed metastably in a suprasubduction zone environment where the chromitites formed, or they may be xenocrysts formed at greater depths and later incorporated into the chromitites.

ACKNOWLEDGEMENTS

First and foremost, I want to thank my supervisor, Dr. Paul T. Robinson, for his constant encouragement, insightful comments and invaluable suggestions. It would not be possible for me to complete this thesis without his support and guidance.

I would also like to thank Prof. W.-J. Bai from the Institute of Geology (CAGS, Beijing) for his invaluable advice, assistance and encouragement. His contacts with government agencies in China made it possible for us to go to Tibet for field investigations. Prof. Q.-S. Fang from the Institute of Geology (CAGS, Beijing) is an expert at diamond separation, and his helpfulness is greatly appreciated. Both of them contributed a great deal in the sample collection and separation. Dr. Mei-Fu Zhou from the University of Hong Kong merits special words of appreciation for his help during the study.

I express much gratitude to Robert MacKay and Dr. T. Stanley Cameron for their help in mineral identification, to Dr. Peter Reynolds and Dr. Jarda Dostal for critical reading of the early versions of the thesis, to Dr. David Scott and Dr. Rebecca Jamieson for their support in photography, to Mr. Golden Brown for his hard work on thin section making, and to Dr. J.-S. Yang from the Institute of Geology (CAGS, Beijing) for permission to access his computer for communication during the field trip in China.

Thanks to Dr. Gareth Davies and Melanie Grislen from the Vrije University (Amsterdam) for their insightful ideas and enjoyable days we shared during field work in Tibet, to Ba-Deng-Zhu, B.-J. Wei and the second Geological Team (Bureau of Geological and Mineral Resources Tibet) for their guidance and support in many ways during the field work.

Special thanks also to the Bureau of Geological and Mineral Resources Tibet, particularly to Mr. Tsewang Duoji, Ping Cuo and R.-J. Lu for their assistance in making the field work successful.

This work was supported financially by NSERC research grants to Dr. Paul T. Robinson.

CHAPTER 1. INTRODUCTION

1-1. Occurrences of diamonds

Natural diamonds are widespread in the Earth's crust and mantle and have been reported from a variety of rocks including those of igneous, metamorphic, and sedimentary origins (e.g., Helmstaedt, 1994; Janse, 1994). Occurrences in kimberlites/lamproites are the most common and best known. Also of commercial importance are numerous beach and placer deposits which are believed to be spatially associated with primary sources. Less common, but of great scientific interest, are occurrences in metamorphic rocks in China, Kazakhstan, and Norway (Xu et al., 1992; Sobolev and Shatsky, 1990; Claoue-Long, et al., 1991; Dobrzhinetskaya, et al., 1995). Diamonds have also been reported from alpine-type ultramafic rocks in ophiolite complexes in the Urals, Caucasus, Sayan, Kamchatka and Transbaikalia of Russian, in the Koryak Range of Armenia, and in the Appalachians and Cordillera of North America. Unfortunately, most of the reported occurrences in alpine ultramafic rocks are unconfirmed, although graphite pseudomorphs after diamond have been recovered from the Beni Bousera massif in Morocco and the Ronda massif in Spain (Davies et al., 1993; Pearson et al., 1989; Slodkevich, 1983). These bodies, however, are believed to consist of subcontinental not oceanic mantle peridotite. Other reported occurrences of diamond include eclogite and peridotite xenoliths from non-kimberlitic rocks in locations such as the east margin of the Siberian Platform, Czech Republic, and the western Burkina Faso

(Upper Volta); and meteorites and meteorite impact structures (see Nixon, 1995; Hough et al., 1995).

Diamonds were also reported to occur in a picrite dike in the Kusya River basin on the western side of the middle Urals (Lukyanova, et al., 1980). Accessory minerals in the picrite dyke and explosive breccias include pyrope-almandine, apatite, zircon, SiC, pyrite, rutile, magnetite, ilmenite, sphene and chromite. This accessory mineral assemblage is very similar to that found in the Luobusa chromitites (see chapter 4).

Despite the many reported occurrences of diamonds only those from kimberlites and metamorphic rocks have been investigated in any detail. Natural diamonds from kimberlites commonly contain syngenetic mineral inclusions, such as forsterite, enstatite, diopside, omphacite, Cr-pyrope, pyrope-almandine, kyanite, K-feldspar, sanidine, coesite (quartz), Cr-spinel, rutile, ruby, ilmenite, zircon, sulphides, chromite, native iron, Fe-Ni metallic alloys, magnesite, calcite, dolomite, wustite, solid CO_2 and moissanite (Arculus, 1985; Meyer and McCallum, 1986; Meyer, 1987; Otter and Gurney, 1989; Schrauder and Navon, 1993; Kinny and Meyer, 1994; Wang et al., 1994; Bulanova, 1995; Stachel et al., 1998). Fluid phase inclusions have also been reported in these diamonds (Navon et al., 1988; Navon, 1991; Schrauder et al., 1993).

Studies of the diamonds and their inclusions have shown that the diamonds are considerably older than the rocks in which they occur (Richardson, 1986; Richardson et al., 1993). Furthermore, many of these diamonds are corroded, etched and partially resorbed. These textural features indicate they were out of equilibrium with the

kimberlitic/lamproitic melts. These diamonds were clearly not crystallised from kimberlitic/lamproitic magmas, but rather were derived from the upper mantle and transported to the surface as xenocrysts (Kirkley, et al., 1991). The relationship of the diamonds to their host kimberlites/lamproites is that of passengers to transporting agencies (Meyer, 1985; Mitchell 1991; Stachel and Harris 1997).

Based on their inclusion mineralogy and carbon isotopic character, kimberlitic diamonds are assigned to either a peridotitic or eclogitic paragenesis (Meyer, 1985; Kesson and Ringwood, 1989; Mitchell 1991). Kirkley et al (1991) compiled a large number of carbon isotopic analyses of diamonds and showed that peridotitic diamonds have $\delta^{13}C$ values predominantly between -10 and -1‰ with a sharp peak near -5‰, whereas eclogitic diamonds have $\delta^{13}C$ values between -34 and +3‰ with a smaller peak near -5‰.

Most of the diamonds from kimberlites whether of eclogitic or peridotitic paragenesis are believed to have formed either from melts or fluids in the upper mantle (Boyd and Gurney, 1986; Boyd et al., 1985; Griffin and Ryan, 1995; Meyer, 1985). Their isotopic character indicates that the carbon from which they formed was derived both from subducted material and from the mantle (Meyer, 1985). However, a small portion of diamonds, e.g., from South Africa and Brazil (Moore and Gurney, 1985; Sautter, et al., 1991) are from the transition zone of the mantle (400-670 km) (Haggerty, 1994). These diamonds contain syngenetic inclusions of majoritic garnet (garnet containing a substantial pyroxene component in solid solution). Other diamonds are probably from the

lower mantle (>670 km). These contain inclusions of cubo-octahedral enstatite (previously $(Mg,Fe)SiO_3$ perovskite) and magnesiowustite, e.g., those from Orrorroo, South Australia (Scott-Smith, et al., 1984) and Koffiefontein, South Africa (Richardson, et al., 1989). Wollastonite (previously $CaSiO_3$ perovskite) and magnesiowustite are also found in diamonds from Sloan, Colorado (Otter and Gurney, 1989). The recognition of a mineral assemblage of (Mg, Fe) perovskite, Ca-perovskite, ferropericlase and a tetragonal almandine-pyrope phase included in diamonds from Sao Luiz, Brazil, also suggests a lower mantle origin (Kerr, 1993; McCammon, et al., 1997; Harris, et al., 1997).

Some microdiamonds are thought to crystallise directly from the kimberlitic or lamproitic magmas which transported them to the surface (Gurney, 1989; Leung et al., 1990; Pattison and Levinson, 1995).

Diamonds from metamorphic rocks, such as those in China and Kazakhstan, are believed to have crystallised in the upper mantle at pressures greater than 40 kbar and temperatures in the range of 900-1000°C (Sobolev and Shatsky 1990; Xu et al. 1992). Diamonds from metamorphic rocks in Norway probably formed in a similar stability regime at pressures exceeding ~35 kbar and temperatures above ~700°C (Dobrzhinetskaya et al. 1995). The occurrence of microdiamonds in metamorphic rocks has significant tectonic implications. Crustal materials were presumably subducted to depths of more than ~100 km where the diamonds crystallised from a fluid phase under static conditions. After formation, the diamond-bearing rocks must have been uplifted

and exhumed rapidly enough to retain evidence of their high-pressure, high-temperature history.

The occurrences of graphitized diamonds in the Beni Bousera and Ronda massifs of Morocco and Spain respectively demonstrate clearly that diamonds can form in Alpine peridotites and that tectonic processes can sample deep mantle sections (Pearson et al. 1989; Davies et al., 1993). However, in these bodies, emplacement was not rapid enough to preserve the original minerals.

In summary, there is general agreement that most natural diamonds are formed in the upper mantle at pressures greater than ~35 kbar and at temperatures more than ~1000°C. Once formed, the diamonds were rapidly brought to the surface by either kimberlite eruptions or tectonic processes. A few diamonds formed in the lower mantle, and some microdiamonds crystallised from their transportation media - kimberlites. A few occurrences of diamonds formed in meteorites and meteorite impact structures.

This dissertation, however, deals with a new occurrence of diamonds and associated minerals, in podiform chromitite hosted in the mantle section of the Luobusa ophiolite, southern Tibet. A similar occurrence of diamonds in chromitite ores in southern Quebec was reported by Dresser (1913), but never confirmed.

1-2. Previous work

Diamonds were first discovered in Tibet in heavy mineral separates of podiform chromitite from the Luobusa and Donqiao ophiolites, selected for study of PGE minerals

(Fang and Bai, 1981). A number of other unexpected minerals, including SiC, graphite, native chromium, Ni-Fe alloy and Cr^{+2}- bearing chromite, were also recovered during that study. Following the initial discovery, additional diamonds were recovered from stream sediments and alluvial fans on the south side of the Donqiao massif. Later, geologists of the Tibetan Geological Bureau independently found diamonds in the podiform chromitite of the Luobusa ophiolite (Yan et al., 1986).

Over 100 diamond grains were recovered during these initial studies, 20 from the chromitite and harzburgites of the Luobusa massif and six from similar rocks in the Donqiao massif. The remainder are placer diamonds from the sediments flanking the Donqiao massif, which is located in the Bangong-Nujiang ophiolite belt (Bai et al., 1989) ca. 500 km northwest of the Luobusa massif.

Most of the Luobusa diamonds are 0.1-0.2 mm in diameter but several exceed 0.5 mm (Fang and Bai, 1981; Bai, et al., 1993). All of the diamonds from Luobusa are colourless and transparent. Many have euhedral octahedral, or cubo-octahedral morphologies, others are broken or fractured cleavage fragments.

Earlier workers suggested that the Luobusa diamonds formed during subduction of the Luobusa ophiolite into the diamond stability field at depths of 150-200 km and that the body was later emplaced rapidly into the crust by tectonic processes (Bai et al., 1993; Nixon, 1995).

Because diamonds were not found in hand specimens or thin sections, the possibility of natural or human contamination could not be completely ruled out. A study

of the infrared (IR) microspectroscopy of the Luobusa diamonds by Taylor, et al. (1995) confirmed that they are natural crystals; but the fact that their high nitrogen aggregation state is inconsistent with formation in a 'cool' subduction model led them to suggest that the diamonds were the result of either natural or anthropogenic contamination.

The carbon sources (mantle or recycled crustal material or a combination) remain unclear.

1-3. This work

In order to confirm the presence or absence of diamonds in these rocks and to obtain abundant material for detailed studies, in 1996 we sampled the chromitite and harzburgite of the Luobusa ophiolite under carefully controlled conditions. Five 1-ton samples were collected from orebodies 11 and 31 and associated harzburgites of the Luobusa ophiolite. The samples were hand washed, air dried, crushed to pass a 1-cm sieve and shipped to the Institute of Multipurpose Utilization of Mineral Resources, Zhengzhou, China, for separation of diamond and heavy minerals. Detailed descriptions of the sampling and separation procedures are given in chapter 2.

About 25 diamonds, as well as an extensive collection of associated minerals, have been hand-picked from the mineral separates and they form the basis for this study. The associated minerals include SiC (moissanite), graphite, Fe-Si, Fe-Ni, Cr-C, Ag-Au alloys, olivine, enstatite, Cr-diopside, chromite, phlogopite, biotite, amphibole, sillimanite, zircon, sphene, apatite, rutile, corundum, wollastonite, plagioclase, K-

feldspar, celestite, gehlenite, native silicon, pyrite, arsenopyrite, sphalerite, pentlandite, matraite, galena, dolomite, calcite, almandine, uvarovite, chlorite, and serpentine.

This study differs from the previous work in that: 1) sampling and separation processes were specially designed for diamond collection, and carefully controlled procedures were used to avoid any possible contamination; 2) one diamond was identified to contain 3 silicate mineral inclusions, a natural fingerprint; 3) an abundant collection of unusual minerals which are seldom observed in hand samples or thin sections were recovered; 4) some minerals are attached to chromite, verifying their primary occurrence in the chromitite; 5) two most likely models are provided for the diamond formation.

The main goals of this study are to 1) confirm the presence or absence of diamonds in the Luobusa chromitites, including collecting diamonds and associated minerals in the Luobusa chromitites; 2) characterise the Luobusa diamonds; 3) collect electron microprobe and X-Ray diffraction data of the mineral assemblage with which the diamonds are associated in order to constrain the formation conditions; and 4) on the basis of the available data and reviews of other occurrences of natural diamonds, develop a likely model(s) for the formation of diamonds in the Luobusa ophiolite. The work is based on study of the diamonds and their inclusions, and the assemblage of associated minerals.

CHAPTER 2. GEOLOGY

2-1. Regional geology

The Tibetan Plateau is the largest and highest such feature on Earth (Fig. 2-1, modified from Fielding et al., 1994). It has an average elevation of about 5 km (Fielding et al., 1994) and is underlain by 65-75 km of continental crust, nearly twice the normal crustal thickness (Hirn et al., 1984; Hirn, 1988; Molnar, 1988). It is proposed by some that the Tibetan plateau was uplifted over the latest 20 Ma years by the injection of crust from beneath the Tarim, Karakumy and Indus-Gangdese spreading basins (Bai and Yang, 1985; 1987; 1988; Bai et al., 1993; 1994). Others suggest that the Tibetan plateau was uplifted in the late Cenozoic as a result of the collision of India and Asia about 50 Ma (Searle et al., 1987; Dewey et al., 1988; Ratschbacher et al., 1994); four models have been proposed to explain the uplift resulting from collision: 1) Underthrusting of the Indian crust beneath Asia (Barazangi and Ni, 1982; Powell, 1986); 2) Crustal shortening and thickening of both Asia and India (Dewey and Burke, 1973; England and McKenzie, 1982; England and Houseman, 1986); 3) Injection of Indian crust into a viscous and ductile lower crust beneath Tibet (Zhao and Morgan, 1985; 1987; Nelson et al., 1996); and 4) removal of part of the Tibetan lithospheric mantle and replacement by hotter and less dense asthenosphere, leading to a decrease in lithospheric mass and isostatic uplift (Houseman et al., 1981; England and Houseman, 1988). In contrast to the above models emphasising uplift in the latest 20 Ma or after collision, Murphy et al. (1997) proposed

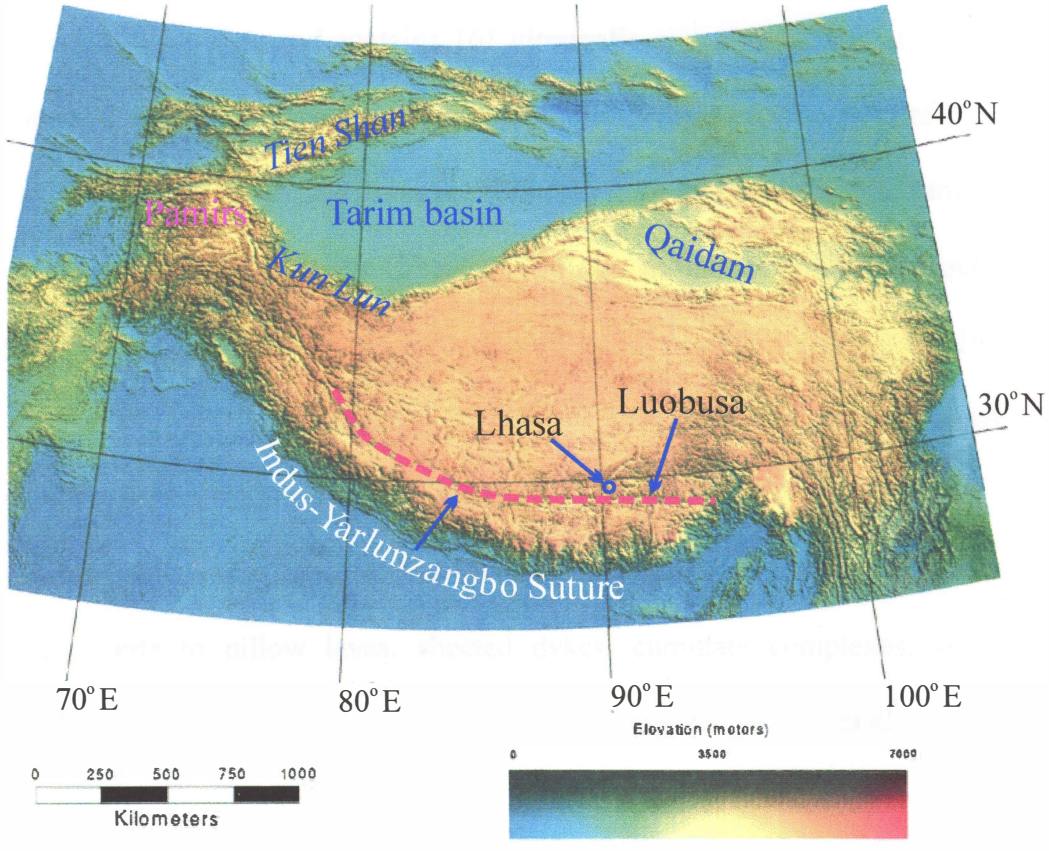

Figure 2-1. Tibetan Plateau (from Fielding et al., 1994)

that the southern part of the plateau was uplifted 3-4 km in the early Tertiary, prior to the India-Asia collision.

The Indus-Yarlunzangbo Suture (IYS) (Fig. 2-1) marks the early Tertiary collision zone between India and Asia (Zhao, 1997). Numerous ophiolitic bodies crop out along the entire length of the IYS, from Burma on the east to Ladakh on the west. The ophiolite belt is over 1500 km long and contains 161 ultramafic or mafic massifs of varying size, which have an overall outcrop area of about 3660 km^2 (Zhou, 1995). All of the known ophiolites in Tibet occur in late Jurassic to late Cretaceous formations (Zhang and Ba, 1996). Those in the IYS are all Cretaceous in age and were emplaced about 50 Ma (Allegre et al., 1984; Nicolas et al., 1981; Girardeau et al., 1985; Wang et al., 1987). In contrast to other collisional orogens, no high-pressure metamorphic rocks have been reported in the IYS.

All of the components of ophiolites, from marine sedimentary rocks and radiolarian cherts to pillow lavas, sheeted dykes, cumulate complexes, and mantle peridotites, are present in the suture zone, although complete sequences are rare. Where present, the different components are almost always in fault contact with one another. A typical ophiolite section is preserved in the Xigaze area in the middle of the suture within the Tibetan Plateau (Girardeau and Mercier, 1988; Bai et al., 1989).

2-2. Geology of the Luobusa ophiolite

The Luobusa ophiolite lies in the eastern part of the IYS about 200 km southeast

of Lhasa (Fig. 2-1 and 2-2). Elevations in the area range from 3500 m above sea level at the Yarlunzangbo River to about 6000 m on the highest peaks (Zhou, 1995). The ophiolite is exposed on the south bank of the Yarlunzangbo River and extends for about 43 km along strike (Zhou, 1995). The ophiolite is bounded on the north by Tertiary sedimentary rocks of the Gangdese Formation or by the Gangdese batholith and on the south by a thick sequence of Triassic sedimentary rocks (Zhou, 1995). Both contacts are reverse faults dipping to the south and the ophiolite itself is cut by numerous north-trending normal faults (Fig. 2-2).

The ophiolite consists predominantly of mantle peridotite, transition zone dunite, and ophiolitic melange. The mantle peridotite includes harzburgite and diopside-bearing harzburgite with abundant dunite and podiform chromitite. It is cross-cut by numerous undeformed gabbro dykes, 1-20 m wide and several hundred meters long. Similar gabbro dykes are also observed in the Triassic rocks in fault contact with the ophiolite to the south. Podiform chromitite orebodies occur chiefly at a particular level in the harzburgite where they are typically surrounded by envelopes of dunite. The harzburgites are composed of 62-85 modal % olivine, 11-32 % orthopyroxene, 0.2-5% clinopyroxene and 0.2-1% disseminated chromite (Zhou et al., 1996). They typically have a well developed porphyroclastic texture, with a fine-grained, recrystallized granoblastic matrix containing a few large porphyroclasts which show deformation lamellae and kink banding (Zhou et al., 1996). The harzburgites have rather uniform bulk rock compositions, with mg-numbers (100 $Mg/(Mg + Fe^{2+})$ of 80-91 and flat, unfractionated, chondrite-normalized

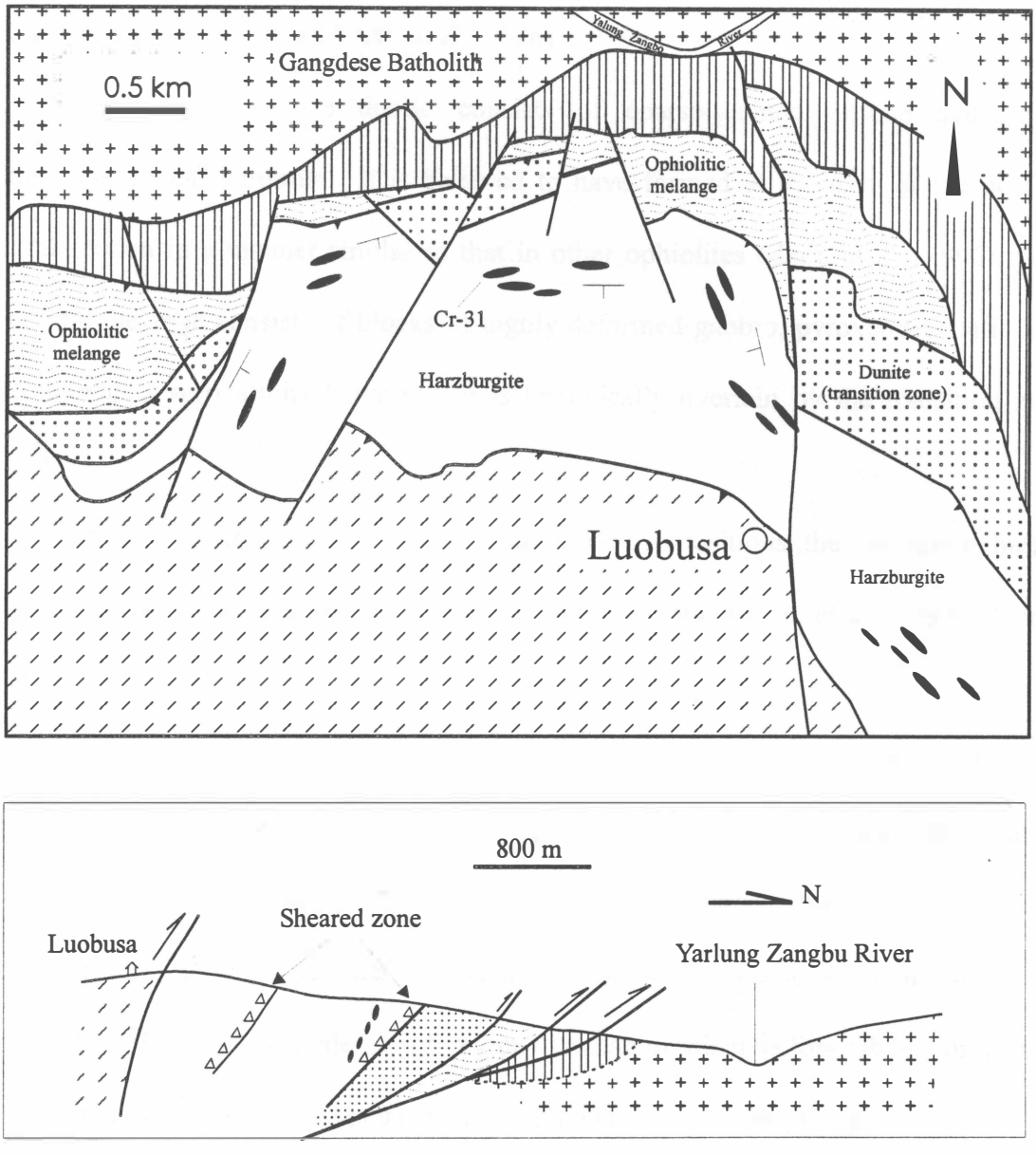

Figure 2-2. A - Geologic map of the Luobusa ophiolite; B - Cross section of the Luobusa ophiolite (from Zhou, et al., 1996)

platinum group element patterns. They are believed to be residual peridotites left after extraction of mafic magmas (Zhou et al., 1996).

The transition zone dunite consists of coarse-grained olivine and minor clinopyroxene and chromite. It is believed to have formed at the base of the oceanic crustal section in a manner similar to that in other ophiolites (Zhou et al., 1996). The ophiolitic melange consists of blocks of highly deformed gabbro, pyroxenite, mafic lava and chert in a serpentinized matrix. It is tectonically overlain by the transition zone dunite.

Based on its rock geochemistry and chromite compositions, the Luobusa ophiolite is believed to have formed in a suprasubduction environment (Bai, et al., 1993; Zhou et al., 1996).

The metamorphic history of the Luobusa massif has not been studied in detail. The peridotites have experienced high-temperature recrystallization and deformation within the mantle (Zhou, 1995). The mantle sequence has also undergone serpentinization of variable intensity from <1% near the top to 40% or more near orebodies. There is no evidence of regional metamorphism before obduction-related serpentinization. No high pressure or high temperature metamorphic phases have been observed, either in the Luobusa area or in the IYS as a whole.

2-3. Characteristics of the Luobusa podiform chromitites

The Luobusa podiform chromitites occur in the depleted mantle sequence of the

ophiolite. Most of the chromitite orebodies in Luobusa are surrounded with sharp contacts by dunite envelopes which grade outward into the enclosing harzburgite. The envelopes range from several centimetres to several meters thick and, in general, the largest orebodies have the thickest envelopes. The chromitite orebodies are typically lens-shaped (Fig. 2-3), although some are tabular or pencil-shaped. They range from 20-250 m long, 10-100 m wide and 0.5-5 m thick (Zhou et al., 1996). Most bodies are concordant or subconcordant to the foliation in the host rock. Massive, disseminated, nodular and brecciated textures are present in most of the orebodies. Massive chromitite is composed of more than 80 modal % chromite, and has a closely packed, coarse-grained texture. Individual chromite grains are anhedral and mostly 1-5 mm across. The interstices between chromite grains are filled with a variety of other minerals, mostly silicates.

Based on the high Cr content, the podiform chromitites are believed to have precipitated from highly magnesian magmas formed by high degrees of partial melting. Precipitation was triggered by interaction between the newly formed magmas and old lithospheric mantle peridotites in an island arc environment (Zhou, 1995; Zhou and Robinson, 1997).

2-4. Characteristics of the diamond-bearing chromitite orebody

Diamonds and associated minerals were first recovered from chromitite orebody No. 31 in 1980 (Fang and Bai, 1981). In 1996 we resampled this orebody and diamonds

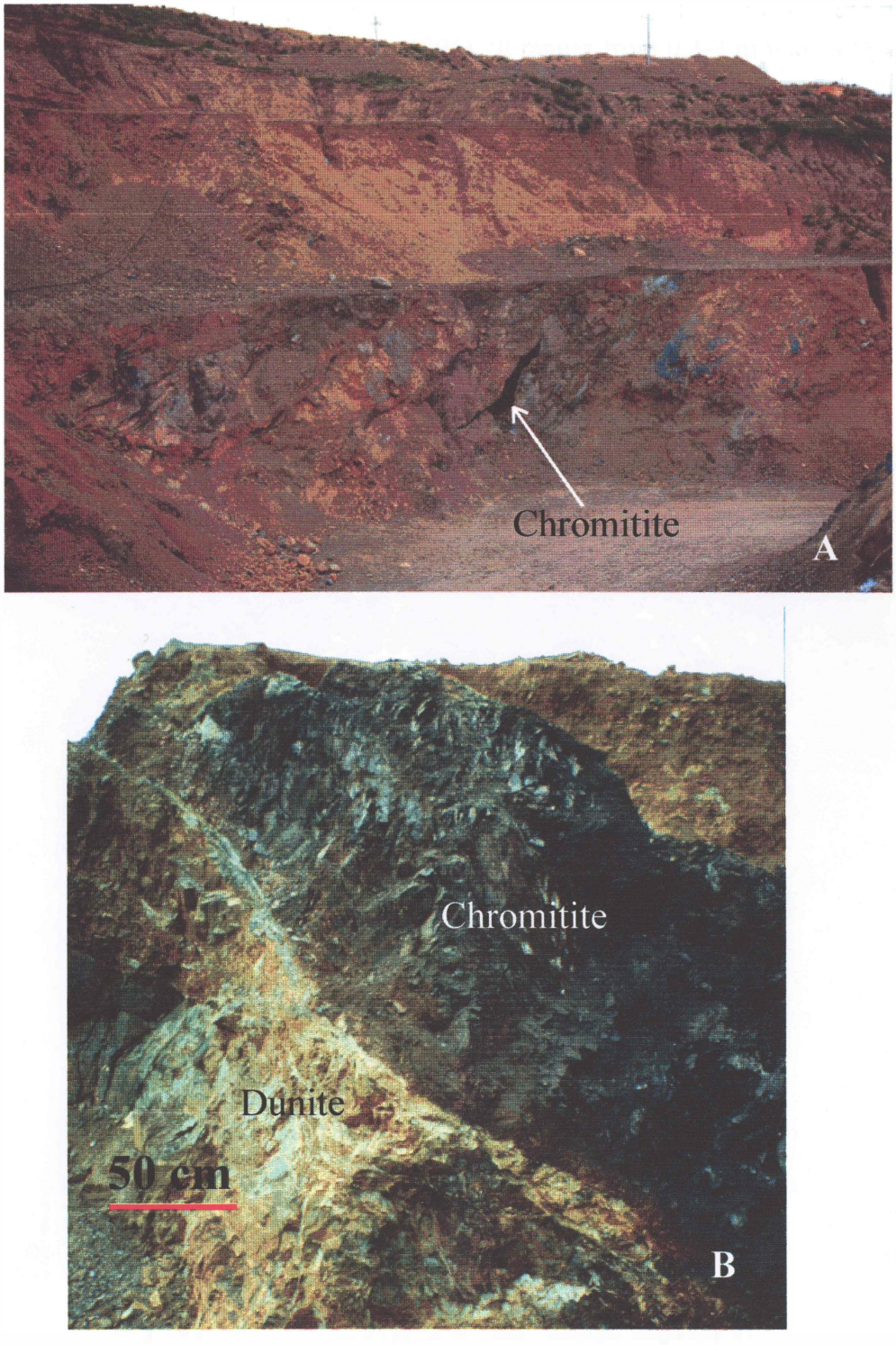

Figure 2-3. A - lens-shaped chromitite orebody (No. 31) in its host harzburgite in the mantle section of the Luobusa ophiolite; B - chromitite orebody (No. 31) and its dunite envelope in Luobusa.

were again recovered from heavy mineral separates of the chromitite. Orebody No. 31 is shaped like a flat bean (Zhang and Ba, 1996). It ranges from 0.3-3 m wide and crops out for more than 300 m along strike. The orebody is in fault contact with the enclosing harzburgite but is generally concordant with the foliation in the host rock. A dunite envelope, up to 5 m thick, is generally present around the orebody. The chromitite has a massive texture (Fig.2-4), composed of closely packed chromite grains with other

Figure 2-4. Massive chromitites of the the orebody number 31 in Luobusa in which diamonds and associated minerals were found

minerals filling the interstices. Other minerals identified in the mineral separates include diamond, graphite, SiC, Cr-C, Si-Fe, Ni-Fe, Ag-Au alloys, native Si in SiC, olivine, enstatite, Cr-diopside, phlogopite, amphibole, biotite, sillimanite, zircon, sphene, apatite, rutile, corundum, plagioclase, K-feldspar, celestite, gehlenite (intergrown/inclusion within SiC), wollastonite ($CaSiO_3$), pyrite, arsenopyrite, sphalerite, pentlandite, matraite (ZnS), galena, dolomite, calcite, almandine, uvarovite, Fe-Mn garnet, chlorite, and serpentine. PGE minerals, native chromium and native copper were also reported in the previous work (Fang and Bai, 1981; Bai et al., 1993; Zhang and Ba, 1996).

2-5. Sampling and separation procedures

In 1996, we collected three 500 kg samples from three sites at different levels of orebody No. 31, with each of the 3 sites being about 10 m higher than the next one (the top site: 29°13.86′ N, 92°11.32′ E, and bottom site: 29°13.88′ N, 92°11.39′ E). In order to minimize the possibility of any natural or anthropogenic contamination, the samples collected in 1996 were selected and processed with the utmost care. Diamond or carbide tools were not employed in any of the sampling or processing steps and no diamond drilling has been carried out in the sampled area. The sampling and processing of the chromitite involved a step by step approach, as discussed below.

a. Sampling in the field.

The Luobusa massif is covered by Quaternary glacial soils which could possibly

have carried diamonds from a distant source. To eliminate possible contamination from this source, samples were removed directly from the chromitite orebody using iron tools. The samples were placed in double-layered plastic bags for transporting by truck to the initial crushing plant in Lhasa. A 200 kg sample of granite from the Gangdese batholith was collected as a blank to check on possible contamination during sample processing (or separation). Because of their magmatic temperatures and high oxygen fugacities, granites should be free of diamonds.

b. Initial crushing.

To avoid any damage to sample bags during train transportation, the samples were initially crushed in Lhasa. They were hand washed, air dried and crushed to pass a 1-cm sieve using specially cleaned equipment. Before processing each sample, the jaw crusher was dismantled and cleaned carefully using brushes and compressed air. A 2 kg piece of each sample was crushed and discarded before crushing proceeded. The crushed material was then placed in plastic bags for shipment to the separation plant in Zhengzhou, China.

c. Separation procedures

The separation procedures (Fig. 2-5) were specially designed for diamond separation. Prior to separation, all the equipment was dismantled and carefully cleaned. The granite control sample was processed first using a procedure similar to that used for the chromitite samples. Fraction size ranges from 3 mm down to 0.3 mm. After the

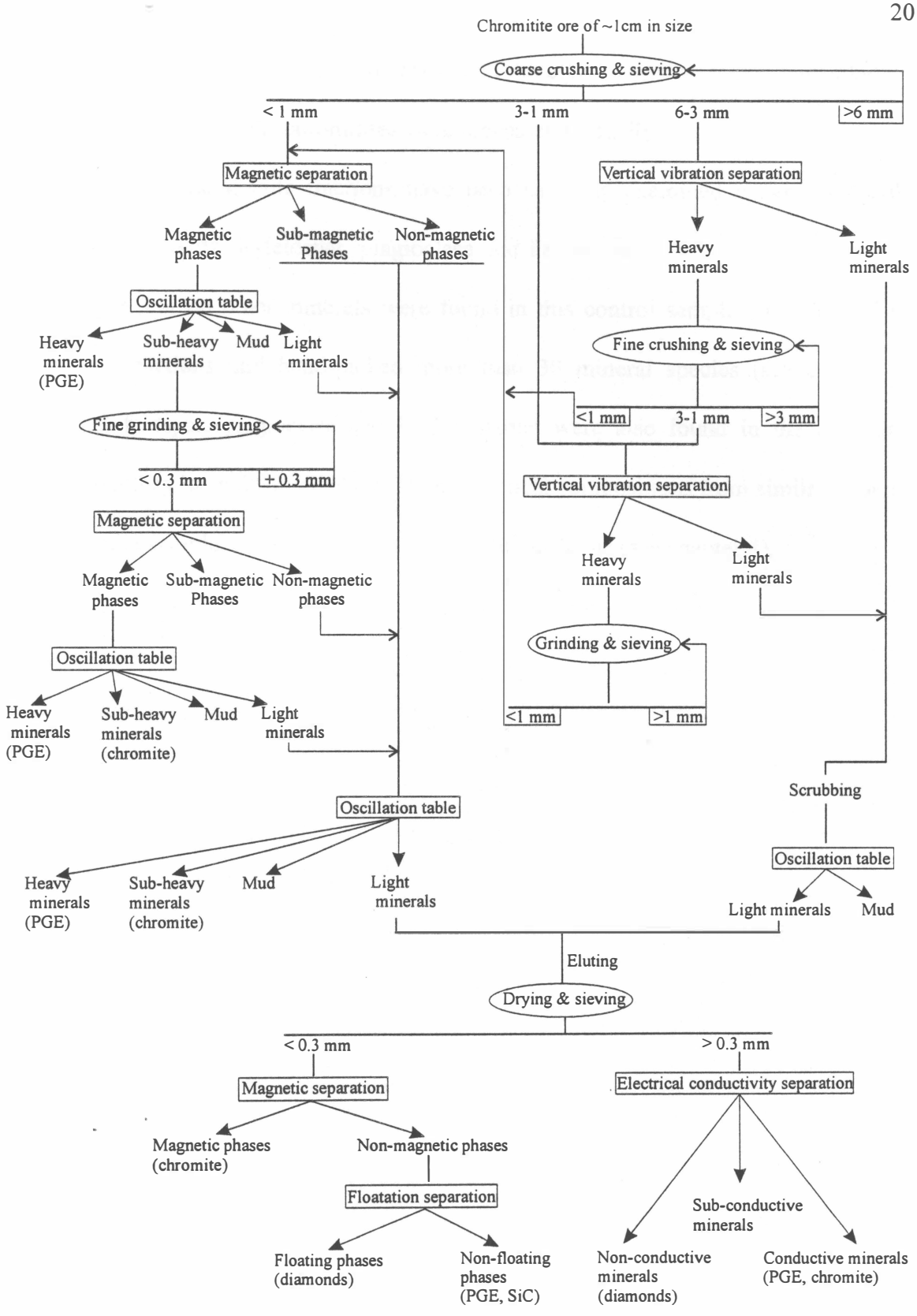

Figure 2-5. Diamond separation procedures

completion of the control sample processing, all the equipment was again dismantled and carefully cleaned, then the chromitites were processed carefully.

Most of the granite fractions have been carefully examined under a binocular microscope. Quartz, K-feldspar, plagioclase and Fe-Mn garnet were hand-picked from this sample, but no other minerals were found in this control sample. I examined the chromitite fractions and hand-picked more than 30 mineral species (see chapter 4). Quartz, K-feldspar, plagioclase and Fe-Mn garnet were also found in the chromitite sample, but they have distinctively different chemical compositions from similar minerals in the granite sample, except that quartz is indistinguishable (see chapter 4).

CHAPTER 3. LUOBUSA DIAMONDS

3-1. Recovered during previous work

The diamonds recovered by Fang and Bai (1981) are colourless and transparent. Most of them are 100-200 μm across, with some exceeding 500 μm. The euhedral diamonds have octahedral, or cubo-octahedral morphologies (Bai et al., 1993). Some of the grains contain numerous dark microinclusions (Yang et al. 1986). None of the diamonds are obviously corroded or etched on the crystal surfaces as is the case for many grains from kimberlites. The diamonds were identified optically and confirmed by X-ray diffraction analysis. Microprobe analyses indicate that they consist of nearly pure carbon (Bai et al., 1993).

IR spectra indicate that the diamonds separated by Fang and Bai (1981) are of type IaAB (Taylor et al., 1995). The total nitrogen contents varies from ~20 atomic ppm to ~700 atomic ppm and aggregation states are high, up to 80% (Taylor et al., 1995).

3-2. Recovered during this project

About 25 diamonds have been recovered thus far from the Luobusa chromitite. They are colourless and transparent. Most of them are euhedral crystals, and exhibit sharp-edged octahedral morphology (Fig. 3-1 A, C and D). Others are broken fragments (Fig. 3-1 B). Euhedral crystals are 150 × 150 μm to 400 × 400 μm, whereas broken fragments range in size from 200 × 250 μm to 900 × 1000 μm.

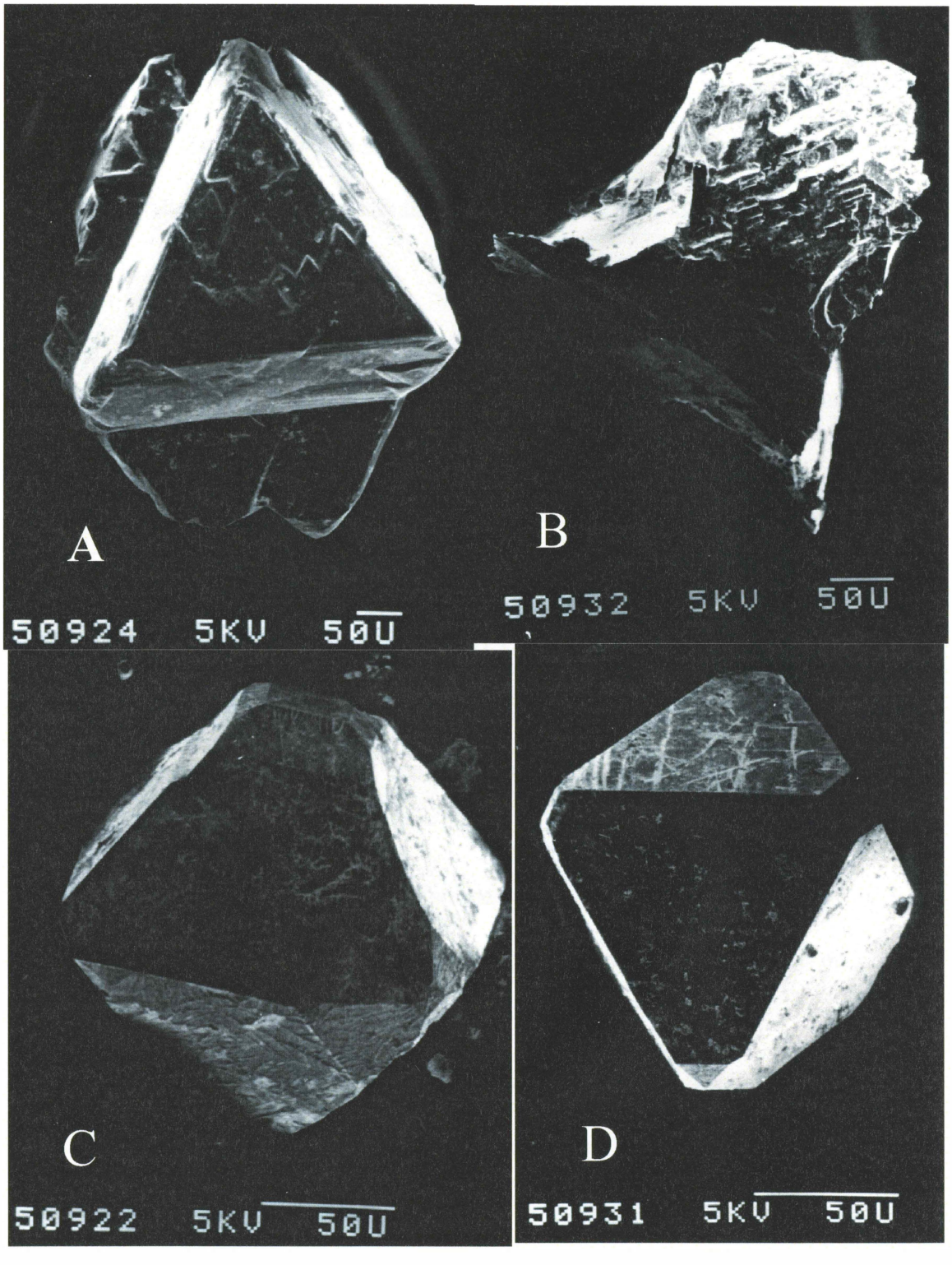

Figure 3-1. A - diamond macle with triangular stepped layer;
B - diamond fragment; C and D - sharp-edged octahedron.

The diamonds were identified by both Raman spectra and X-ray diffraction techniques (Fig. 3-2, and Table 3-1). Raman Spectra for the Luobusa diamonds show a peak ranging from 1329.9 to 1331.9 cm^{-1} typical for diamonds (Fig. 3-2). The X-ray diffraction data of the Luobusa diamonds match those of standard samples very well (Table 3-1).

Table 3-1. Representative X-ray diffraction data of the Luobusa diamonds (JCPDS 6-0675 - diamond standard)

1		2		3		4		JCPDS 6-0675		
d(A)	I/Io	d(A)	I/Io	d(A)	I/Io	d(A)	I/Io	d(A)	I/Io	hkl
2.042	100	2.050	100	2.042	100	2.048	100	2.06	100	111
1.256	57	1.258	44	1.256	52	1.256	58	1.261	25	220
1.072	15	1.072	13	1.071	17	1.073	30	1.075	16	311
0.8897	17	0.8913	17	0.8890	19	0.8904	34	0.8916	8	400
0.8165	9	0.8170	7	0.8176	13	0.8168	25	0.8182	16	311
				0.6030	6					

Moka radiation; 47.5 KV; 20 mA; Scan 4-75 degrees 2θ

One grain is a macle (contact-twinned form, Trautman et al., 1997) (Fig. 3-3 and 3-1 A). It is about 450 × 550 μm in size. Typical triangular plates which originate with crystal growth clearly appear on its crystal surface (Fig. 3-1 A and 3-3). This grain also contains dark bundles inside the crystal (Fig. 3-3).

One crystal fragment is 900 × 1000 μm in size. It contains, or is intergrown with, three discrete patches of silicate minerals (Fig. 3-4). The three inclusions or intergrowths are small, 425 × 170, 200 × 190, and 190 × 100 μm, respectively, monomineralic, and yellow to yellowish green in colour. They are separate and do not touch one another.

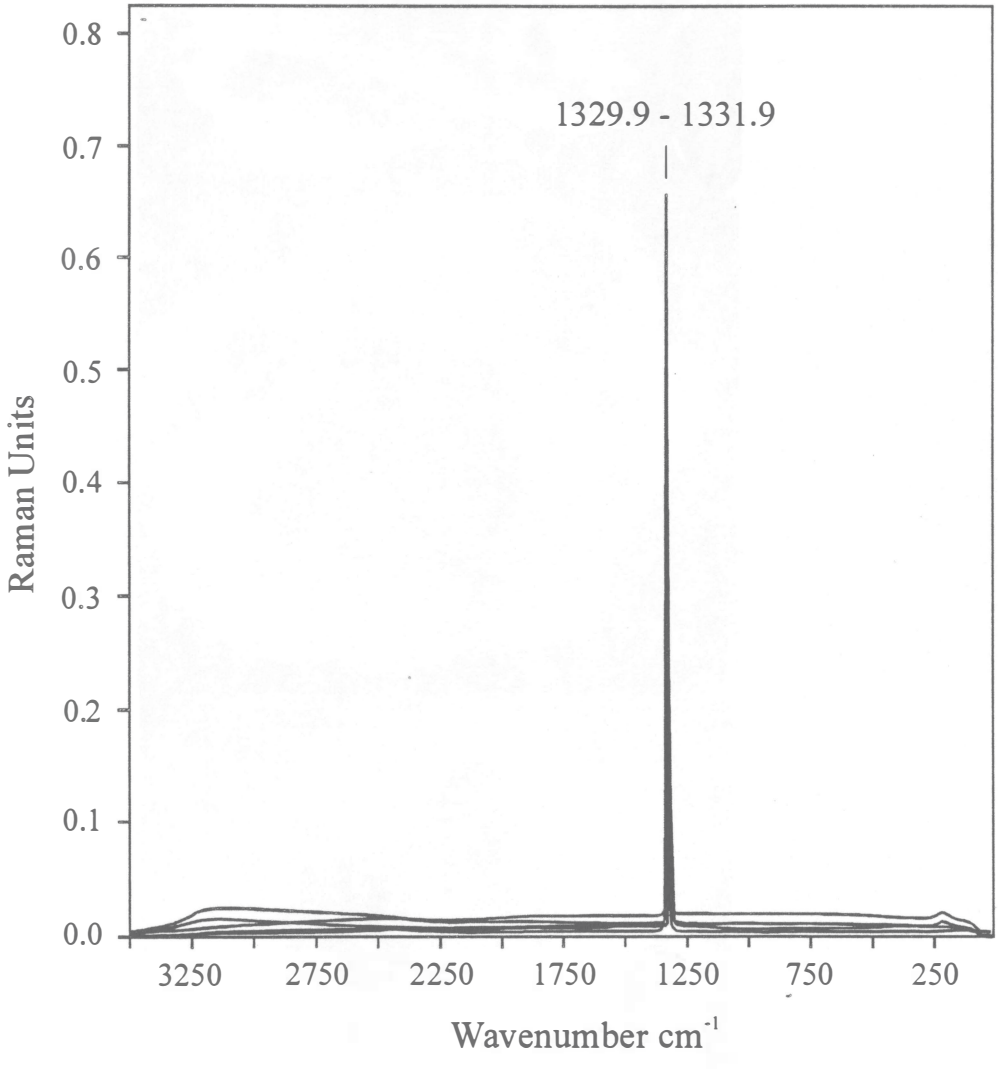

Figure 3-2. Raman Spectra patterns of the Luobusa diamonds

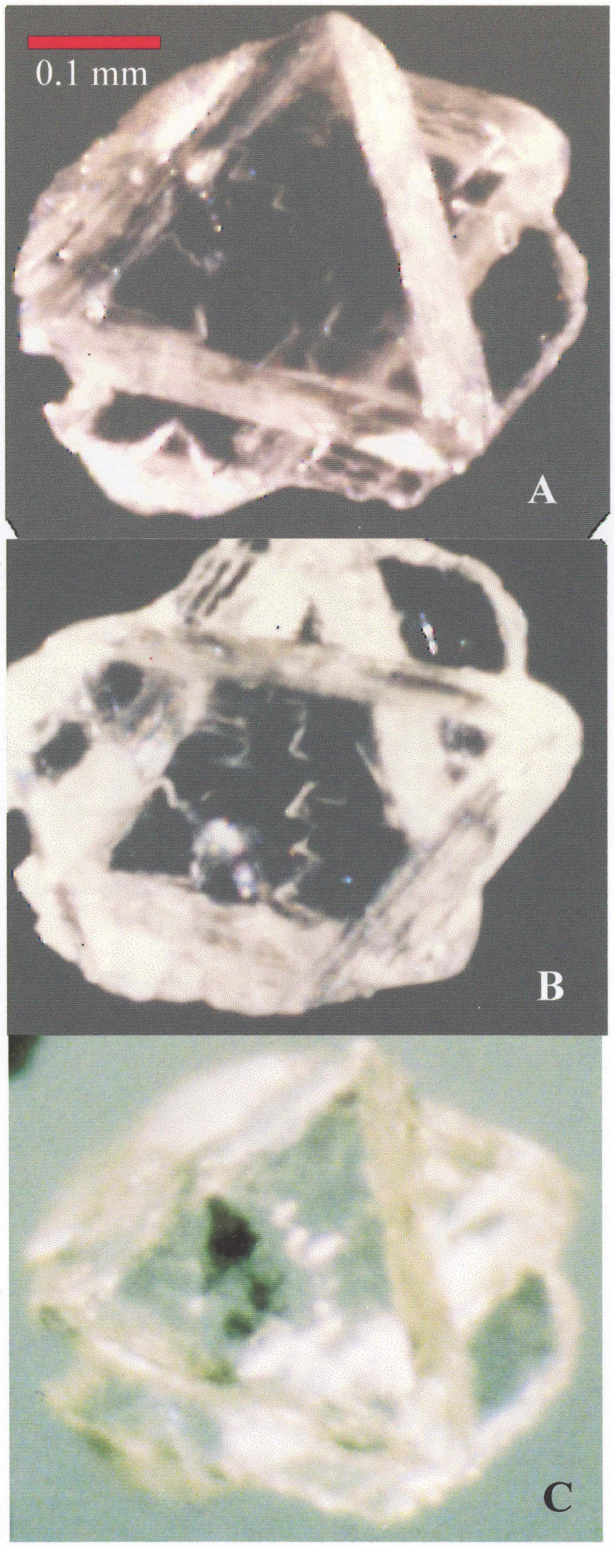

Figure 3-3. A - diamond macle showing stepped-growth layers on the crystal surface; B - the reverse side of the macle; C - showing the dark inclusions inside the macle

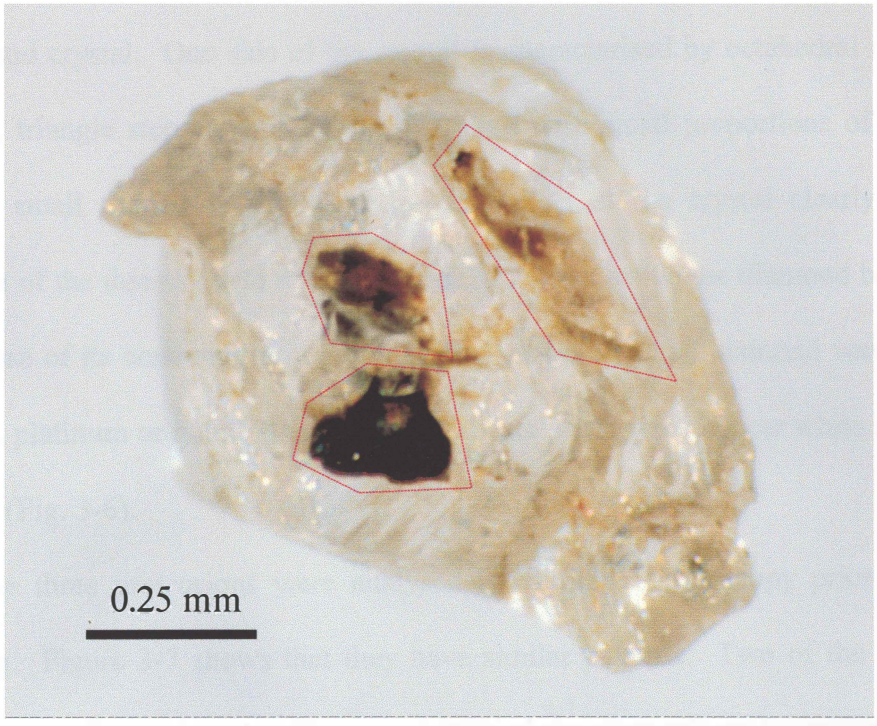

Figure 3-4. Diamond and its 3 inclusions in the Luobusa chromitites, Tibet

Secondary electron images (SEI) were taken to characterise the surface detail of this diamond crystal. One side of the crystal is characterised by octahedral morphology (Fig. 3-5); triangle step-layers are well preserved with small proportions of negatively-orientated small trigons (Fig. 3-5). The other side of the crystal clearly shows the occurrence of the three silicate minerals - part of each is inside the diamond body (Fig. 3-6). Because of its conductivity, during the SEI processing, the diamond was not coated by carbon, platinum or gold. As a result the silicate protrusions appear white in colour on the image (Fig. 3-6).

The three protrusions were analysed by Raman spectroscopy prior to the SEI processing. Figure 3-7 shows that they have similar patterns. Two of the spectra also show a typical diamond peak. The appearance of the diamond peak confirms the close association of the two minerals. One of the three minerals was detached from the diamond body during the SEI processing. A SEI of this intergrowth (Fig. 3-8) shows that it possesses an octahedral morphology typical of that imposed on many syngenetic inclusions by the contemporaneous growth of the surrounding diamond (Scott-Smith, et al., 1984). Electron microprobe analyses were also done for this mineral and these show a composition of SiO_2 64 wt%, FeO 5 wt%, and MgO 31 wt% (Table 3-2). The identification of a silicate mineral occurring in the diamond is strong evidence of its natural origin.

Table 3-2. Electron microprobe analysis of the inclusion in the Luobusa diamond

wt%	1	2
SiO_2	63.95	64.15
Al_2O_3	0.36	0.46
FeO	4.69	4.52
MgO	30.57	30.78
CaO	0.00	0.24
Na_2O	0.42	0.00
Total	99.97	100.14

3-3. Comparison of the diamonds from the two studies

On the basis of morphology, colour and size, the diamonds recovered from this study and previous investigations are very similar. The only difference is that more inclusion-bearing diamonds or ones with silicate intergrowths were collected in this work.

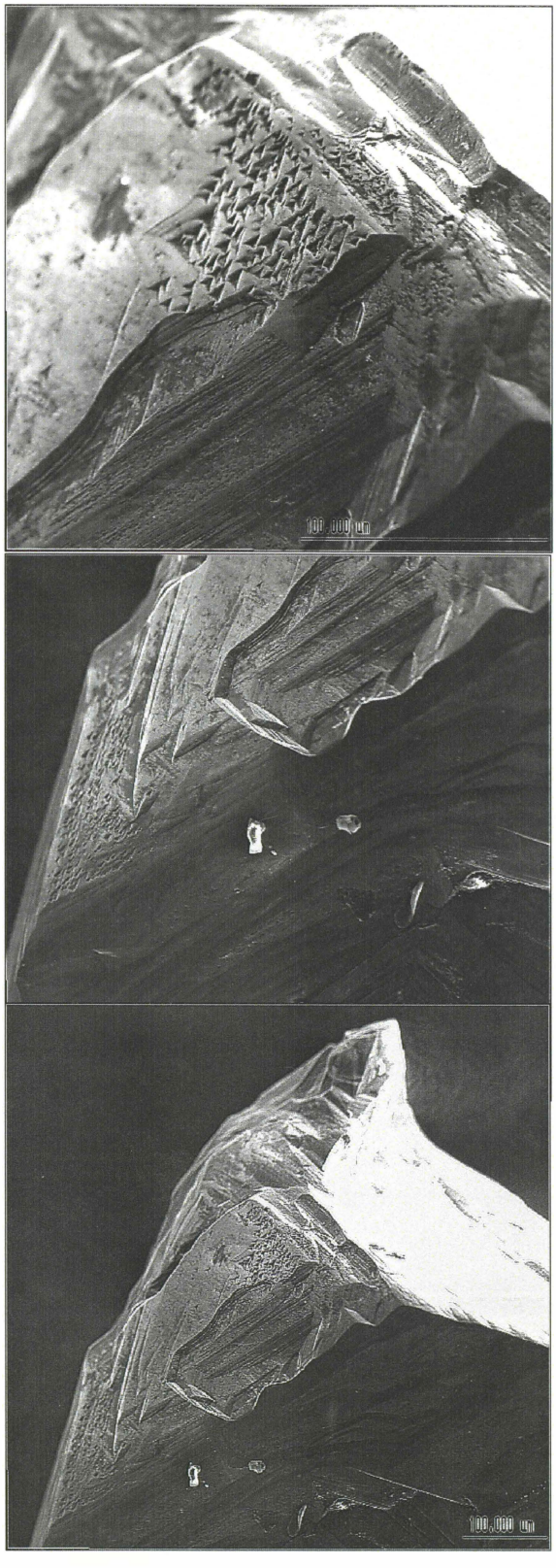

Figure 3-5. SEI of a diamond in the Luobusa chromitites, Tibet, showing its detailed surface characters

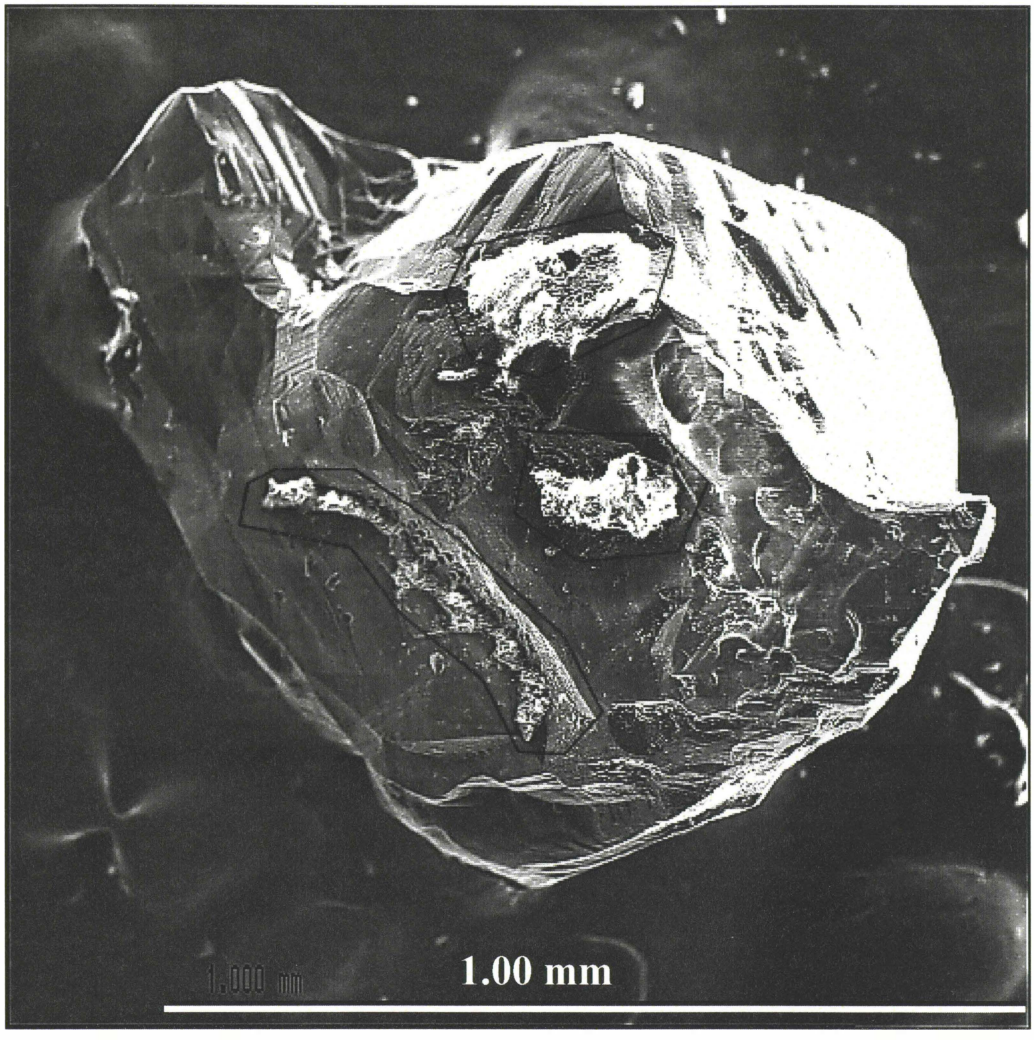

Figure 3-6. SEI image of the diamond with 3 inclusions

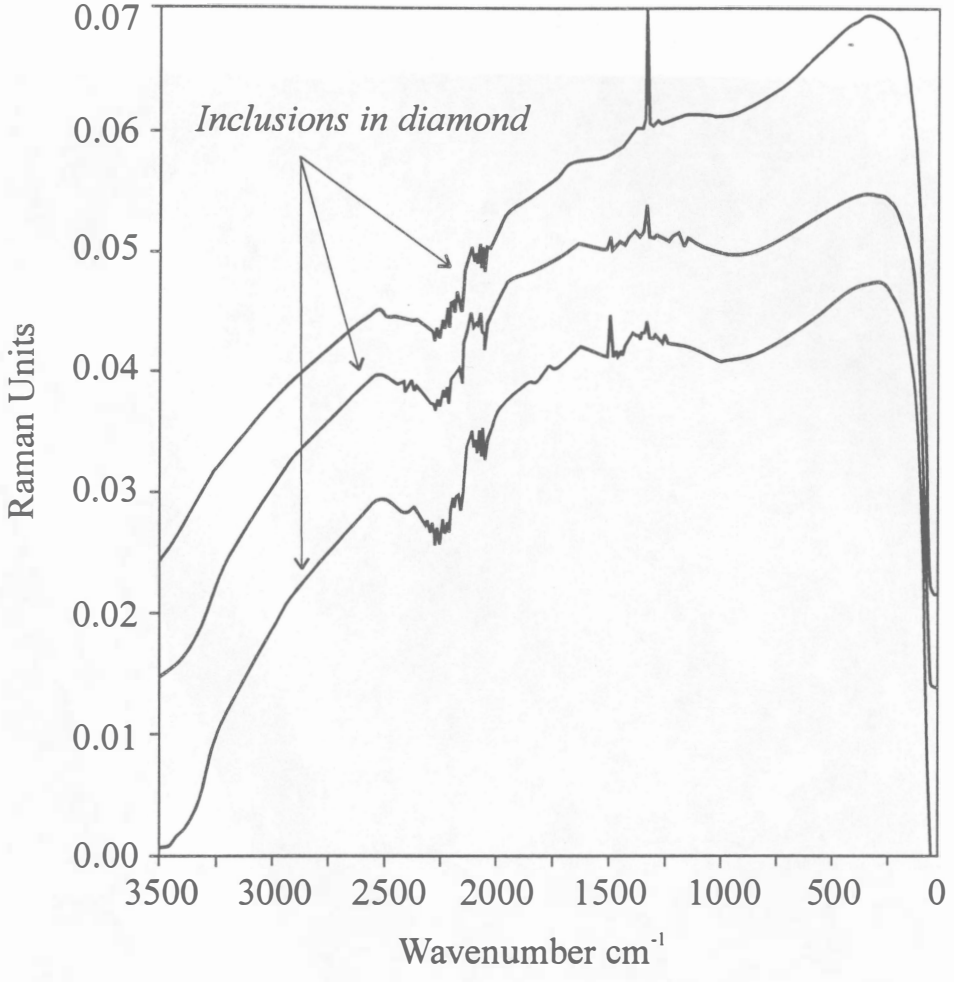

Figure 3-7. Raman Spectra patterns of inclusions in the diamond from the Luobusa chromitites

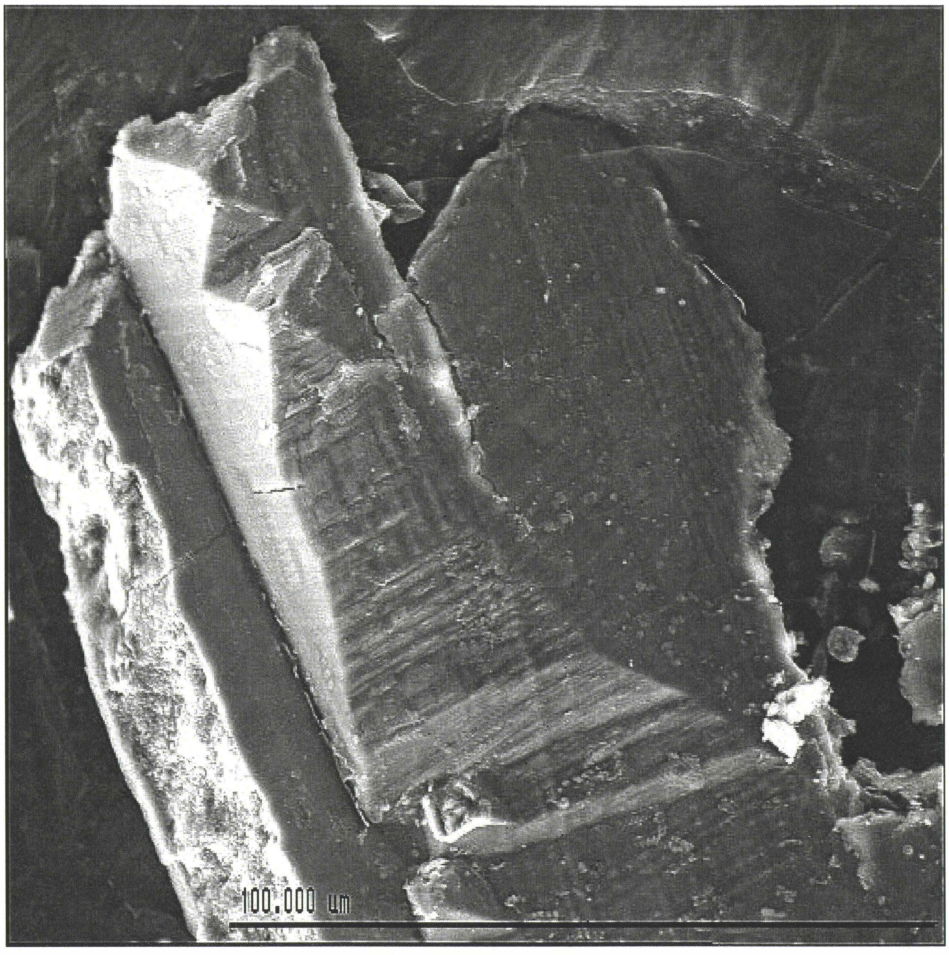

Figure 3-8. SEI image of one of the 3 inclusions in the Luobusa diamond

CHAPTER 4. MINERALOGY/MINERAL CHEMISTRY

A wide variety of minerals including native elements, alloys, sulphides, oxides, phosphates, sulfates, carbonates and silicates have been hand-picked from the podiform chromitite of the Luobusa ophiolite (Table 4-1). The minerals were identified optically, by X-ray diffraction analysis by Dr. T. Stanley Cameron at Dalhousie University in 1998, and by electron microprobe analysis (Table 4-1). Some of the electron microprobe analyses were made by Robert Mackay at Dalhousie University in 1998, such as Cr-C and Au-Ag alloys, SiC, gehlenite and graphite. Most of these minerals occur in small quantities, and are rarely, if ever, observed in thin sections.

Olivine is the most common matrix mineral in the podiform chromitites, although small amounts of orthopyroxene and clinopyroxene are also present (Zhou, 1995). Chlorite occurs as veins in chromite and as interstitial material between chromite grains (Fig. 4-1). Cracks and veinlets in the chromitite are very commonly filled with serpentine, and sulphides occur in these veins (Fig. 4-2). In a few cases, cracks and veinlets are filled with carbonate (Zhou et al., 1996). Primary inclusions of euhedral to subhedral PGE minerals and sulphides occur in massive chromite free of fissures or cracks; and the PGE minerals are rich in Os and Ir (Wen-Ji Bai and Qin-Song Fang, personal communication, 1998), a finding consistent with the work of Zhou (1995).

Table 4-1. Minerals recovered from the Luobusa chromitites, Tibet

Mineral group	Minerals	Abundance	Means of identification		
			XRD	MP	RAM
Native Elements	Diamond	VR	X		X
	Graphite	R		X	
SiC	moissanite	R	X	X	
Alloys	Fe-Si	R	X	X	
	Cr-C	VR		X	
	Fe-Ni	R		X	
	Au-Ag	VR		X	
Sulphides	Pyrite	C		X	
	Arsenopyrite	C		X	
	Pentlandite	C		X	
	Sphalerite	C	X	X	
	Galena	C		X	
	Matraite	R	X		
Oxides	Chromite	A	X	X	
	Corundum	R		X	
	Rutile	R		X	
	Quartz	C	X	X	
Phosphates	Apatite	R		X	
Sulfates	Celestite	VR		X	
Silicates	Olivine	A	X	X	
	Enstatite	A		X	
	Cr-diopside	A		X	
	Zircon	R		X	
	Sphene	R		X	
	Sillimanite	C	X	X	
	Wollastonite	R	X		
	Gehlenite	VR		X	
	Amphibole	R		X	
	Biotite	R		X	
	Phlogopite	R		X	
	Uvarovite	R		X	
	Almandine	R	X	X	
	Plagioclase	R		X	
	K-feldspar	R		X	
	Chlorite	A		X	
	Serpentine	A		X	X
Carbonates	Dolomite	C		X	
	Calcite	C		X	

Note: XRD - X-ray diffraction, MP - electron microprobe, RAM - Raman spectra; A - abundant, C - common, R - rare, VR - very rare.

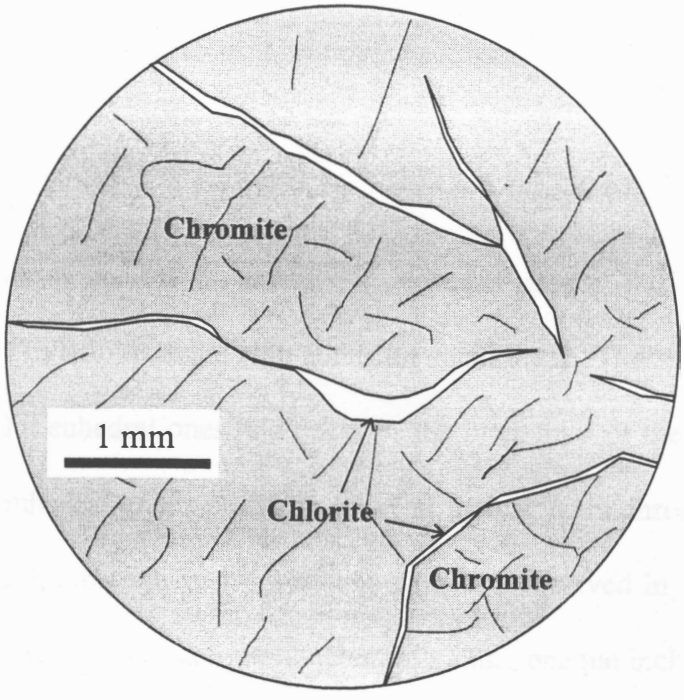

Figure 4-1. Chlorite as veins in the Luobusa chromitites

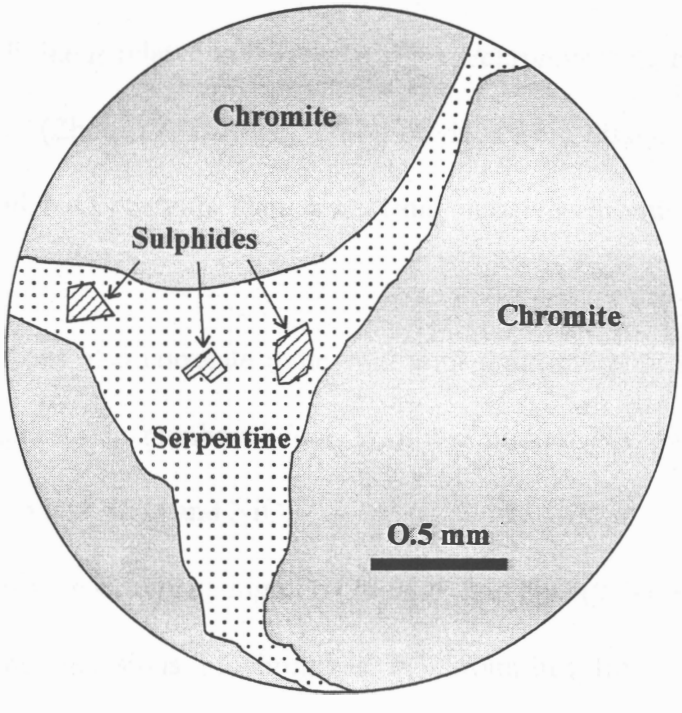

Figure 4-2. Sulphides in the serpentine veins in the chromite matrix of the Luobusa chromitites

Silicate minerals

Olivine $(Mg, Fe)_2SiO_4$

Olivine occurs as colourless, anhedral to euhedral grains, 0.05-0.6 mm across, many of which are of indefinite shape with abundant small faces. The anhedral grains are usually larger than the euhedral ones and occur in the interstices of the chromite grains (Zhou, 1995). The euhedral grains probably occur as inclusions in chromite (Melcher et al., 1997; Auge, 1987), although such inclusions were not observed in the thin sections examined. The euhedral olivines commonly contain minute opaque inclusions which are presumably high-chrome chromites (Fig. 4-3 A, B, C and D).

The olivine grains are all forsterite, with compositions varying from Fo_{91} to Fo_{98}. Corresponding NiO contents range from 0.3 to 1.35 wt% (Fig. 4-4) (Appendix II 1). The composition of the olivine is related to the modal silicate/chromite ratio in the chromitites with different textures (Zhou, 1995; Auge, 1987); olivines from disseminated chromitite have lower MgO and NiO contents than those from massive chromitite (Zhou, 1995; Auge, 1987).

The compositions also correlate quite well with grain morphology: the euhedral olivines have the highest Mg numbers ($Fo_{97.4-98.4}$), and highest NiO contents, whereas anhedral grains contain less MgO and NiO.

Those olivines with extremely high Fo (96-98.4) and NiO (0.7-1.35 wt%) contents are similar to olivine inclusions in chromites in chromitites from the ophiolite of Kempirsai (Melcher et al., 1997) and Oman (Auge, 1987). As suggested by many authors

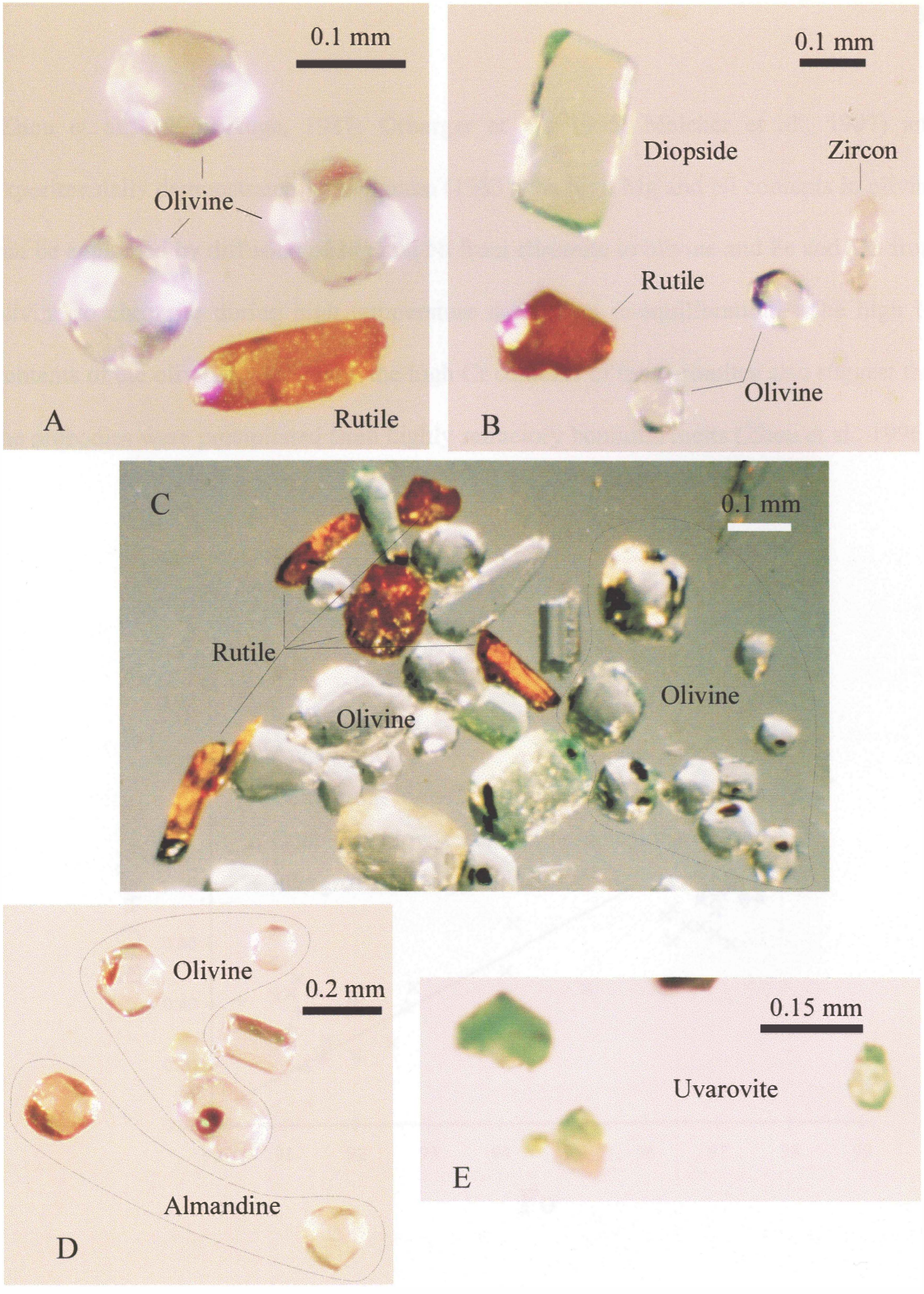

Figure 4-3. Olivine, zircon, garnet and rutile in the Luobusa chromitites, Tibet

(Zhou et al., 1996; Auge, 1987; Orberger et al., 1995; Melcher et al., 1997) and experimentally demonstrated by Lehmann (1983), the high Mg and Ni contents in olivine can be explained by diffusion of Mg and Ni from chromite to olivine and Fe and Mn from olivine to chromite during high temperature subsolidus re-equilibration. The high Ni contents of the olivines, along with the high Cr contents of the chromites also suggest that the orebodies were precipitated from highly refractory boninitic melts (Zhou et al., 1996).

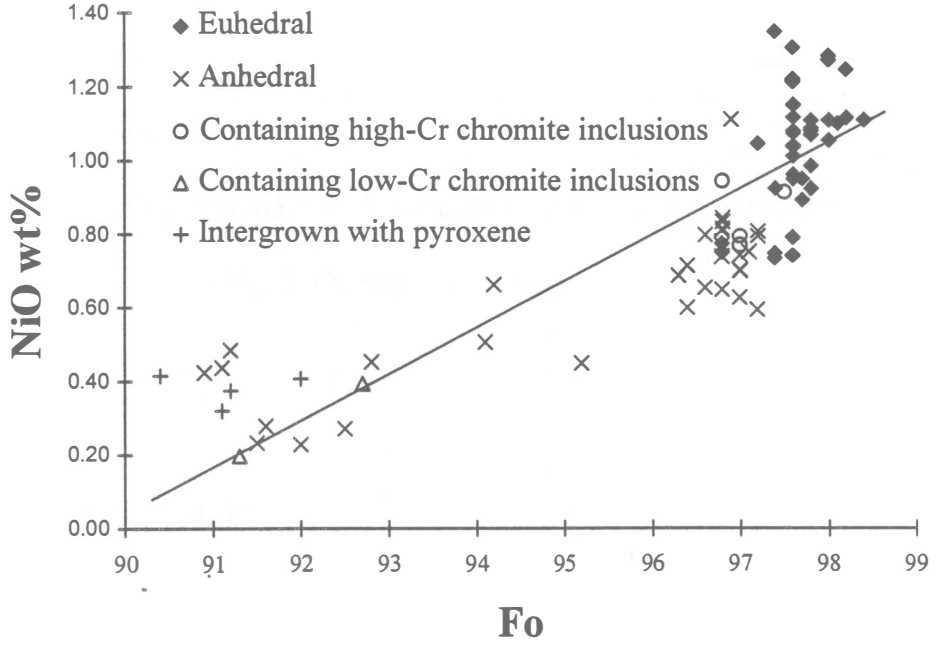

Figure 4-4. Fo versus NiO of the olivine from the Luobusa chromitites

Zircon $ZrSiO_4$

Zircons from the Luobusa chromitite are colourless to brownish-pink, and range in size from 0.03 to 0.4 mm. Most of them are euhedral, showing long-prismatic and prismatic forms (Fig. 4-5 D and 4-3 B); a few are oval in shape or irregular fragments. No zoning or core-overgrowth relationships were observed under the microscope, suggesting that these crystals grew during a single, discrete event rather than by addition to pre-existing igneous or metamorphic zircons. One grain which was analysed by electron microprobe from its center to its edge, showed a constant major element composition (IV-45Za - IV-45Ze, Appendix II 2).

Rounded zircons are commonly regarded as detrital in origin, however, rounding may also be caused by magmatic corrosion (Maria and Heinz, 1989). Some zircons, such as those in the Finero chromitites, are believed to have formed by alkali metasomatism (Von Quadt et al., 1992).

Analysed grains have 65.7-67.2 wt% ZrO_2 and 31.6-33.2 wt% SiO_2. They also contain small amounts of HfO_2, Y_2O_3 and Ta_2O_5 (Appendix II 2).

Sphene $CaTiSiO_4$(O, OH, F)

Sphene occurs as irregular colourless fragments, about 0.4 mm in size. Microprobe analyses show that titanium may be partly replaced by aluminium and iron (Appendix II 3). Sphene is a wide-spread accessory mineral.

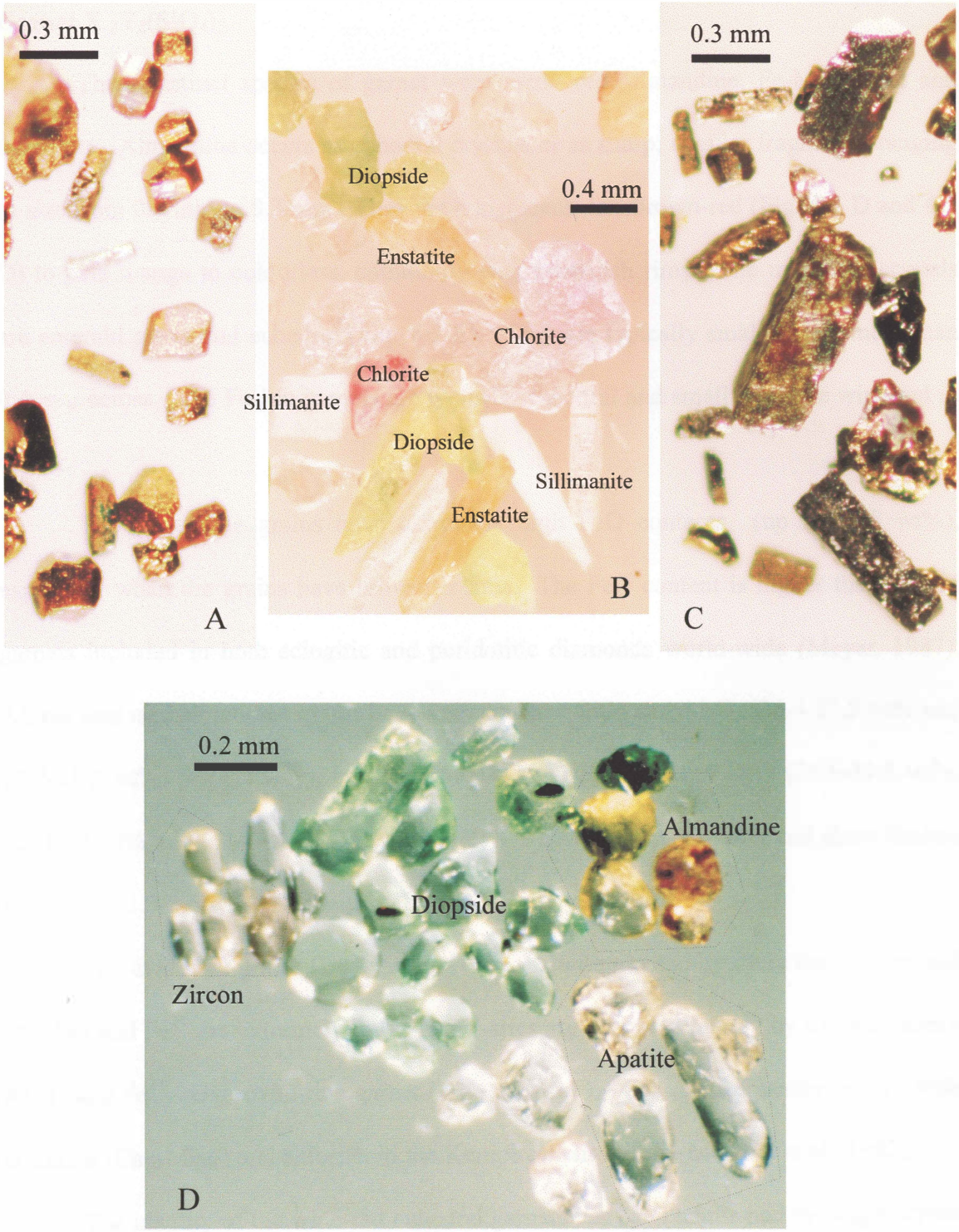

Figure 4-5. A - pyrite; B - enstatite, diopside, sillimanite and chlorite; C - arsenopyrite; D - zircon, diopside, apatite and almandine in the Luobusa chromitites, Tibet

Garnet $X_3Y_2(SiO_4)_3$

Three distinct species of garnet were recovered: almandine, Fe-Mn garnet and uvarovite. Almandine occurs as euhedral crystals or as sharp, angular fragments, ranging in size from 0.1 mm to 0.3 mm. They are transparent, and brown-red (Fig. 4-3 D and 4-5 D) to pale orange to colourless, commonly with brownish rims. The uvarovite crystals are emerald green and euhedral (Fig. 4-3 E). They are typically small, rarely more than 0.4 mm across. The Fe-Mn garnets are typically euhedral and small; they are wine-red in colour.

The almandine grains have extremely high FeO contents (up to 39.8 wt%), especially when the grains have brownish rims. The FeO content is higher than that of garnets included in both eclogitic and peridotitic diamonds world-wide (Meyer, 1987). All the analysed almandine grains have very constant SiO_2 and Al_2O_3 (36.4-37.5 wt% and 20.2-21.2 wt%, respectively), but vary widely in FeO, MnO and CaO (24.6-39.8 wt%, 0.2-13.2 wt% and 0.7-14.6 wt%, respectively). MgO contents are low and show limited variability (1.3-3.6 wt%) (Appendix II 4).

The uvarovite grains ($Uv_{92.3}$ $And_{4.2}$ $Grs_{3.4}$) are dominated by Ca in the X-sites, and Mn, Mg and Fe^{2+} are extremely low. The Y-sites are occupied mainly by Cr, with minor Al, Ti and Fe^{3+}. Uvarovite-rich garnet (Uv_{77-88} And_{7-22} Grs_{1-4}) frequently occurs, with dolomite ($Ca_{50}Mg_{50}$) and chlorite, in the Kempirsai chromitite (Melcher et al., 1997).

The identity of the wine-red euhedral garnets has been confirmed by single crystal X-ray diffraction analysis. Electron microprobe analyses indicate these are Fe-Mn garnets, with SiO_2 35 wt%, Al_2O_3 20 wt%, FeO 23 wt% and MnO 18 wt%.

All of these garnets are interpreted as secondary minerals that formed at relatively low-temperatures.

Sillimanite Al_2SiO_5

Sillimanite is common in the Luobusa chromitites. The sillimanite grains occur as prismatic crystals with at least one perfect cleavage (Fig. 4-5 B). They are white to colourless. The composition (Appendix II 3) is very close to the ideal formula Al_2SiO_5, and the identity was confirmed by X-ray diffraction analysis. A few grains were found attached to chromite grains, showing clearly that they are part of the mineral assemblage.

Orthopyroxene $MgSiO_3$

Orthopyroxene grains are colourless to pale yellowish and rectangular in shape with good cleavage (Fig. 4-5 B). They are commonly intergrown with olivine and chrome diopside and some grains contain exsolution lamellae of chrome diopside.

All of the orthopyroxenes are highly magnesian (En = 88-95, Fs = 4-9, Wo = 0.4-5) (Fig. 4-6) and contain significant amounts of Cr_2O_3 (0.15-0.90 wt%), consistent with the analyses reported by Zhou (1995). Alumina contents are relatively uniform (Al_2O_3 = 1.32-3.85 wt%) but the most magnesian grains have as little as 0.52 wt% Al_2O_3. Alumina and silica show a consistent negative correlation (Appendix II 5).

Clinopyroxene

Clinopyroxene occurs as colourless to bright emerald green, euhedral to subhedral crystals. They are often of indefinite shape with abundant small faces, many of which are

elongate (Fig. 4-5 B and D). Some of the grains are intergrown with olivine or orthopyroxene. When plotted on the pyroxene quadrilateral, all of the analysed grains cluster within or close to the diopside field (Fig. 4-6).

Most of the diopsides display very uniform compositions (En = 46-48, Fs = 0.85-2.1, Wo = 48-50, and Ac = 1.7-3.7), particularly in SiO_2, MgO, Al_2O_3, Cr_2O_3 and CaO, and have low Al contents (Al_2O_3 = 0.49-1.44 wt%) in contrast to those of the peridotites (Zhou et al., 1996). Clinopyroxenes intergrown with olivine or orthopyroxene have distinctive compositions with relatively lower Cr_2O_3 and Na_2O contents and higher FeO and Al_2O_3 contents than other clinopyroxenes analysed (Appendix II 6).

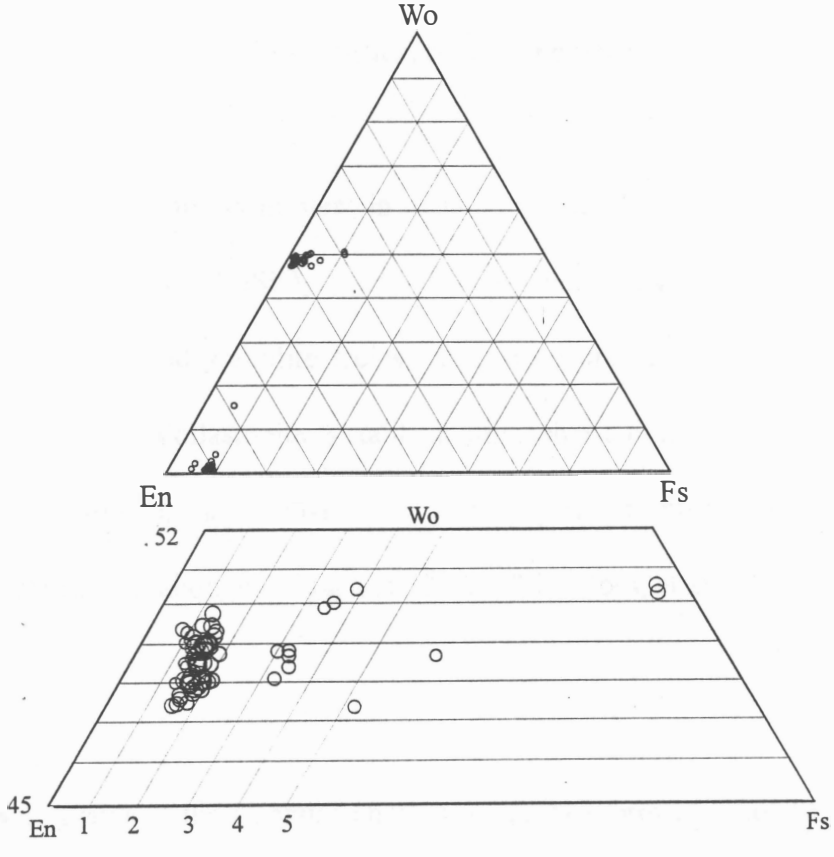

Figure 4-6. Wo - En - Fs diagrams of the OPX and CPX from the Luobusa chromitites

A few augite grains were recovered. They are prismatic and colourless, and have higher Fs and Wo, and lower En contents than diopsides.

All the chromium diopsides have a uniformly higher Cr_2O_3 content (0.99-1.75 wt%) than augite (0.07 wt%). The chromium diopsides have uniform major element compositions, although they vary in colour from colourless to emerald green.

Wollastonite $CaSiO_3$

These are colourless translucent crystals with a prismatic form. Grains range from 0.3 mm to 1.0mm in size. X-ray diffraction analysis demonstrates the prismatic grains have cell parameters of a = 7.27Å, b = 7.88Å, c = 7.03Å. This structure is referred to as the low-temperature form (α-$CaSiO_3$), a typical triclinic polytype – wollastonite-Tc (Deer et al., 1995).

Wollastonite is a common mineral in metamorphosed limestones, resulting from the reaction $CaCO_3 + SiO_2 = CaSiO_3 + CO_2$. In regional metamorphic rocks, it may occur in the amphibolite and granulite facies. It also occurs in some alkaline igneous rocks (Deer et al., 1995). Wollastonite is stable at atmospheric pressure, but it transforms to garnet at about 0.7-0.9 Gpa and 873-1073 K, and the garnet formed in this way further transforms to perovskite at about 6-7 Gpa and 973-1573 K (Ross, et al., 1986).

Amphibole

Amphibole grains in the Luobusa chromitite are dark brown in colour. They are sheet-like fragments, less than 0.9 mm in size. Electron microprobe analyses (Appendix

II 7) show they have a narrow range of composition: SiO_2 = 42.3-43.2 wt%, Al_2O_3 = 10.4-10.6 wt%, TiO_2 = 2.9 wt%, FeO = 8.2 wt%, MgO = 15.5-16.4 wt%, CaO = 11.8 wt%, Na_2O = 2.7-3.1 wt%, K_2O = 1.3 wt%, and Cr_2O_3 = 0.2 wt%. This composition is very similar to that of amphiboles, which were derived from metasomatism in the upper mantle, in peridotites in Pulvermaar, Germany and the Massif Central, France (Menzies et al., 1987) (Fig. 4-7).

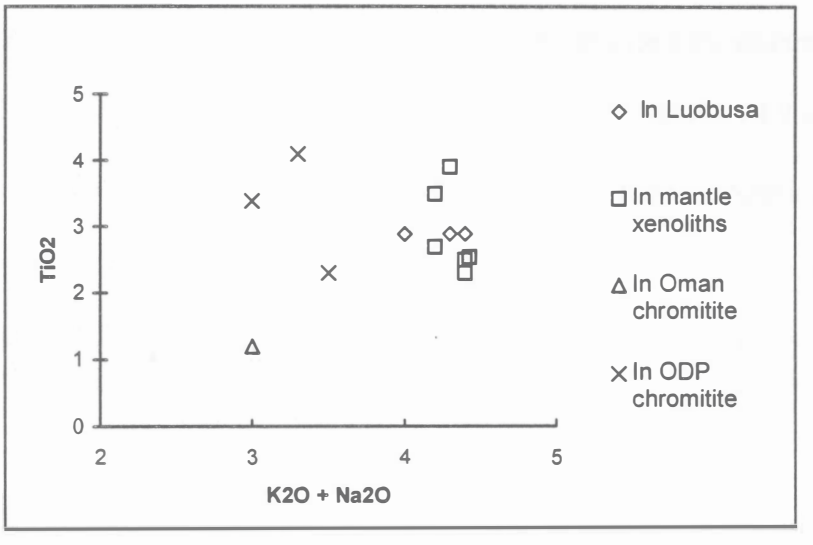

Figure 4-7. Variation in Ti versus total alkalis for amphiboles

This composition of the Luobusa amphiboles is also generally similar to that of amphiboles in chromitites of the Oman ophiolite (Auge, 1987) and of the Hess Deep drilling on ODP Leg 147 (Arai et al., 1997) (Fig. 4-7). However, in the latter two occurrences the amphiboles have higher MgO (17.8-18.1 wt%) and Cr_2O_3 (1.9-3.4 wt%), and lower FeO (2.5-3.5 wt%) than those from Luobusa. The amphiboles from Luobusa have lower Mg/Mg+Fe ratios (0.77-0.78) than the other two occurrences (0.91-0.93), but have similar high incompatible element contents, indicating a similar origin – probably by

melt/rock interaction (Arai et al., 1997).

The amphiboles in the Luobusa chromitites are easily distinguished in high TiO_2 content from alteration amphibole in the Oman chromitite, which never contains more than 0.2 wt% TiO_2 (Auge, 1987).

Biotite

Biotite grains from the Luobusa chromitites are brown in colour, less than 0.8 mm in size. They are sheet-like fragments. One grain was analysed by electron microprobe (Appendix II 7), showing a compositions of SiO_2 37.7 wt%, Al_2O_3 19.7 wt%, TiO_2 1.3 wt%, FeO 15.7 wt%, MgO 11.4 wt%, and K_2O 7.8 wt%. This composition is similar to that of one biotite grain in a diamond from the Prairie Creek lamproite, Arkansas, which has higher FeO (20.7 wt%) and K_2O 9.3 wt%, and lower MgO (8.9 wt%) (see Meyer, 1987).

Phlogopite

The recovered phlogopite grains are dark yellow sheet-like fragments, less than 0.6 mm in size. They are similar in composition to phlogopite inclusions in the Oman chromitite (Auge, 1987) and in the Hess Deep chromitite recovered during ODP Leg 147 (Arai et al., 1997). Their SiO_2 contents range from 38.5-38.8 wt%, TiO_2 2.2-2.6 wt%, Al_2O_3 13.6-13.7 wt%, FeO 7.6-8.3 wt%, MgO 20.4-21.5 wt%, Na_2O 1.4-1.7 wt% and K_2O 6.8-7.5 wt% (Appendix II 7). The MgO and Cr_2O_3 contents are lower and FeO content is higher than the phlogopite in Oman and Hess Deep, but the incompatible

element contents, e.g., Ti and Na are similar (Auge, 1987; Arai et al., 1997). Like the Luobusa amphibole, the phlogopite also has lower Mg/Mg+Fe ratios (0.82-0.84) than similar minerals in the Oman and Hess Deep chromitites (0.96-0.98).

Chlorite

The chlorite grains from the Luobusa chromitite are irregular fragments and pink in colour (Fig. 4-5 B). They can be divided into two groups: one is chromium-rich (Cr_2O_3 2.02-6.27 wt%), and the other is chromium-poor. Except for their Cr_2O_3 contents, the chlorites of the two groups are similar in composition, with SiO_2 31.46-35.72 wt%, Al_2O_3 9.69-16.27 wt%, MgO 32.12-36.66 wt%, and FeO <1 wt% (Appendix II 8).

Serpentine

Serpentine grains are colourless to yellowish. They are irregular fragments. Microscopic study shows they occur as veins cutting chromite grains. The serpentine grains have a narrow range of composition, with SiO_2 34.92-43.93 wt%, MgO 39.05-41.17 wt%, and FeO 3.05-7.30 wt% (Appendix II 9).

Plagioclase $(Ca,Na)(Al,Si)AlSi_2O_8$

Plagioclase occurs as angular fragments, up to 0.7 mm in size. The plagioclase grains display uniform compositions, with An ranging from 28 to 34, Ab from 65 to 72, and Or from 0 to 4 (Appendix II 10). Plagioclase has been described in aluminous chromitites from other ophiolitic complexes (e.g., Leblanc and Violette, 1983). It also

occurs as inclusions in the Oman chromitite where it has a more calcic composition (An = 81-97) (Auge, 1987).

K-feldspar $KAlSi_3O_8$

K-feldspar occurs as colourless, angular fragments, 0.6 mm across. Microprobe analyses reveal some replacement of K by Na and Ba. Ab end-member ranges from 12 to 23, and Or from 77 to 89. The Na_2O and BaO contents are 1.23-2.21 wt% and 0.56-1.39 wt%, respectively (Appendix II 10).

Quartz

Quartz grains recovered from the chromitites are colourless fragments and range in size from 0.3 to 1 mm across. Some very fine strations can be observed on the faces of some crystals. The quartz has been identified by both electron microprobe and X-ray diffraction techniques.

Quartz is a widespread mineral commonly found in association with diamonds. Olivine, orthopyroxene and clinopyroxene in diamond-bearing peridotite from kimberlites in southern Wyoming are locally replaced by quartz and carbonate (McCallum, 1976). Quartz is also intergrown with SiC from kimberlite (Leung et al., 1990). The coesite polymorph has been found enclosed by diamond (Meyer, 1985) and it has been speculated that SiO_2 as stishovite is present in the lower mantle (>670 km) (Knittle and Jeanloz, 1991). The two polymorphs of quartz are transformable with depth.

Alloys

Fe-Si alloy

Irregular fragments of Fe-Si alloys were recovered from the Luobusa chromitites. The Fe-Si grains are black and very shiny, and up to 1 mm in size. All the grains are fractured, and crystal faces are rarely observed. Microprobe analyses (Appendix II 11) show a constant composition with an Fe/Si ratio of approximately 2.76:7 (Fe 44.3-45.4 wt% and Si 55.5-56.1 wt%). These alloys contain less than 1 wt% Au, Sn, Mn, Co and Bi.

Mathez et al. (1995) reported a ferrosilicite (Fe_3Si_7) occurring as an inclusion in SiC from the Yakutia kimberlite which is very similar in composition to those reported here. Another similar occurrence is ferrosilicite (Fe_2Si_3) associated with moissanite in igneous rocks in the Northern Azov region (Gevorkyan, 1969, cited from Lyakhovich, 1980).

Micrometer- to centimeter-sized globules of irregular Fe_xSi_y alloy (including Fe_3Si_7, FeSi, $FeTiSi_2$ and Si) are found in a glassy fulgurite occurring on a morainal ridge in southeastern Michigan. They are suggested to have formed by lightning strikes on the Earth's surface which produced the extremely reduced conditions and high temperatures responsible for formation of these phases (Essene and Fisher, 1986). On the other hand, high pressure and temperature experiments suggest that the Fe_xSi_y alloy is one of the common components of the lower mantle (>670 km).

Ni-Fe alloy

Ni-Fe alloy was only found as irregular patches in pentlandite grains, 0.02-0.05 mm in size (Fig. 4-8). Electron microprobe analyses (Appendix II 11) show the grains have a formula of $Ni_{7.01-7.40}Fe_{2.89-2.60}$.

A similar occurrence was reported in the Kempirsai podiform chromitites where awaruite (Ni_3Fe) occurs as composite grains with Ni sulphides in the serpentine matrix (Melcher et al., 1997). Ni-Fe alloys are common in the Salt Rock chromitites, Southwestern Oregon where they occur as thin veins or as irregular patches and are exclusively associated with cracks in the chromitites (Stockman and Hlava, 1984).

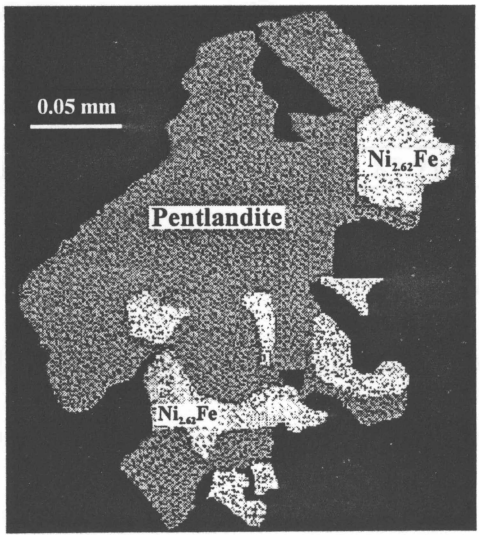

Figure 4-8. Intergrowth of pentlandite and Ni-Fe alloy in the Luobusa chromitites

Cr-C alloy

Acicular crystals of Cr-C were recovered from the Luobusa chromitites. They are steel grey in colour with well-developed crystallographic faces (Fig. 4-9 A). Two grains were mounted in epoxy resin, machine-polished, and analysed by electron microprobe. The results in which carbon was not analysed (Table 4-2) show that they contain around 80 wt% Cr, which approximately fits the formula Cr-C.

Although native chromium has been reported in the Luobusa chromitites (Fang and Bai, 1981; Yang and Song, 1982; Zhang et al., 1996), these grains could not be native chromium, because they have distinctive Cr contents from the control sample of pure Cr metal (Table 4-2).

Table 4-2. Electron microprobe analysis of Cr-C alloy

wt%	Standard Cr metal	1	2	3
Cr	100.78	79.69	80.03	76.71
Ti		0.16	0.13	0.00
Fe		1.92	1.66	1.57
Ni		1.59	1.40	1.40
Total	100.78	83.36	83.21	79.68

To further confirm the presence of carbon in the two grains, pure Cr metal and the two grains were reanalysed. The results show that pure Cr metal has only a small carbon peak which is believed due to the coated carbon, whereas the two grains have significant higher carbon peaks. A rutile crystal in the same thin section, which is believed not to contain any carbon, was also analysed for carbon content. Compared to the pure Cr metal

standard and the two Cr-C crystals, the rutile has a carbon peak much closer to that of pure Cr, rather than the two Cr-C crystals, confirming that these grains have more carbon than either the Cr standard or the rutile grain. It is thus concluded that the two grains are Cr-C mineral.

Au-Ag alloy

Au-Ag grains from Luobusa are irregular in shape and range in size from 0.2 mm to 0.4 mm. They are yellow in colour. Electron microprobe analyses show Au 14-17 wt%, Ag 86-82 wt% (Table 4-3).

Table 4-3. Electron microprobe analysis of Au-Ag alloy

wt%	1	2	3
Ag	16.48	16.79	13.93
Au	81.82	83.53	86.16
Total	98.30	100.32	100.08

SiC (moissanite)

Numerous crystals and crystal fragments of SiC were recovered from the Luobusa chromitites. These crystals are transparent (if not deeply coloured) and gem-like with a strong, brilliant adamantine luster. The colour ranges from colourless to grey-blue to pale green to yellow to yellow-blue to bluish-green to blue-black (Fig. 4-10). Many SiC grains are colour-zoned with one colour grading into another colour gradually. The colour variations are probably caused by small amounts of impurities such as N (Mathez, et al., 1995) and Al (Leung, et al., 1996).

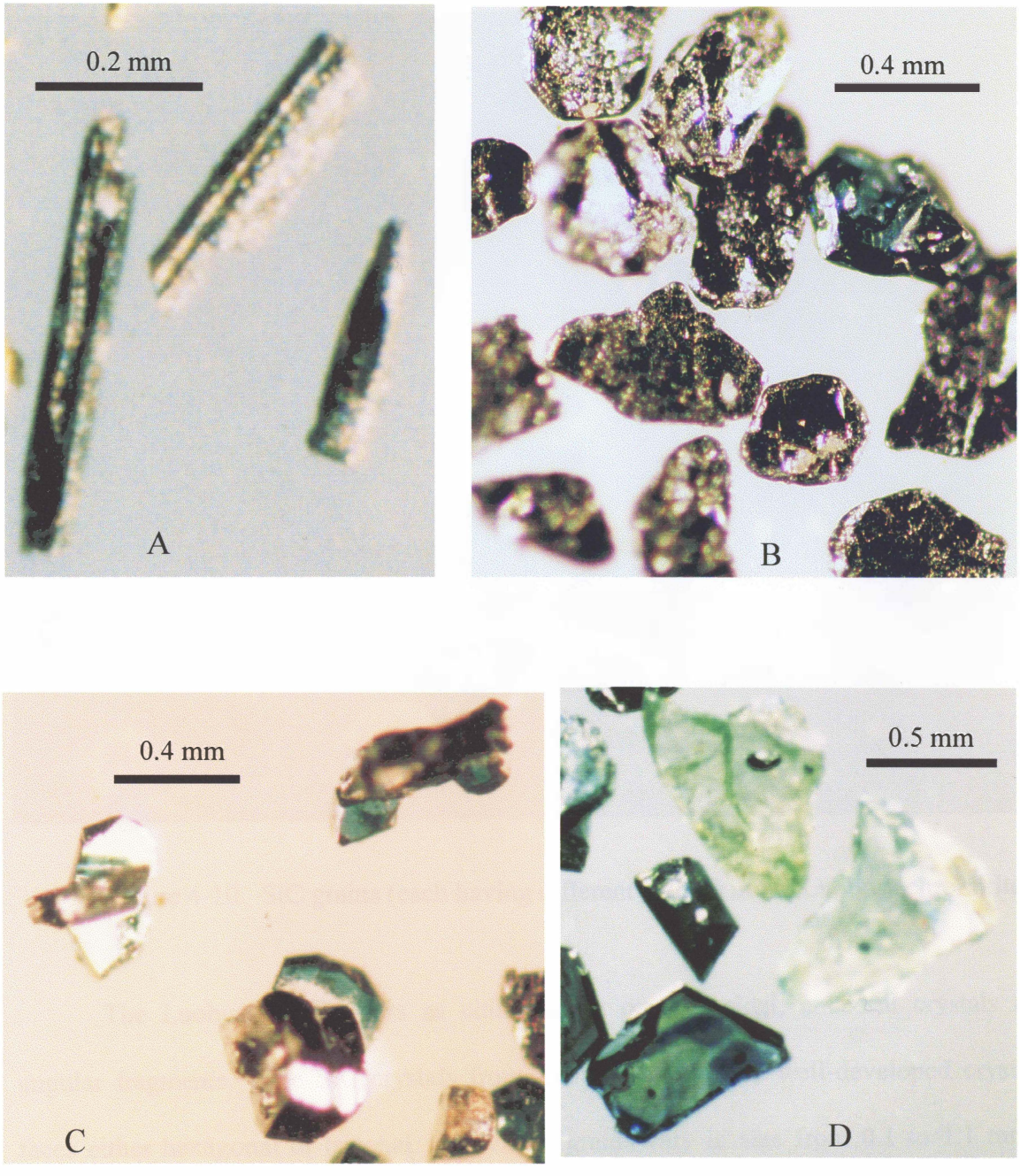

Figure 4-9. A - Cr-C alloy; B - graphite; C - twinned SiC crystals; D - SiC with dark inclusions (possibly native Si) in the Luobusa chromitites, Tibet

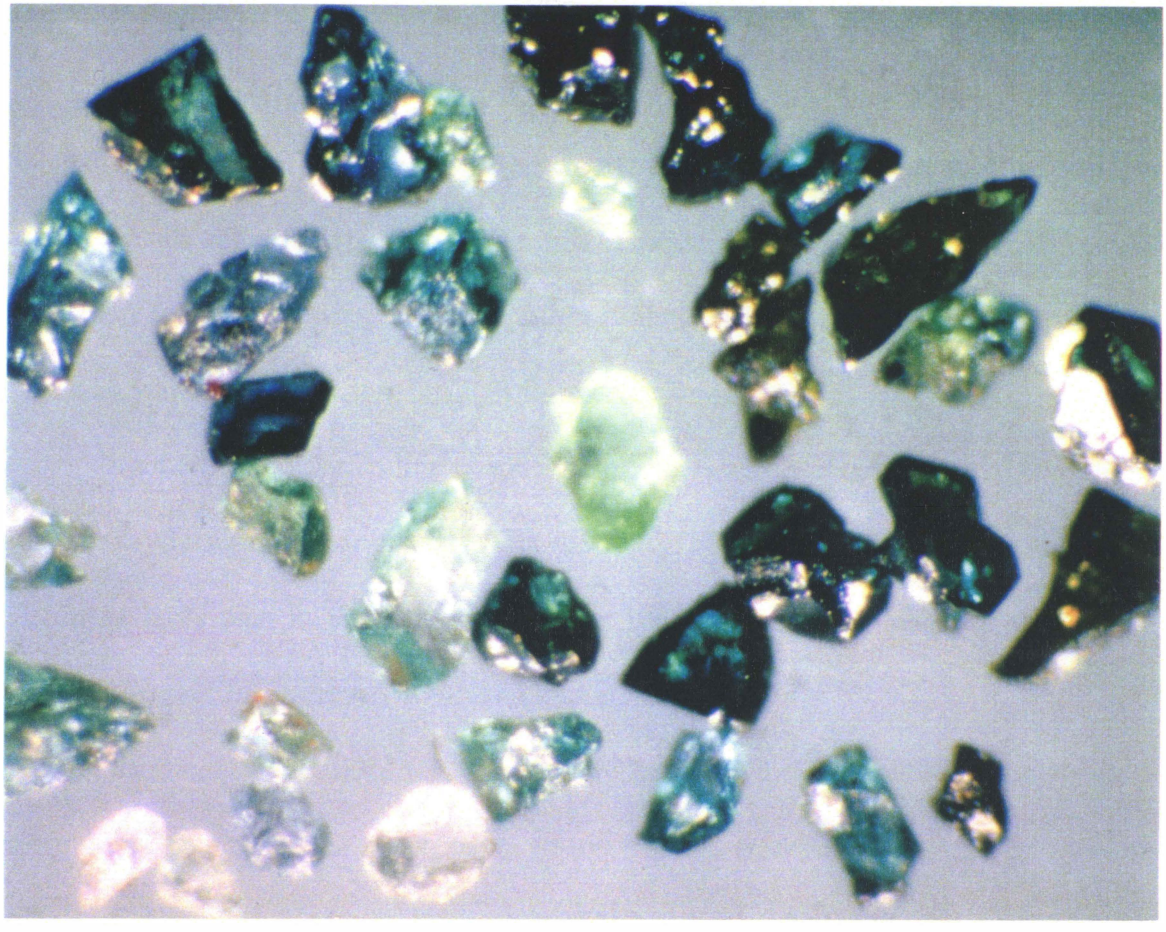

Figure 4-10. SiC grains (each having different colour) in the Luobusa chromitites

The Luobusa SiC occurs as either single or pinacoidal, euhedral crystals or angular fragments. The SiC crystals from Luobusa show very well-developed crystal faces either hexagonal or trigonal. Individual grains vary in size from 0.1 to 1.1 mm. The euhedral crystals exhibit well-formed faces on all sides, and the angular fragments commonly display at least one side that is a well-formed crystal face. Syntactic

intergrowths of different SiC crystal forms are common, either on or across the pinacoidal face. Two pinacoidal crystals have been found to decussate (i.e. *to cross in the form of an X*) with each other (Fig. 4-9 C).

SiC from Luobusa was confirmed by both electron microprobe and single crystal X-ray diffraction analysis. The microprobe analyses were performed on polished surfaces of the crystals mounted in epoxy. The Si/C atomic ratio is very close to 1:1. X-ray diffraction analysis on a single idiomorphic crystal gives cell dimensions of a = 3.083Å, b = 3.083Å and c = 75.5Å, being the 30H form of the mineral.

Minute oval or needle-like opaque inclusions were observed in some idiomorphic granular crystals and planar crystals (Fig. 4-9 D). The presence of dark-coloured native silicon as inclusions in the Luobusa SiC has been confirmed by electron microprobe analysis (Wen-Ji Bai, personal communication, 1998).

Occasionally, euhedral SiC crystals are intergrown with a white to pale-yellow mineral. One such grain was mounted on carbon tape and analysed by electron microprobe (Table 4-4). It consists mainly of SiO_2 38 wt%, Al_2O_3 28 wt%, CaO 40 wt%, and MgO 2 wt% (Total 108 wt%), an analysis which closely fits the composition of gehlenite.

One deep blue, broken SiC crystal has a crudely rectangular cavity, half of which is filled by a white material. This material is considered to be a solid mineral inclusion, rather than decrepitated material. This unpolished grain was also mounted on carbon tape and analyzed by electron microprobe. It has a composition of SiO_2 = 24 wt%, Al_2O_3 = 29 wt%, CaO = 33 wt%, and MgO = 1 wt% (Total 87 wt%) (table 4-4). This composition is

similar to that of the intergrowths described above, which are believed to be gehlenite ($Ca_2Al(AlSi)O_7$).

Table 4-4. Gehlenite intergrown with and enclosed in SiC

wt%	ING	INC	INC	INC	Gehlenite*	
SiO_2	38.4	19.9	22.7	23.7	22.9	21.9
Al_2O_3	28.2	26.0	29.7	29.2	32.1	37.2
FeO					3.0	
MgO	1.7	0.7	0.0	0.9	0.85	
CaO	39.7	30.4	30.0	33.1	41.3	40.9
Total	108.0	77.0	82.4	86.9	100.1	100.0
Si	1.788	0.166	0.174	0.174		
Al	1.549	0.256	0.269	0.254		
Mg	0.116	0.009	0.000	0.009		
Ca	1.978	0.272	0.247	0.261		
O	8.000	1.000	1.000	1.000		

Note: ING - intergrowth; INC - inclusion. * from Anthony, et al., 1990.

Occurrence of SiC in nature

Increasingly SiC has been documented as a naturally-occurring mineral closely associated with diamond-bearing rocks. Moissanite inclusions in diamonds have been found from many locations, e.g., the Monastery Mine in South Africa (Moore et al., 1986; Moore and Gurney, 1989), the Sloan diatreme in North America (Otter and Gurney, 1989), the Argyle lamproite in Western Australia (Jaques et al., 1989), and the Fuxian kimberlite in China (Leung et al., 1990, 1996; Leung, 1990). SiC has also been reported as an accessory mineral in diamond-bearing rocks from the Mirny and Aykhal kimberlite pipes in Yakutia, Russia (Mathez et al., 1995; Leung et al., 1996), the Mengyin kimberlite pipes of Shandong, China (He, 1987), and the Kimberley kimberlite, South Africa (Leung et al., 1996). A ß-SiC intergrowth with diamond and graphite was described in mineral

pitch in Turkestan, Central Asia (Novgorodova et al., 1984). The recent work on SiC from the Fuxian (Leung et al., 1990; 1996) and Yakutia (Mathez et al., 1995) diamond-bearing kimberlites has convincingly demonstrated the existence of natural SiC, and established its very close relationship with diamond.

SiC and diamond both are carbon-bearing and share a common atomic structure. They have similar chemical/physical properties (i.e. similar tetrahedrally oriented sp^3 hybrid bonds and identical glide planes) (Leung et al., 1996). These facts indicate that diamond has a much closer relationship with SiC than with any other indicator minerals traditionally used in tracing for diamond deposits. SiC is a more common accessory mineral in diamond-bearing rocks than was previously thought (Mathez, et al., 1995; Leung, 1990; Leung, et al., 1990, 1996).

The possible sources of contamination for SiC are carborundum fragments used in polishing rock samples, drilling equipment bonded with euhedral carborundum crystals used in mining operations, and pollution by industrial waste (Milton and Vitaliano, 1985). The SiC from Luobusa is believed to be natural because the possible contamination sources were eliminated by careful sampling and processing as described in chapter 2. The SiC crystals from Luobusa exhibit a wide range of colour and are relatively large, whereas most synthetic SiC is blue and smaller in grain size. The presence of native silicon and gehlenite inclusions in the Luobusa SiC also argue for a natural origin.

Natural SiC occurs in hexagonal and trigonal polyforms known as α-SiC, as well as cubic polyform known as ß-SiC. The hexagonal form of SiC is termed moissanite (Kunz, 1905; Leung, 1990), whereas no mineral name has been given for the cubic form.

Cubic SiC has been recovered in the Luobusa chromitites during previous work (Yang et al., 1986). None of the analysed grains in this study show cubic structure; the chemical formula SiC refers to α-SiC in this thesis.

Native elements

Native Si

Native Si is found only as inclusions in SiC crystals. They are oval in shape and black in colour (Fig. 4-9 D). Microprobe analyses show they consist of 100 wt% silicon (Wen-Ji Bai, Personal communication, 1998).

Graphite

The Luobusa graphite exhibits tabular prisms, 0.1 to 0.7 mm in size (Fig. 4-9 B). The grains do not show sharp-edged features, and most of the corners of the crystals are rounded, but the hexagonal outline is clearly recognized. The rounded crystal corners are most likely to have resulted from abrasion during the separation processes, due to their softness. Electron microprobe analyses show that they consist of pure carbon.

Oxides

Chromite

On average, chromite makes up 20-90% of the chromitite orebodies which have a range of textures including massive, disseminated, nodular and brecciated. It occurs

mainly as framework grains and occasionally as inclusions in interstitial silicate minerals, particularly olivine and chrome diopside. Framework chromite grains are mainly 1-5 mm across and are typically anhedral, whereas inclusions in silicate minerals are usually less than 0.02 mm across and are subhedral or euhedral.

The Luobusa chromites fall mainly into three compositional groups based on their cr-numbers (100Cr/(Cr+Al)) and mg-numbers (100Mg/(Mg+Fe)) (Fig. 4-11). Most of the analysed grains have cr-numbers between 77 and 84 and mg-numbers between 62 and 76 (group A on Fig. 4-11). Some euhedral grains are richer in both Al and Fe (mg-numbers 49.4-53.2, cr-numbers 69.8-71.4) (group B on Fig. 4-11), and some have relatively high Cr and high Fe (mg-numbers 37.5-48.3, cr-numbers 78.3-82.8) (group C on Fig. 4-11).

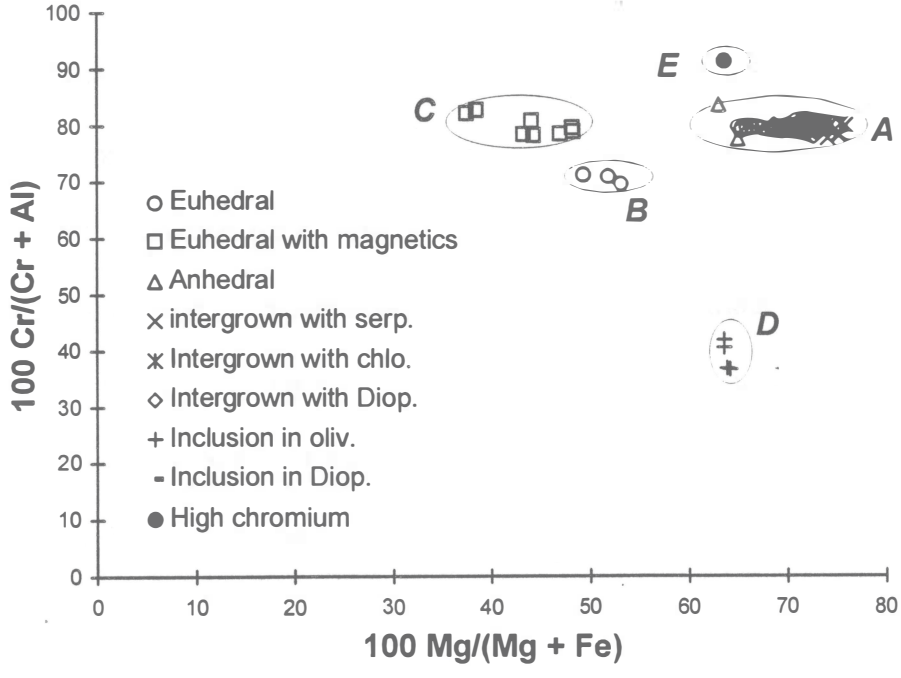

Figure 4-11. Cr# versus Mg# of the chromite in the Luobusa chromitites

Group B and C chromites are common in alpine chromitites, e.g., in Kempirsai (Melcher et al., 1997) and south-western Oregon (Stockman and Hlava, 1984). These Fe-rich chromites are alteration products of primary chromites (Melcher et al., 1997; Stockman and Hlava, 1984).

Chromite inclusions in silicate minerals fall into two compositional groups. A high Cr variety (mg-numbers 68.7-70.1 and cr-numbers 78.5-80.4), which corresponds to group A on Figure 4-11, occurs in highly magnesian olivine (Fo 96.8-97.5), whereas an aluminous variety (mg-numbers 63.6-64.2 and cr-numbers 36.6-41.9) (group D on Fig. 4-11) occurs in less magnesian olivine (Fo = 91.3-92.7). A few grains are extremely rich in chromium (Cr_2O_3 up to 68.7 wt%). These have high cr-number (91.5), and low mg-number (63.7), low $Fe^{3+}/\sum(Cr+Al+Fe^{3+})$ (0.4) and low Ti contents (group E on Fig. 4-11) (Appendix II 12).

Most of the chromites have TiO_2 contents greater than 0.2 wt%, distinctly higher than residual chromites from the host harzburgite (Zhou 1995). The high cr-numbers of the chromites also distinguish them from the residue chromites (Zhou, 1995).

All of the chromite grains are compositionally uniform without detectable zoning. Most are similar to those of typical podiform chromites. Group A chromites have relatively uniform cr-numbers over a range of mg-numbers (Fig. 4-11). Dick and Bullen (1984) suggested that variations in mg-numbers of chromites reflect the partition coefficients of Mg and Fe between chromite and olivine. However, the massive chromitites of Luobusa have only small quantities of silicate minerals, thus exchange of Mg and Fe^{+2} between chromite and olivine must have been very limited (Auge, 1987). It

appears more likely that the variations in mg-number observed in the Luobusa chromitites reflect subsolidus exchange between $FeCr_2O_4$ and $MgCr_2O_4$.

Corundum Al_2O_3

Corundum grains occur as irregular, colourless fragments which are 0.6 mm across in size. Electron microprobe analyses (Table 4-5) show they consist essentially of pure Al_2O_3, with minor TiO_2 (0.77-1.13 wt%) and MgO (0.16-0.23 wt%).

Table 4-5. Microprobe analysis of corundum from the Luobusa chromitite

wt%	IV-45	IV-46	IV-58
SiO_2	0.08	0.13	0.06
TiO_2	1.13	1.09	0.77
Al_2O_3	99.76	99.75	99.97
FeO	0.07	0.00	0.00
MgO	0.23	0.16	0.22
CaO	0.02	0.00	0.02
NiO	0.07	0.17	0.00
BaO	0.02	0.08	0.07
Total	101.38	101.38	101.11

Rutile TiO_2

Rutile grains are generally small, rarely exceeding 0.5 mm in length. They occur either as euhedral crystals with well-developed pyramidal termination, or as slender prisms and prismatic fragments. 'Knee-shaped' twins are sometimes present (Fig. 4-3 B). The rutile grains are blood red in colour and contain very minor amounts of FeO, BaO and Cr_2O_3 (Table 4-6). Some crystals are attached to chromite grains (Fig. 4-3 C).

Table 4-6. Mineral chemistry of rutile from the Luobusa chromitite

wt%	1	2	3	4	IV18	IV19	IV20	IV21	IV22	IV24	IV25
TiO_2	99.3	95.8	99.5	96.1	96.0	95.1	95.7	95.3	95.0	94.6	94.8
FeO	0.0	0.6	0.5	0.3	0.3	0.3	0.5	0.5	0.5	0.5	0.8
SiO_2	0.0	0.0	0.0	0.0	0.2	0.2	0.2	0.2	0.1	0.2	0.1
BaO	0.0	0.0	0.0	0.0	0.3	0.5	0.2	0.6	0.4	1.4	0.2
Total	99.3	96.4	99.9	96.4	96.7	96.2	96.5	96.7	96.1	96.6	96.0

Sulphide Minerals

A variety of sulphide minerals are present in the chromitites, including pyrite (FeS_2), arsenopyrite (FeAsS), pentlandite ($Fe_{5.5}Ni_{3.1}S_8$), galena (PbS), matraite (ZnS), and sphalerite (ZnS). Typically the sulphide minerals occur as discrete euhedral crystals.

Pyrite is the most abundant variety and it forms cubic and pyritohedral crystals, 0.1 to 0.7 mm in size (Fig. 4-5 A). A few anhedral grains are also present. The composition is close to the ideal formula (FeS_2) with no apparent zoning but with minor cobalt, zinc, and gold substituting for iron. Euhedral grains contain 1.07-4.28 wt% arsenic; whereas anhedral ones have much lower arsenic contents (0.1-0.4 wt%) (Appendix II 13).

Arsenopyrite grains are columnar in form and steel grey in colour. The grain size is up to 0.5 × 1.25 mm (Fig. 4-5 C). Minor Co, Zn and Au may substitute for iron, but the composition is close to the formula FeAsS (Appendix II 13).

Pentlandite forms anhedral grains about 0.2 mm across. One grain contains

patches of Fe-Ni alloy (Fig. 4-8). Pentlandite analyses show an iron-to-nickel ratio of 5.5:3.1, and formula $(Fe_{5.56}Ni_{3.10}Co_{0.11})_{8.77}\ S_8$ which is close to the standard formula $(FeNi)_9S_8$ (Appendix II 13).

Galena occurs in crudely columnar grains 0.4-0.6 by 0.2-0.3 mm in size. Electron microprobe analyses indicate that the galena is very nearly pure PbS. One grain contains patches of sphalerite (ZnS) and dolomite (Fig. 4-12) (Appendix II 13).

Sphalerite occurs not only in galena but also as discrete colourless cubic crystals. X-ray diffraction studies revealed the presence of both matraite and cubic sphalerite. One grain shows cubic structure and possibly has pyrite on its surface. The matraite is an

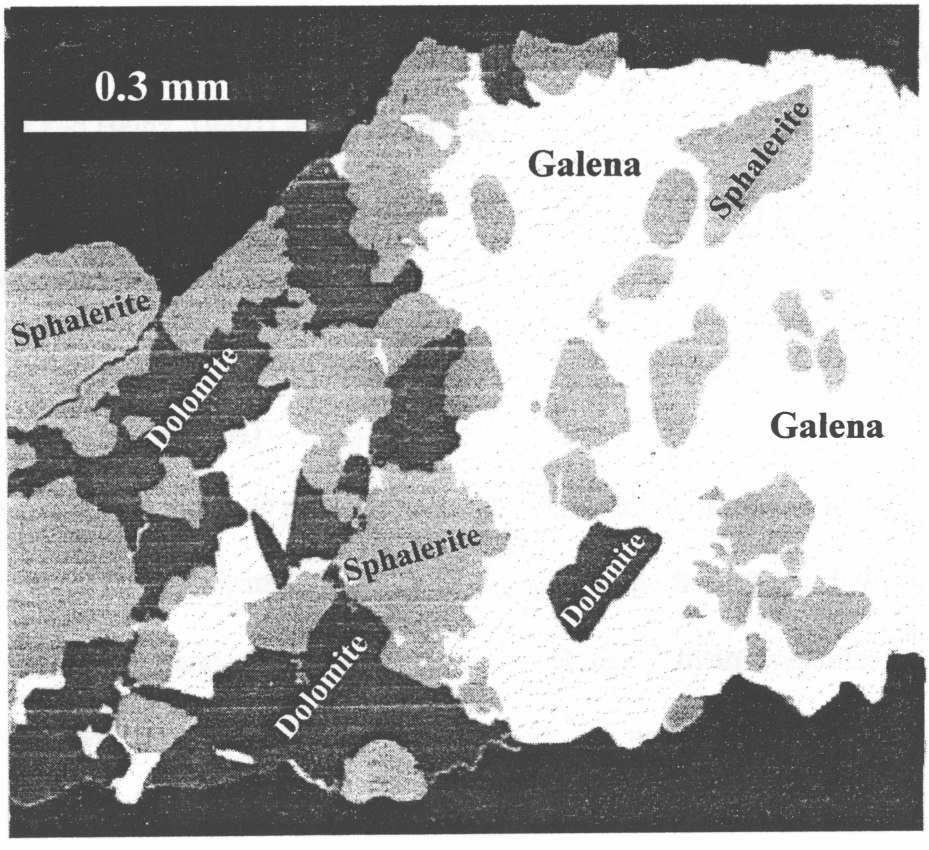

Figure 4-12. Intergrowth of galena, sphalerite and dolomite from the Luobusa chromitites

unusual form of ZnS formed over a temperature range of 600-1200°C (T. Stanley Cameron, personal communication, 1998). Sphalerite is a common mineral in hydrothermal metalliferous veins and in contact metamorphic rocks (Mange and Maurer, 1989).

Sulphates

Celestite $SrSO_4$

Celestite occurs as colourless, euhedral, prismatic crystals, about 0.4 mm across in size. Its composition is close to the ideal formula with minor Ba and Ca. Like sphalerite, celestite has an affinity to some carbonates. Celestite commonly occurs in hydrothermal veins (Maria and Heinz, 1989) (Appendix II 14).

Phosphates

Apatite $Ca_4(PO_4)_3(F,Cl,OH)$

Apatite occurs either as prismatic crystals with smooth or curved termination and edges or as irregular fragments (Fig. 4-5 D). Crystals range from 0.2 to 0.9 mm in size and are colourless to greyish pink. They are most likely hydroxyapatites. Electron microprobe analyses show very low Cl contents, and no F was detected (Appendix II 14). Apatite is found in almost all igneous rocks as an early-formed accessory mineral. It also occurs commonly in high temperature hydrothermal veins and in regional and contact

metamorphic rocks (Mason and Berry, 1968). Apatite occurs often with carbonates (Deer et al., 1995).

Carbonates

Dolomite

Dolomite was observed only in association with galena and sphalerite (Fig. 4-12). Electron microprobe analyses show the dolomite has a Ca/Mg ratio close to 1:1 (Appendix II 14).

Calcite

Calcite occurs as irregular, colourless fragments about 0.4 mm in size. Electron microprobe data indicate a composition of pure CaO (54.77-55.48 wt%), with only traces of MgO. Carbon was not analysed (Appendix II 14).

Granite sample

As mentioned in the previous chapter, 200 kg of Gangdese granite was collected and processed as a blank sample. Plagioclase, K-feldspar, quartz and garnet were recovered from this granite sample. These minerals were mounted in epoxy and polished, then analysed by electron microprobe. Electron microprobe data show they have distinct chemistry from those recovered from the Luobusa chromitites (Fig. 4-13).

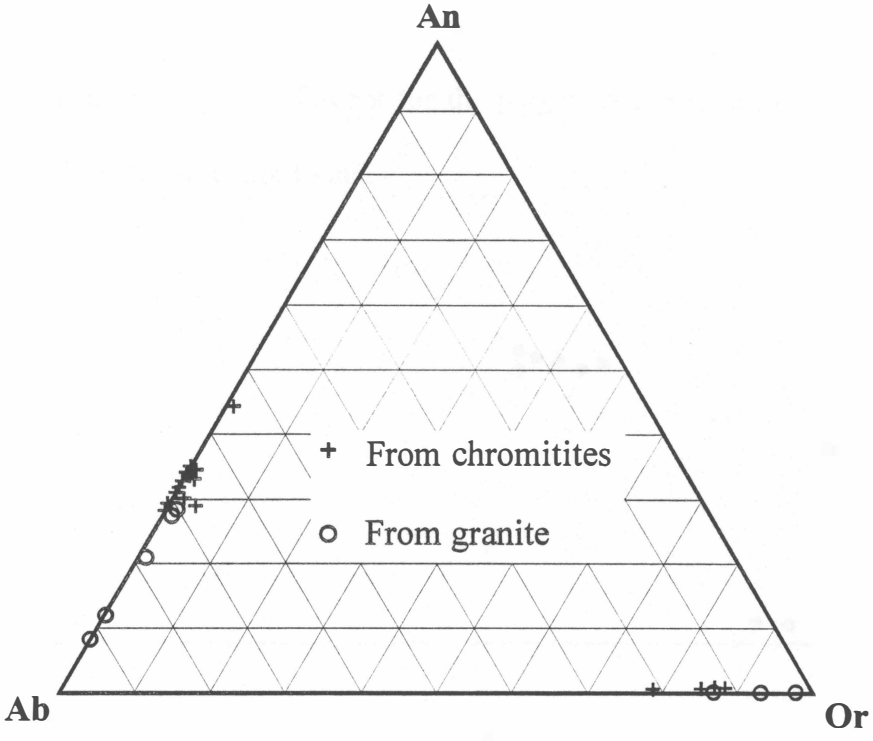

Figure 4-13. An - Ab - Or diagram of the plagioclase and K-feldspar from the Luobusa chromitites and the Gangdese granite

Plagioclase from the granite is more sodic (Ab_{8-29}) than that from the chromitites (Fig. 4-13). K-feldspar is higher in Or (88-96.5) and lower in Ab (3.5-12) than that in the Luobusa chromitites. All the garnets recovered from the granite are the Fe-Mn variety. They have a distinct crystal size and colour. Garnets from the granite are 1-2 mm across, and yellow to brown in colour, whereas those from the Luobusa chromitite are euhedral, <0.3 mm across, and wine-red in colour. The garnet from the granite contains lower MgO (0.9-1.2 wt%), CaO (0.1-0.5 wt%) and higher MnO (16.5-17.6 wt%), FeO (24.5-25.4 wt%) than that from the Luobusa chromitites (Fig. 4-14) (Appendix II 15). Quartz from the two rock types is indistinguishable.

Most of mineral fractions of the granite sample have been carefully examined under binocular microscope. Except for the plagioclase, K-feldspar, garnet and quartz, other mineral phases were not found.

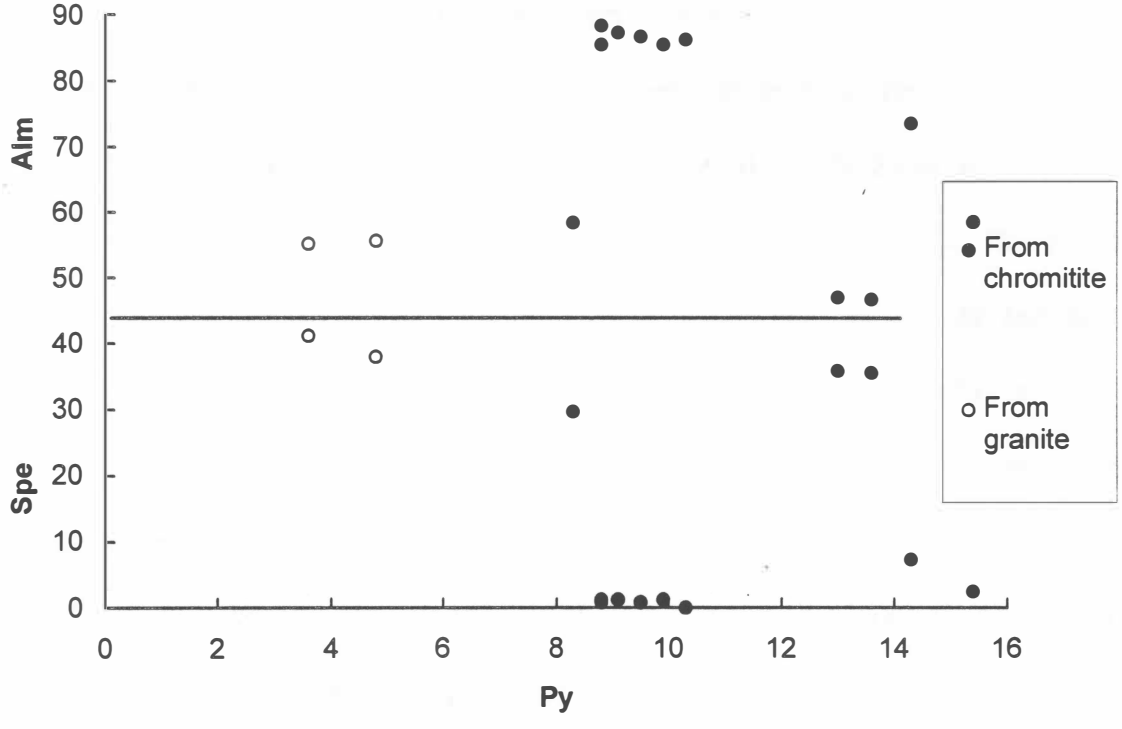

Figure 4-14. Py - Alm and Py - Spe diagrams of the garnet from the Luobusa chromitites and the Gandese granite

CHAPTER 5. DISCUSSION

5-1. Formation of the Luobusa chromitites

5-1-1. Melt - rock interaction in a suprasubduction zone environment

It is widely believed that podiform chromitites in ophiolites form in suprasubduction zone environments, and that melt/mantle rock interaction plays an important role in their formation (Zhou 1995; Zhou et al., 1996; Zhou and Robinson, 1997; Roberts, 1992; Leblanc, 1995; Orberger et al., 1995; Melcher et al., 1997). This melt/rock reaction mechanism for chromitite crystallization requires the melt and mantle rock to be out of equilibrium, i.e., they were derived from distinctively different sources (Zhou, 1995). Suprasubduction zone environments are ideal sites to satisfy this requirement. Dehydration of hydrous minerals from subducted material produces fluid phases (Wilson, 1989; Kesson and Ringwood, 1989). Upward migration of these fluids from the subducted slab triggers partial melting in overlying mantle peridotites. When ascending up to the depth where chromitite crystallized, these melts, whose composition may vary from tholeiitic to boninitic (Robinson et al., 1983), become considerably out of equilibrium with the host peridotites, thus facilitating reactions between the melts and peridotites to form the podiform chromitite.

On the basis of primary hydrous mineral inclusions in chromite from ophiolitic chromitites, Lorand and Ceuleneer (1989), Ferrario and Garuti (1990) and Melcher et al. (1997) suggest that hydrous fluids are involved in podiform chromitite formation. The

mineral chemistry indicates hydrous minerals, such as amphibole, biotite, and phlogopite, are original phases in the Luobusa chromitites. The presence of these hydrous silicates, and of olivine replacing orthopyroxene (Zhou et al., 1996), indicate that fluids were involved during formation of the Luobusa chromitite in a suprasubduction zone environment (Melcher et al., 1997; Orberger et al., 1995).

5-1-2. fO_2 of the Luobusa chromitite formation

Chromitite forms under variable oxygen fugacity conditions. Experimental studies from 'dry' melts show that chromitite forms at fO_2 around ±1 log units from the FMQ buffer and temperatures of 1250±100°C (Murck and Campbell, 1986; Roeder and Reynolds, 1991). Calculations from chromite-olivine-orthopyroxene equilibria demonstrate that the oxygen fugacities for most of the Kempirsai podiform massive chromitites are around 1 log units above FMQ at 1000-1200°C (Melcher et al. 1997). Some of the podiform chromitites in the Nan Uttaradit ophiolite complex of Thailand record an oxygen fugacity around the FMQ buffer (Orberger et al., 1995). However, occurrences of podiform chromitite forming under reducing or strongly reduced conditions are frequently reported, e.g., the Rae Nan and Mae Charim massive chromitites in the Nan Uttaradit ophiolite complex of Thailand which contains graphite (Orberger et al., 1995); the Cyprus chromitite with pure hydrogen inclusions (McElduff, 1989); and the Kempirsai amphibole-chromite veins probably carrying hydrogen in the chromite lattice (Melcher et al., 1997).

One group of chromites in the Luobusa chromitites is extremely high in chromium (Cr_2O_3 up to 68.7 wt%), with a high cr-number (91.5), and low $Fe^{3+}/(Cr+Al+Fe^{3+})$ ratio (0.4) and TiO_2 content. This group of chromites is very similar to those reported in the Rae Nan and Mae Charim massive ophiolitic chromitites, which have high Cr_2O_3 contents (up to 68.1 wt%) (cr-number up to 95) and are almost devoid of Ti and ferric iron (Orberger et al., 1995). On the basis of the very low $Fe^{3+}/(Cr+Al+Fe^{3+})$ ratio and the presence of a graphite matrix and graphite inclusions in the chromitites, Orberger et al. (1995) suggest that the Mae Charim chromitite formed under strongly reducing conditions. It may have originated in a source which incorporated carbon-rich, reducing fluids.

The unusually high Cr_2O_3 contents of some Luobusa chromites are above the stoichiometric 67.9 wt% necessary to completely fill the octahedral sites of chromite (Orberger et al., 1995). The study of chromites from meteorites and diamonds suggests that above this threshold, tetrahedrally coordinated divalent chromium should be present (Bunch and Olsen, 1975; Meyer, 1975) requiring strongly reduced conditions, at least 3-4 log unit below FMQ (Roeder and Reynolds, 1991). The extremely high Cr_2O_3 contents of some chromites and reports of Cr^{+2}- bearing chromite from the Luobusa chromitites (Bai et al., 1993) signify that some of the Luobusa chromites formed under strongly reducing conditions.

5-1-3. Paragenesis of the minerals in the Luobusa chromitites

On the basis of the descriptions in chapter 4, all the recovered minerals are tentatively grouped into four series (see the table below).

group 1	group 2	group 3	group 4
primary phase	*serpentine - related*	*secondary phase*	*UHP*
chromite	chlorite	zircon	diamond
olivine	serpentine	rutile	SiC
enstatite	sulphides	sphene	native Si
Cr-diopside	calcite	apatite	Si-Fe alloy
	dolomite	corundum	Cr-C alloy
	celestite	sillimanite	
	uvarovite	plagioclase	
	almandine	K-feldspar	
	wollastonite	biotite	
	graphite	amphibole	
	Fe-Ni alloy	phlogopite	
	Au-Ag alloy		

The group 1 minerals are the primary phases of the Luobusa chromitites. They are typical components of podiform chromitites.

Textural study in thin sections shows that the Luobusa chromitites did not undergo high/ultrahigh pressure metamorphism. This is consistent with the overall field relationships and the presence of unmetamorphised rock in the melange unit and unmetamorphised dykes cutting the peridotites. Therefore the Luobusa chromitites have never subducted into the deep mantle to depths equivalent to the diamond stability field; they formed in the upper mantle around 15 km deep as did most podiform chromitites worldwide.

The chromite mineral chemistry is consistent with previous work by Zhou (1995), which suggests that the Luobusa chromitites crystallized from a boninitic melt under high-temperature conditions.

Study of the Kempirsai chromitites by Melcher et al. (1997) suggests that they formed at 1000°C and fO_2 1-2 log units above FMQ, and at 1200°C and fO_2 0.5-1 log units above FMQ, indicating that reduced conditions require higher temperatures. An experimental temperature of 1250±100°C at fO_2 around ±1 log units from the FMQ buffer has been calculated for chromitite formation (Roeder and Reynolds, 1991). Some of the chromites in the Luobusa chromitites are believed to have formed under highly reducing conditions. It is therefore suggested that the minimum temperature for the formation of some Luobusa chromitites is ~1250°C. Klingenberg and Kushiro (1996) demonstrated that at 5 kbar (~15 km depth) boninitic melts contain 10-19 wt% MgO. In Figure 5-1, such boninitic melts have a temperature range from 1300 - 1500°C. The Luobusa chromitites have crystallized from high magnesian boninitic melts at around 15 km depth, therefore their crystallization temperatures are probably less than 1300 - 1400°C.

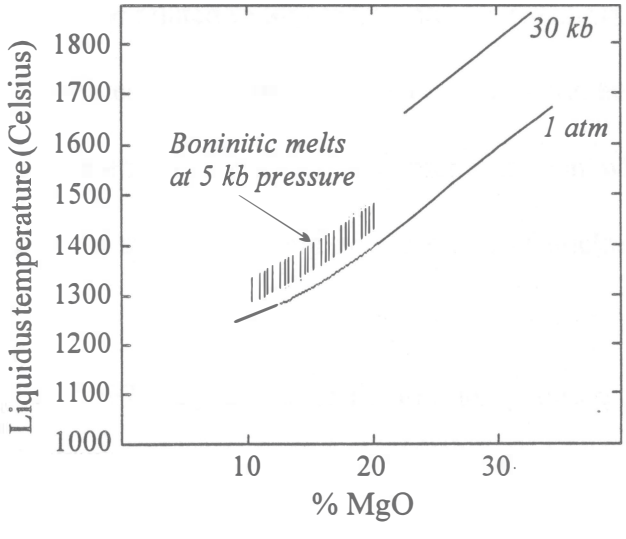

Figure 5-1. Temperature versus MgO content of magmas at 1 atm and 30 kb (from Figure 29.2, in Nisbet, 1982)

The group 2 minerals probably formed during serpentinization of the Luobusa chromitites. Fe-Ni alloys have been reported from other ultramafic rocks around the world (Taylor, et al., 1995), and most of them are believed to form by serpentinization processes (Melcher et al., 1997). The Luobusa Fe-Ni alloy occurs within pentlandite, whereas sulphides from this study are observed only in serpentine veinlets. Chlorite also occur as veins in the Luobusa chromites. The above textural characteristics indicate that these minerals have formed by serpentinization under the conditions of low temperatures and low sulphur and oxygen fugacities.

The wollastonite in the Luobusa chromitites is a low-temperature mineral and uvarovite is a very common alteration mineral in ultramafic rocks. The formation of the uvarovite grains in the Luobusa may be related to the presence of wollastonite and carbonate (Deer et al., 1995; Melcher et al., 1997). Carbonate minerals were also found as veins in the Luobusa chromitite (Zhou et al., 1997), and along with celestite and almandine, are believed to be related to low-temperature serpentinization.

Some of the chromites have high chromium and iron contents (group C in Fig. 4-11), possibly reflecting re-equilibration during serpentinization which increases Cr, Ti and Fe^{3+}, and decreases Al and Mg in primary chromites (Stockman and Hlava, 1984; Melcher et al., 1997).

Melcher et al. (1997) suggest a formation temperature for the chlorite and uvarovite in the Kempirsai chomitites of 400-500°C. The group 2 phases might have formed under similar conditions.

The occurrence of fluids/melts enriched in Na, K, Ti, and P, and their interaction with peridotites in the upper mantle have been well-documented (Ringwood, 1990; Kesson and Ringwood, 1989). During the melt or fluid - rock interaction, compatible elements, such as Cr, and incompatible elements (Na, Ti, etc.) in the melts are enriched, resulting in the precipitation of both chromites and group 3 minerals, e.g. zircon, apatite, rutile, sphene, amphibole, and phlogopite (Arai et al., 1997), and probably plagioclase and K-feldspar.

Melts characterized by high contents of silica, alumina and volatile components are widespread in sub-oceanic mantle (Schiano and Clocchiatti, 1994). Corundum and sillimanite in the Luobusa chromitites may have been derived from such melts during or after formation of the chromitites, and therefore are assigned into group 3.

Study of the secondary fluid/melt inclusions and their micrometer-size daughter minerals (e.g., rutile, amphibole, ilmenite) in olivine and pyroxene in the ultramafic xenoliths, indicates that the trapping conditions of these inclusions are 0.7- 1.4 Gpa at 1250°C (Schiano and Clocchiatti, 1994). Similar temperatures and pressures may apply to the group 3 minerals in the Luobusa chromitites. These conditions are compatible with those of chromitite formation.

The group 4 phases have a paragenesis clearly different from their host chromitites. It is commonly accepted that diamonds, SiC, Si-Fe and Cr-C alloys are

highly reduced phases, below the iron-wüstite buffer (Fig. 5-2). They form under high temperature and pressure conditions in the diamond stability field (Fig. 5-3).

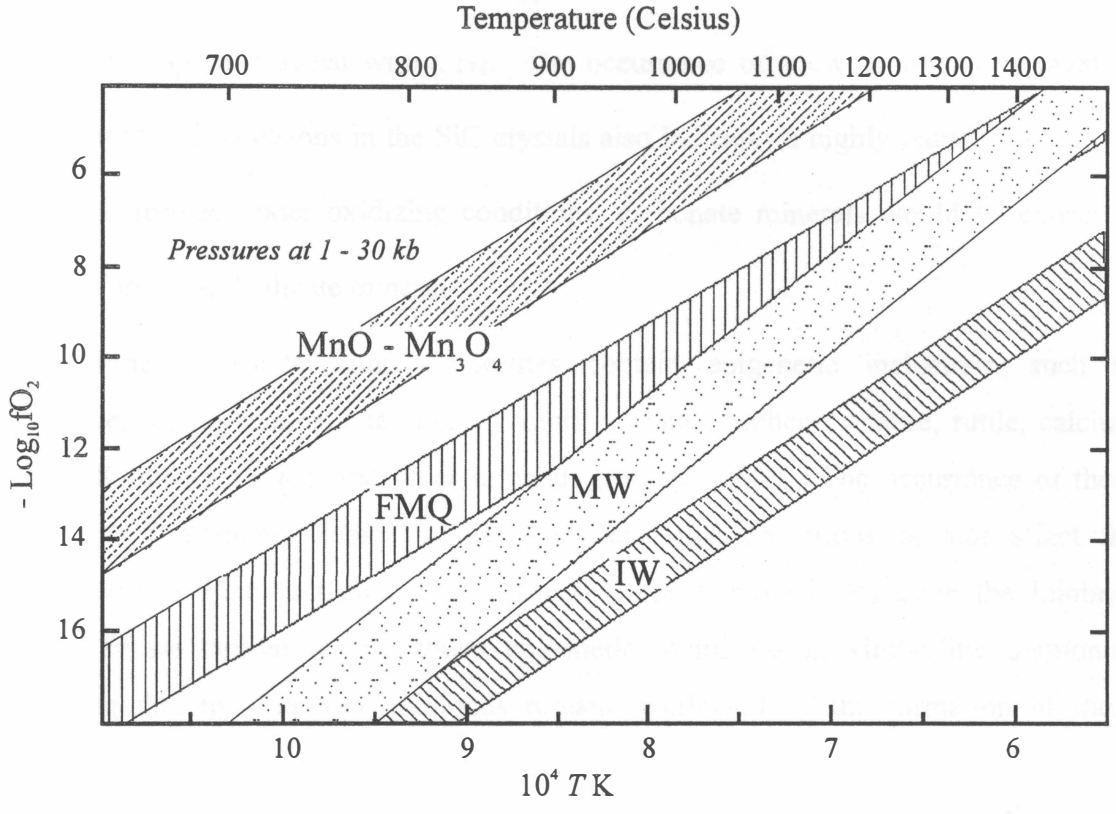

Figure 5-2. Temperature - oxygen fugacity diagram with experimental buffers at pressures from 1 to 30 kb (modified from Haggerty and Tompkins, 1983).
FMQ: fayalite - magnetite - quartz; MW: magnetite - wustite; IW: iron - wustite

The texture characteristics of the Luobusa chromitites and the regional geology do not show any evidence that the ophiolite massif ever reached ultrahigh pressure conditions. Therefore, the group 4 phases from the chromitites must either be xenocrystic in origin, i.e., they have formed in deeper mantle in diamond stability field, then later were captured in the chromitites, or they must have formed outside their normal stability fields at shallow depths in the upper mantle.

In the presence of excess Si, the reaction $2Si + CO_2 = SiC + SiO_2$, produces ß-SiC and quartz, forming a quartz and SiC intergrowth (Leung et al., 1990). The presence of native Si in the Luobusa SiC may thus suggest a deficiency of CO_2 in the system, whereas the system may be reduced with CH_4. The occurrence of a Ca-Al silicate mineral as intergrowths and inclusions in the SiC crystals also indicates a highly reduced condition. If the SiC formed under oxidizing conditions, carbonate minerals would be expected, instead of the Ca-Al silicate mineral.

Some diamonds from kimberlites contain epigenetic inclusions, such as phlogopite, biotite, talc, calcite, quartz, chlorite, anatase, sphene, apatite, rutile, calcium silicate, K-feldspar, mica, and other minerals (Jaques, 1989). The occurrence of these inclusions in diamonds indicates that their formation conditions do not affect the preservation of their host diamonds. Group 2 and 3 mineral phases in the Luobusa chromitites are similar to the above epigenetic inclusions in kimberlitic diamonds, suggesting that the Luobusa diamonds remain unaffected by the formation of these phases.

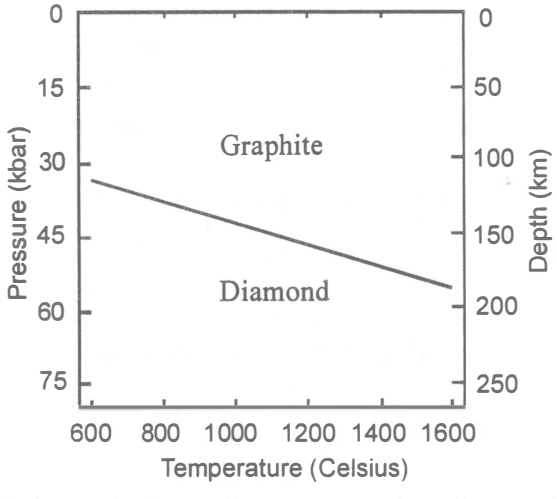

Figure 5-3. Schematic P - T diagram showing diamond and graphite stability fields (from Davies, et al., 1993)

5-2. Formation of the Luobusa diamonds

5-2-1. Review of the origin of natural diamonds

As pointed out in chapter 1 natural diamonds occur in a variety of rock types, but only those from kimberlites and metamorphic rocks have been investigated in detail. The following discussion focuses on diamonds from these two occurrences.

Many different types of studies have been carried out on natural diamonds in order to understand better their origin and mode of formation. Such studies include carbon isotopic analysis, determination of the content and aggregation state of nitrogen, trace element analysis, determination of physical properties by cathodoluminescence and IR-microscopy, identification of mineral inclusions and intergrowths with diamonds, and petrological investigations of diamondiferous xenoliths in various host rocks (Meyer, 1985; Bulanova, 1995; Pattison and Levinson, 1995; Boyd, et al., 1994; Navon, et al., 1988; Garanin and Kudryavtseva, 1990). It is increasingly accepted that natural diamonds grow in a variety of chemical environments; they may crystallize over a significant range of temperatures and pressures and under different fO_2 conditions. In many cases they appear to form by multiple processes. Natural diamonds form over a depth range from the lower mantle (>670 km) to the Earth's crust, and range in age from 3.3 Ga to as young as the eruption of their host kimberlites.

5-2-1-1. Natural diamonds grow in a variety of chemical environments

Natural macrodiamonds from kimberlites contain a variety of syngenetic inclusions which have been broadly grouped into two suites: eclogitic and peridotitic.

Members of these two suites are mutually exclusive in origin, i.e., minerals of one suite do not equilibrate with minerals of the other suite. This clearly indicates that diamonds grow in more than one geochemical environment (Meyer, 1985).

Clinopyroxene inclusions from peridotitic diamonds show that 100 × Ca/(Ca + Mg) values range from sub-calcic (<40) to normal diopsides, some of which are Cr-rich (Sobolev, et al., 1975). It is unlikely that the Cr-rich diopside inclusions would have formed in the same environment as the sub-calcic clinopyroxenes, and thus it is probable that diamonds form in more than one type of ultramafic rock.

Sobolev et al. (1972) documented the relationship between eclogitic mineral inclusions in diamonds and the constituent minerals of the host eclogite. They found that the two assemblages were chemically equivalent, suggesting that the diamond formed contemporaneously with the eclogite host in the mantle. Diamond-bearing ultramafic rocks which occur as xenoliths in kimberlites range from lherzolites (garnet + olivine + clinopyroxene + orthopyroxene), to harzburgites (garnet + olivine + orthopyroxene), to dunites (garnet + olivine), also suggesting that diamonds form in more than one type of ultramafic rock.

Further evidence in support of diamonds having grown in varying chemical environments is the variation of $\delta^{13}C$ values and nitrogen contents. The $\delta^{13}C$ values of diamonds range from +3 to -34‰ (Deines, 1980; Milledge et al., 1983; Kirkley et al., 1991), which has a bearing on the sources of carbon and the chemical reactions that produce diamonds (Meyer, 1985). In some cases diamonds occur as inclusions in bigger diamonds. Garanin and Kudryavtseva (1990) report that the enclosed diamonds are richer

in the light carbon isotope than their host diamonds. Nitrogen contents of diamonds range from 0 up to 3000 ppm (Evans and Harris, 1989; Gurney, 1989, and the different nitrogen contents reflect different chemical environments (Evans and Harris, 1989; Meyer, 1985).

Detailed studies have shown that individual diamonds may also be zoned with respect to their carbon compositions and nitrogen aggregation states (Javoy et al., 1984; Cartigny et al., 1997), which are best explained by formation of diamonds from a reservoir that was either compositionally diverse and/or whose composition changed with time (Griffin et al., 1988).

Some diamonds from Yakutian kimberlites exhibit different cathodoluminescence colours from the centre to the rim of individual crystals. These differences correlate with different inclusion mineral assemblages. The central, extremely heterogeneous zones of the host diamonds contain omphacite, pyrope-almandine garnet and pyrrhotite (eclogitic assemblage) and exhibit yellow-brown to orange-red cathodoluminescent glow. In the intermediate and peripheral zones of the diamonds, the included minerals are pyrope, olivine, enstatite, chromite and pentlandite (ultramafic assemblage) and the grains exhibit light to dark blue cathodoluminescence (Garanin and Kudryavtseva, 1990). This abrupt change in cathodoluminescence, corresponding to the presence of two distinct inclusion assemblages, demonstrates a dramatic change in chemical and P-T conditions during diamond formation (Gurney et al., 1986; Garanin and Kudryavtseva, 1990). Such 'mixed' paragenesis diamonds have also been reported in Argyle, western Australia (Griffin et al., 1988), Monastery, South Africa (Moore and Gurney, 1989), Sloan,

Colorado, North America (Otter and Gurney, 1989), and Mwadui, Tanzania (Stachel et al., 1998).

About 58 elements have been recognized in natural diamonds, and most of them occur in trace quantities. However, the trace element compositions of natural diamonds vary widely (Sellschop, 1979), also suggesting diamonds form in a variety of chemical environments.

Recently micro-inclusions which differ in composition from the more common large inclusions of peridotitic and eclogitic character have been found in natural (cubic and coated) diamonds from Zaire and Botswana. These micro-inclusions resemble potassic magmas in their compositions; they are very enriched in H_2O, CO_3^{2-} and K_2O and depleted in MgO (Navon, et al., 1988; Schrauder et al., 1996). This composition represents a volatile-rich fluid or melt from the upper mantle, which was captured during growth of the diamonds (Navon, et al., 1988). Fibrous coats on macrodiamonds and most euhedral microdiamonds are believed to have crystallized from the kimberlitic magma that transported them to the surface (see Boyd et al., 1994 for a review; Pattison and Levinson, 1995). The validity of this suggestion was also demonstrated by high pressure-temperature experiments (Arima, et al., 1993). These data indicate yet another environment of formation for natural diamonds.

Abundant diamonds from the Mbuji Mayi kimberlites, Zaire, display a clear core surrounded by a coat of fibrous diamond; apatite, biotite and carbonate are present as inclusions in the coat (Walmsley and Lang, 1992). This occurrence indicates the diamond coat crystallized in a silica-carbonate-water-rich system (Kinny and Meyer,

1994). It is suggested that these Zaire diamonds may have formed in at least two distinct geochemical environments: a peridotitic or eclogitic paragenesis in which the core crystallized, and volatile-rich fluids or melts in which the coat formed (Kinny and Meyer, 1994).

The fact that diamonds form in varying chemical environments is best documented by the study of Garanin and Kudryaavtseva (1990). They proposed a four-stage model for the formation of diamonds from the Yakutia kimberlites on the basis of their physical properties, carbon isotopic compositions, and enclosed minerals. In the earliest stage, diamonds nucleated and grew under high pressure and extremely reducing conditions, indicated by inclusions of low-nickel pyrrhotite, wustite and native iron. Continuous growth under mantle conditions formed the inner zones of the diamond crystals in which the inclusions are eclogitic minerals. In the third stage, the dominant mass of the diamonds crystallized under mantle conditions, forming the outer part with peridotitic mineral inclusions. During the final stage, the diamonds crystallized from the kimberlite melt itself.

Diamond formation depths and formation ages also reflect the fact that natural diamonds can form in a variety of chemical environments. Natural diamonds occur from the lower mantle (>670 km) to the Earth's surface where impact diamonds are formed through chemical vapour deposition processes (CVD). Most macrodiamonds are xenocrysts in kimberlites and radiometric model ages for some are as old as 3.0-3.3 Ga (Richardson et al., 1984). On the other hand, most type Ib diamonds (see the next page for an explanation), fibrous coats on macrodiamonds and most euhedral microdiamonds,

which are believed to have crystallized from the host kimberlite magmas (Gurney, 1989; Leung et al., 1990), are Phanerozoic in age (e.g., 350-71 Ma, Boyd et al., 1994). Within these widespread depth range and time scales, the environments in which diamonds formed experienced extensive changes in chemistry. This change is also reflected in the compositions of diamond inclusions. Olivine inclusions in diamonds from Precambrian kimberlites have higher mean Cr_2O_3, Al_2O_3, CaO, Na_2O, and Li than those from Mesozoic ones (Hervig et al., 1980), suggesting a temporal change of either chemistry or temperature or both in diamond formation regions.

5-2-1-2. P-T, fO_2 conditions

The nitrogen content and aggregation state of diamonds reflect different crystallization and heating/cooling histories. Nitrogen tends to occur in an atomic form within diamond lattice as a simple 1:1 substitution for carbon (type Ib diamond) during the initial stages of growth. At mantle temperatures this structure is unstable and the single nitrogen atoms aggregate to form pairs (types IaA); with continued heating the pairs join together to form groups of four nitrogen (type IaB) (Evans and Harris, 1989; Taylor et al., 1990). The occurrence of all these types of natural diamonds (Meyer, 1985), indicates that natural diamonds grow over a range of temperatures and have variable residence times in the mantle.

Many natural diamonds show a series of geometric layers on polished and etched surfaces. This crystallographically discontinuous growth reflects variations in formation conditions (Meyer, 1985; Bulanova, 1995).

Diamonds with simple internal structures typically have inclusions with homogeneous compositions, indicative of a single stage of continuous growth (Sobolev et al., 1997). On the other hand, some diamonds with complex internal structures indicative of interrupted growth and intermittent resorption contain heterogeneous inclusions (Bulanova, 1995). These heterogeneous inclusions within single diamond crystals commonly reflect a wide range of temperature, suggesting that individual diamonds may grow over a significant temperature range (Sobolev et al., 1997). The largest range of temperature yet recorded from a single diamond is ca. 400°C, measured by Ni thermometry of two Cr-pyrope grains in a diamond from Mir (Griffin et al., 1992).

Geothermometry on coexisting mineral inclusions in diamonds yields a temperature range of 900-1,400°C at pressures estimated to be about 35-60 kbar (130-200 km) (Haggerty, 1986; Dobrzhinetskaya et al., 1995). The presence of inclusions of ferropericlase, and native iron rimmed by wustite in Tanzanian diamonds suggests a lower mantle or ultra-deep origin (>670 km) (Stachel, et al., 1998). Some euhedral microdiamonds from kimberlites are believed to form metastably at shallower depths, e.g., the Fuxian diamonds along with SiC at a depth of 60-90 km, which is in the graphite stability field (Leung et al., 1990).

The conclusion that diamonds have grown in a reducing environment is corroborated by inclusions of metallic iron, sulphides, magnesiowustite, and Cr^{2+}-bearing olivine (Haggerty, 1986). However, syngenetic/primary microinclusions dominated by water, CO_2, quartz and carbonate have been found in some natural diamonds, e.g., coated fibrous diamonds (Navon et al., 1988; Guthrie et al., 1991; Boyd et al., 1994). This

indicates that not all diamonds have formed under reducing conditions because it points to growth from oxidized fluids or melts rich in water and carbon dioxide. When such fluids encounter a pre-existing diamond, one would expect the diamond to be resorbed, however, in many cases where this has occurred, for instance diamonds from Zaire and Udachnaya, the sharp edges of the octahedral cores are preserved (Boyd et al., 1994). Recent finding of native iron, wustite and magnetite inclusions coexisting in a single diamond from Tanzania also demonstrates that diamonds form in varying fO_2 conditions (Stachel et al., 1998).

In summary, most natural diamonds probably form in the Earth's mantle and crust under varying fO_2 conditions.

5-2-1-3. Formation processes and preservation

Natural diamonds form in a variety of ways, such as by metamorphic reaction (Boyd and Finnerty, 1980), by metasomatism (Navon et al., 1988; Boyd et al., 1994), by igneous crystallization (Pattison and Levinson, 1995), and perhaps by hydrothermal processes (DeVries, 1997).

Boyd and Finnerty (1980) and Boyd and Gurney (1986) applied various geothermobarometers to ultramafic inclusions in diamonds and found that most inclusions have equilibration temperatures below 1150°C. On the basis of estimated temperatures and pressures, they cautiously suggest that peridotitic diamonds form in a subsolidus environment. Their suggestion is supported by the studies of Shimizu and Richardson (1987) and Griffin et al. (1988) which showed that single diamonds contain

numerous disequillibrium inclusion phases that record a large range of crystallization temperatures (>=400°C) and large compositional changes of the system during diamond crystallization, indicating the diamonds grew at solid-state conditions, enhanced by a fluid flux with introduced or liberated carbon.

A metasomatic origin was proposed by Haggerty (1986; 1994) and Cartigny et al. (1997) for the formation of euhedral microdiamonds. In this model, C-containing, volatile-rich fluids or carbonaceous fluids percolate upward from relatively oxidized parts of the upper mantle and, upon encountering the relatively reducing mantle, are themselves reduced, leading to microdiamond precipitation. The presence of mantle-derived fluid inclusions in diamonds also suggests that diamonds may form by metasomatism (Navon et al., 1988; Boyd et al., 1994; Schrauder et al., 1996).

Macrodiamonds from kimberlites are typically characterized by varying degrees of resorption, indicating that they are unstable in kimberlite magmas. The microdiamonds, because of their small size, should be more susceptible to resorption than macrodiamonds, however, the opposite is commonly observed. Many microdiamonds are euhedral with an octahedral morphology (Pattison and Levinson, 1995). Thus, it has been suggested that type Ib diamonds, fibrous coats on macrodiamonds and most euhedral microdiamonds crystallize from the host magma as phenocrysts, or as condensates from fluids that were liberated from the C-bearing magmas due to decompression ascent (Boyd et al., 1987; Gurney, 1989; Leung et al., 1990; Pattison and Levinson, 1995).

Recent experiments demonstrate that diamonds can grow under relatively low pressures and temperatures (1.4 kbar and 800°C) (Zhao et al., 1997). In this experiment

diamonds were grown on seeds in a hydrothermal environment from a mixture of carbon, water and metal, and it is speculated that this process "may be responsible for most natural diamonds" (DeVries, 1997). Studies on coated diamonds (Navon et al., 1988) strongly support the presence of liquid C-H-O phases during diamond growth, and DeVries (1997) suggests that the very small diamonds found in metamorphic rocks (Sobolev and Shatsky, 1990) probably grew from similar C-H-O liquids.

Natural diamonds may form in the mantle in the diamond stability field from recycled carbon or from mantle carbon, then be transported to Earth's surface either by kimberlitic eruption or by tectonic emplacement, e.g., microdiamonds in metamorphic rocks in the Dabei Mountain in China (Xu et al., 1992). They may also form metastably from kimberlitic magmas by decompression during ascent.

Natural diamonds formed under stable conditions in the mantle require rapid emplacement to keep them from being retrograded to graphite such as has occurred in the Beni Bousera and Ronda Massifs (Davies et al., 1993) or completely resorbed. The factors affecting diamond stability are temperature, particularly the length of residence time at high temperatures and pressures outside the diamond stability field, and oxygen fugacity (Meyer, 1985).

In summary, the growth of natural diamonds is rarely continuous or simple and large variations in pressure, temperature, fO_2, chemical environment and carbon sources have been documented (Meyer, 1985). "The growth of diamonds is not unique to a single rock but can take place in any mantle material in which chemical interactions produce

elemental carbon" (Meyer, 1985; Griffin et al., 1992), and diamonds have formed throughout geological time (Kinny and Meyer, 1994). Preservation of diamonds at Earth's surface requires either rapid emplacement from their stability fields or formation at relatively shallow levels and low temperatures. There are many ways of producing natural diamonds. Diamond formation is no longer considered a unique process, instead diamonds can be expected in a variety of natural environments. The major control on the occurrence of natural diamonds appears to be preservation in their host media after growth rather than mode of formation.

5-2-2. Occurrence of diamonds in the Luobusa chromitites

Thus far diamonds, because of their low concentrations, have not been found in thin sections or hand samples of the Luobusa chromitites; all of them are from mineral concentrates; therefore any possibility of contamination has to be carefully examined. There are three possible sources of contamination: artificial diamonds, natural diamonds from geologic sources, or natural diamonds acquired during separation processes.

The high nitrogen aggregation states of those diamonds recovered in 1980's (Fang and Bai, 1981) indicate that they are of natural origin (Taylor, et al., 1995). The recognition of magnesian-silicate mineral inclusions in the diamond completely rules out the possibility that the diamonds are of artificial origin. Therefore they must be of natural origin.

Contamination from natural sources during sampling can be ruled out because our samples were removed directly from the massive chromitite orebody. Contamination

during separation processes can also be excluded because, (1) the sampling and separation processes were specially designed for diamond collection and these processes were conducted with great care, (2) the separation equipment had not been used previously for diamond-bearing materials and was carefully cleaned before being used; and (3) no diamonds or SiC or other exotic minerals were found in the granite control sample.

Diamonds have been recovered from the Luobusa ophiolite by three independent groups in different separation plants, and all the recovered diamonds and associated minerals have similar characteristics, e.g., colour, size and morphology. It seems most improbable that this level of similarity could be coincidental; most likely it indicates a primary origin in the Luobusa ophiolite.

Taylor et al. (1995) suggested that the diamonds recovered by Fang and Bai (1981) may have resulted from natural contamination. This conclusion was based on the high nitrogen aggregation states of the diamonds which are not consistent with a model of "cool subduction with a relative short residence time in the mantle". However, it is unlikely that the Luobusa diamonds formed during subduction.

A similar argument was applied to the origin of some natural diamonds from metamorphic rocks in Kazahkstan. The previous model suggested they formed by subduction, but this is debatable because continental crust is probably too buoyant to be carried down into the deep mantle (Monastersky, 1995), and an entirely new mechanism is speculated for their formation (Stephen E. Haggerty, cited in Monastersky, 1995).

The Luobusa diamonds represent the first documented occurrence of ultrahigh-pressure minerals in ophiolites. Here two models are proposed that could explain the characteristics of the Luobusa diamonds, including their nitrogen aggregation state.

5-2-3. Origin of the Luobusa diamonds

Diamond nucleation requires oxidation of CH_4 or reduction of CO_2. Pattison and Levinson (1995) suggest that euhedral microdiamonds might precipitate either directly from a saturated melt as phenocrysts (Navon et al., 1988), or from a C-bearing fluid phase (e.g., Leung et al., 1990). Ballhaus and Frost (1994) speculated that highly reduced kimberlitic melts (in association with CH_4-rich fluids) might dissolve elemental (uncomplexed) C, such that simple decompression due to ascent might induce solid C (diamond or graphite) precipitation from the melt.

Whether microdiamonds would precipitate would depend on the evolution of $fO2$ in the magma during ascent (cf., Taylor and Green, 1989), the oxidation conditions of the rocks through which the magma passes (e.g., Taylor and Green, 1989), and the degree of interaction between the two.

A solid-gas reaction of the form $2FeS + CO_2 = 2FeO + S_2 + C$ has been suggested as a mechanism for diamond nucleation (see, Haggerty, 1986). Although not all diamonds contain sulphides and not all carbon was produced by sulfur or sulfide interaction, large concentrations of sulphides as inclusions in diamonds might be indicative of their role in maintaining a reduced buffered environment, critical to diamond nucleation and growth (Haggerty, 1986). Sulphides have been found as

abundant primary inclusions in chromites of the Luobusa chromitites (Wen-Ji Bai and Qing-Song Fang, personal communication, 1998). This occurrence of sulphides might have played an important role in the formation of diamonds during chromitite crystallization outside of the diamond stability field.

Carbonaceous, partially serpentinized peridotite is reduced. Serpentinization reactions are capable of generating highly reducing conditions near the serpentinization front (Frost, 1985), and graphitic material may be locally precipitated if the serpentinizing fluids are carbonaceous (Mathez et al., 1995). It is probable that serpentinization would occur before, or at an early stage of, the reaction between melts and host peridotites, which is responsible for chromitite formation, thus producing a highly reducing environment in which diamond, SiC, Si-Fe and Cr-C alloys, and some high-chromium chromites could form and/or be preserved.

Model 1 – metastable formation in a suprasubduction environment

This model suggests that the Luobusa diamonds may have formed metastably in the upper mantle at the depth where the chromitites were precipitated. During chromitite formation, the chromitites were invaded by metasomatic fluids/melts supersaturated in carbon. Under appropriate fO_2 conditions, the lowered capacity of the fluids/melts to dissolve C-bearing volatiles would result in the precipitation of euhedral microdiamonds and SiC (Pattison and Levinson, 1995).

This model is consistent with the following data currently available.

The Luobusa ophiolite consists chiefly of depleted harzburgite and dunite with high Cr magnesiochromite orebodies. The mineral assemblages and compositions are quite different from those of peridotite inclusions in diamonds and xenoliths in kimberlites. Knorringite garnet has not been found in the Luobusa chromitites. Instead lower pressure almandine is relatively common, together with such minerals as corundum, zircon, rutile, etc.. The lack of other ultra-high pressure minerals other than SiC, and possibly Si-Fe and Cr-C alloys, in the mineral assemblage from Luobusa is difficult to reconcile with crystallization in the diamond stability fields.

For a given nitrogen concentration, the rate of aggregation depends on residence time and temperature. Evans and Harris (1989) suggested that conversion of type IaA to type IaB nitrogen aggregation at temperatures of 1200-1300°C would occur over times of tens of millions of years. The high nitrogen aggregation state of the Luobusa diamonds (type IaAB) (Taylor et al., 1995) suggests that they formed under high temperatures and/or had a long residence time in the mantle after formation. This is consistent with the inference that the Luobusa chromitites formed by melt/rock reaction at high temperatures (Zhou, 1995), and with a formation age of late Jurassic to early Cretaceous and an probable Tertiary emplacement age (Bai et al., 1993). There would have been several tens of million years between formation of the ophiolite in the mantle and its emplacement. This residence time is long enough for nitrogen to aggregate into high state forms, such as IaAB.

It is also difficult to envisage a mechanism by which the euhedral Luobusa diamonds could have formed in the mantle in the normal diamond stability field, and then

together with their host ophiolite massif of more than 50 km^2, have been tectonically emplaced into the crust with sharp-edged diamond crystal forms well-preserved.

The forms of diamonds are commonly modified by various processes subsequent to initial growth, either while resident in the host region or during transportation, which reduce diamond size and generate a variety of secondary forms (Trautman, et al., 1997), i.e., graphitization on {110} and combustion (oxidization) on the {111} and {110} faces of primary forms resulting in rounded dodecahedra (Eggler, 1989). The post-growth history of diamonds has been ascribed to deformation, resorption and late-stage processes such as corrosive etching, which are commonly reflected on the crystal surfaces. All the Luobusa diamonds display the most common primary growth forms: sharp-edged octahedra, along with cubo-octahedra and macled form. Only slight degrees of modification are observed in a few grains, i.e., etch pits and corrosion sculpture. Neither corrosion sculpturing nor etching is extensive. Rounding or resorption along crystal edges and corners, which are typical features of kimberlitic diamonds, are not observed. The well-preserved crystal forms can best be explained by formation at shallow depths, a relatively short distance from where the ophiolite was emplaced.

A metastable origin is also supported by the character of the associated SiC. It is significant that the SiC grains from Luobusa have perfect crystal faces and show no signs of resorption. All of the recovered grains exhibit at least one well-developed crystal face with others fractured, and some are euhedral hexagonal crystals with all the faces well developed. It is difficult to understand how such crystals could have been transported from the deep mantle to the surface without losing their pristine crystal habits. The well-

developed and well-preserved crystal morphology may signify moissanite growth under metastable conditions (Mathez et al., 1995). The possibility of metastable growth is also supported by the reported growth of moissanite by combustion of graphite at low pressure (Chan, 1993).

High temperature/high pressure experiments (Lane et al. 1988) on man-made α-SiC show that ductile deformation takes place at more than 1400°C when a constant compressive stress of 0.41 Gpa (4.1 kbar) is applied. Ductile bending and lamellar structures in Kimberley α-SiC were interpreted to have formed under high temperature, implying a deep source (Leung et al., 1996). No such deformation features have been observed in the Luobusa SiC crystals, which may imply that they formed at relatively shallow depths under high temperatures.

The SiC crystals from Luobusa are also distinct from those of Yakutia kimberlites. None of the Yakutian SiC crystals, which are believed to have formed in the diamond stability field, have well-formed faces on all sides, and most crystals exhibit one side that is rounded (Mathez et al., 1995).

The metastable origin is also supported by: (1) the extensive literature on formation of diamonds under low-pressure conditions, e.g., chemical vapour deposition processes (Sato and Kamo, 1992); (2) synthetic formation of diamonds under low pressures (Zhao et al., 1997); (3) the absence of omphacite, pyrope-almandine, magnesian-chromium pyrope and magnesian ilmenite in the Luobusa chromitites, all of which are typical of eclogitic and peridotitic inclusions in kimberlitic diamonds which grew in the diamond stability field; (4) the occurrence of microdiamonds as inclusions in

most of the rock-forming minerals (e.g. biotite, phlogopite, quartz, diopside and secondary sericite-calcite-chlorite aggregates) in metasedimentary gneiss in the Kokchetav massif (Kazakhstan), suggesting metastable growth outside the diamond stability field (Dobrzhinetskaya et al., 1994; DeVries (1997); (5) nanometre-size diamonds in interstellar and intergalactic space nucleating and growing without ultrahigh pressures or extreme kinetic conditions (Badziag et al., 1990); and (6) increasing documentation that some natural diamonds may form outside the diamond stability fields. A wide range of conditions in the mantle, corresponding to depths of 30-60 km (Eggler, 1989) and 60-90 km (Leung et al., 1990) exists, where fluid liberation and solid C precipitation could occur. Leung et al. (1990) inferred that the diamonds and SiC from the Fuxian kimberlite formed at pressures of 2-3 Gpa (60-90 km depth), which is within the graphite stability field. Pattison and Levinson (1995) also suggest that most euhedral microdiamonds from kimberlites may grow metastably under low pressures. The coexistence of diamond, SiC and graphite in the Luobusa chromitite suggest an origin similar to that of the Fuxian diamonds and SiC.

The growth habit of a crystal, reflected in the interface and face morphology, is very sensitive to the conditions of crystallization, and reveals the conditions and mechanism of crystal growth (Bulanova, 1995). A polyhedral shape (e.g., octahedral) and atomically smooth interfaces are characteristic features of crystals that have grown from a gaseous or liquid phase (Modern Crystallography, 1979). The Luobusa diamonds exhibit poly-euhedral crystal shapes, which strongly argue for their free growth from a carbon supersaturated solution in a silicate melt or fluid (Bulanova and Spetsius, 1990;

Bulanova, 1995). Some of the Luobusa euhedral diamonds exhibit planar triangle growth layers on crystal faces (Fig. 3-1, 3-3 and 3-5), and this feature also suggests they crystallized from a melt or fluid (e.g., Sunagawa, 1982; Gurney, 1986). The euhedral morphology of SiC is also indicative of formation from melt or fluid.

A critical factor in this model is then being able to demonstrate the presence of such a melt/fluid (containing CH_4 or CO or CO_2) in the suprasubduction zone environment where the Luobusa chromitites formed. In fact, metasomatism has proved to be a ubiquitous process in the mantle (Schiano and Clocchiatti, 1994). The involvement of melt/fluid in chromitite formation has been widely documented, e.g., in Kempirsai (Melcher et al., 1997), Troodos (McElduff and Stumpfl, 1991), south-western Oregon (Stockman and Hlava, 1984), and New Caledonia (Johan, 1984). Evidence for similar fluids in the oceanic upper mantle and transition zone has been reported from ODP Leg 147 (Arai et al., 1997). The importance of H_2O/CO_2 -rich fluids and volatile-rich melts in oceanic and continental mantle and crust has been widely accepted (Falloon and Green, 1989; Wyllie, 1987; Menzies and Hawkesworth, 1987). Evidence for such fluids comes from mantle xenoliths and mineral inclusions trapped in diamonds (Schrauder et al., 1996). Peacock (1993) argued that during subduction, oceanic lithosphere undergoes progressive metamorphism and devolatization. Upward migration of the slab-derived fluids can trigger partial melting of the mantle wedge and add H_2O, CO_2, SiO_2, and incompatible elements to the overlying mantle wedge and lithospheric plate. Study of melt inclusions in oceanic peridotites (Schiano and Clocchiatti, 1994) also indicates that small amounts of migrating metasomatic melt exist in the oceanic mantle; these originate

at depth and are characterized by high contents of alumina, silica and volatile components, which provide elemental sources for SiC, etc.. The existence of incompatible element-bearing minerals in the Luobusa chromitites (e.g., zircon, rutile, apatite, sphene, carbonate, K- or Na-bearing phases and celestite) provides evidence that at least small amounts of metasomatic fluid were involved in chromitite formation.

The occurrences and forms of carbon and silicon from which SiC and diamond/graphite grow are probably diverse and complex. The carbon might be derived from decarbonation reactions or dissociation of hydrocarbons, such as methane (CH_4) in the mantle (Leung et al., 1996), or from subducted biogenic carbon (Mathez et al., 1995). The carbon could be as CH_4, CO_2, CO, C or in a variety of carbon-containing species. Silicon in the mantle might be supplied by silicate melts, or be delivered by gaseous carriers, such as CO_2, CH_4, H_2O, N_2, S, F, and Cl. The most important Si-bearing molecules are probably chlorides ($SiCl_2$ and $SiCl_3$) and chlorosilanes (SiH_3Cl, SiH_2Cl_2 and $SiHCl_3$) (Leung et al., 1996). Fluids related to serpentinization are reactive and have the possibility of carrying significant quantities of dissolved silica (Moody, 1976), providing a silica source for SiC formation.

Model 2 – xenocrystic origin from the deep mantle

Although a metastable origin in the chromitites is most preferable, a deep mantle origin can not be completely ruled out. In this model the diamonds, SiC, Si-Fe and Cr-C alloys, along with previously reported native iron and chromium would have formed at depths possibly up to around the transition zone, or deeper. They were then carried to

shallower levels by a mantle plume (Kerr, 1993) which eventually underwent partial melting to form the boninitic magmas from which the chromitites crystallized. The diamonds and other ultra-high pressure (UHP) minerals would then be picked up by the melts and carried to the upper mantle where they were entrapped during chromite crystallization.

The best evidence for this model comes from one diamond grain which contains three inclusions of an unknown silicate mineral. This grain is a typical broken fragment which is believed to result from the separation processes, with the silicate crystals being exposed on its broken surface. A scanning electron image of one of the inclusions shows that it has a characteristic morphology imposed by the growth of the host diamond, like many inclusions in diamonds from kimberlites. The unusual composition of the inclusions does not fit any known mineral, but is close to that of enstatite $(Mg,Fe)SiO_3$, except for excess Si and Al, $(Mg_{0.77}Fe_{0.06}Al_{0.01}Si_{0.07})_{0.91}SiO_3$. Experimental evidence demonstrates that Al would substitute for Mg+Fe in perovskite at depths equivalent to the lower mantle (Irifune, et al., 1996). Possibly Si can also substitute into the (Mg,Fe) site of silicate minerals formed at great depths. The crystal structure of the inclusions is being analyzed by T. Stanley Cameron using X-ray diffraction techniques. Because of their unusual composition, the inclusions may also have an unusual structure, something like enstatite having perovskite structure.

Another possible piece of evidence for this model is the occurrence of some alloys, particularly Fe-Si. Abundant Si-C, Fe-Si and minor Cr-C alloys were recovered from the Luobusa chromitite; native chromium, iron and silicon have also been reported

in the Luobusa ophiolite (Fang and Bai, 1981). Formation of these metallic phases requires extremely reduced conditions and high temperatures (T > 1727 °C) (Essene and Fisher, 1986).

High pressure-temperature experimental studies have suggested the occurrence of Fe_xSi_y alloys, where x and y are uncertain, in the lower mantle (>24 Gpa, i.e., >670 km). Fe_xSi_y alloys along with stishovite (the high-pressure polymorph of SiO_2), $MgSiO_3$ perovskite, and $(Mg,Fe)_xO$ wustite are products of molten iron reacting with $(Mg,Fe)SiO_3$ perovskite, the major component of the lower mantle (Knittle and Jeanloz, 1986; 1991).

This model requires a long transportation for the uplift and emplacement of the xenocrystic UHP phases. It is difficult to reconcile such an emplacement process with the euhedral morphology of the UHP minerals and the absence of corrosion or resorption features. Chemical re-equilibration would be expected during transportation of the minerals to an entirely different physical-chemical environment.

Either of formation mechanism could have occurred in the Luobusa ophiolite; without in situ observation of texture relationships of the diamonds with other phases, it is difficult to determine which is most probable; but on the basis of available data, the metastable model is preferred.

CHAPTER 6. CONCLUSIONS

Diamonds and more than 30 associated mineral species were identified in the Luobusa chromitites. The specially designed sampling and separation procedures, together with the careful implementation of these procedures, as well as the characteristics of the diamonds and other minerals, clearly demonstrate that these are original phases in the Luobusa chromitites.

All the mineral species are assigned into four groups. 1 - primary phases, such as chromite, forsterite, enstatite, and Cr-diopside; they are the major components of the Luobusa chromitites and have a typical podiform chromititic paragenesis. 2 - secondary minerals, including zircon, rutile, sphene, apatite, amphibole, biotite, phlogopite, plagioclase, K-feldspar, corundum, sillimanite, wollastonite, and celestite; they are suggested to have formed through fluid influxes during or shortly after chromitite formation. 3 - alteration minerals, including serpentine, chlorite, sulphides, calcite, dolomite, almandine, Fe-Mn garnet, uvarovite, and Fe-Ni and Au-Ag alloys; they were derived from low-temperature serpentinization of the chromitites. 4 - highly reduced phases, including diamond, SiC, Si-Fe and Cr-C alloys, gehlenite enclosed in SiC, native iron, chromium and silicon, and possibly graphite.

Group 4 phases are unusual occurrences in the podiform chromitites. Two models are proposed for their formation: 1) they formed metastably in the chromitites at shallow levels in the upper mantle; this model fits most of the data currently available. 2) they may have formed at great depth and were later carried by a rising plume to shallower

depths, where the plume experienced partial melting. The UHP minerals were then picked up and transported further up by a reduced fluid/melt, and carried to the depths where the chromitites crystallized.

The Luobusa diamonds are colorless, and range in size from 150 ×150 μm to 900 × 1000 μm. Most of them are euhedral crystals, and are sharp-edged octahedrons; others are broken fragments.

The well-developed crystal morphology of the diamonds, SiC and Cr-C alloy signifies that they crystallized from melts/fluids. Their well-preserved character indicates they have not been involved in any resorption processes subsequent to formation.

Magnesian silicate inclusions were identified in the Luobusa diamonds. They possess an octahedral morphology which was imposed by their host diamond during growth, and have a composition of $(Mg_{0.77}Fe_{0.06}Al_{0.01}Si_{0.07})_{0.91}SiO_3$ never before documented. The composition best fits the enstatite formula $(Mg,Fe)SiO_3$, but with excess Si and Al.

No pseudomorphs of graphite after diamond were found in the Luobusa chromitites, but flat-shaped hexagonal graphite crystals are abundant in the chromitites, implying that the Luobusa diamonds have not been graphitized. This graphite may have formed together with diamond under metastable conditions.

Larger diamond crystals (i.e. >1mm) are expected to be found in the Luobusa ophiolite. Thus far the biggest diamond grain is 0.9 × 1 mm in size. This is a broken diamond crystal with one side having octahedral morphological features, and others being fractured.

It is possible that diamonds in Alpine peridotite are more common than heretofore expected. There are similar occurrences in the Beni Bousera massif in Morocco and in the Ronda massif in Spain, although these were formed in subcontinental mantle. It may also be common for ophiolite sequences to contain highly reduced xenocrysts, such as metallic silicon in the Josephine ophiolite (Bird and Weather, 1975).

The extremely high chromium chromites were identified in the Luobusa chromitites by electron microprobe analyses. It is suggested that they formed in reducing conditions, similar to those of Mae Chirum, Kempirsai and Cyprus. This suggestion is supported by the identification of Cr^{2+}-bearing chromites in the Luobusa chromitites (Bai et al., 1993). Such reduced conditions are favorable for the metastable formation of the UHP minerals, or/and the preservation of them as entrapped xenocrysts.

The presence of hydrous minerals, such as amphibole, biotite and phlogopite, suggest that fluid phases have been involved in the formation of the Luobusa chromitites.

This study also shows that none of the rocks in the ophiolite sequence display evidence of high or ultra-high pressure metamorphism that would be expected if the body had been subducted to the diamond stability fields. Pillow lavas, cherts, layered gabbros and pyroxenites are preserved in the melange zone at the base of the ophiolite and unmetamorphised diabase dykes are common in the mantle peridotites. In addition, high pressure metamorphic rocks have not been observed elsewhere in the Indus-Yarlunzangbo Suture (IYS) in which the Luobusa ophiolite lies. Kimberlites/lamproites are also absent along the IYS zone. The mineral assemblage recovered in this study strongly suggests that the Luobusa chromitites did not form in the

diamond stability fields. The evidence indicates that the diamonds and other UHP phases are either of metastable origin in the chromitites, or of xenocrystic origin.

CHAPTER 7. RECOMMENDATIONS FOR FUTURE STUDY

1. A potentially important further study would involve investigation of the C-isotope ratios of the SiC, graphite and diamonds. Results of such research might provide information on the C cycle, particularly with regard to the sources of C, isotopic fractionation processes, presence or absence of biogenic C or recycling by subduction.
2. Structural analysis of the silicate inclusions in the diamonds and SiC, and SiC, Fe-Si and Cr-C alloys might help support the xenocrystic model.
3. Mathez, et al. (1995) suggested that in the system Si-Mg-Fe-C-O at high pressures, ß and spinel polymorphs of Mg_2SiO_4 and the stishovite polymorph of SiO_2 would be involved in the formation of diamonds and SiC. The finding of such phases would lend credibility to the xenocrystic model.
4. Quartz coexisting with SiC has been reported by Leung et al. (1990). Whether or not the formation of quartz recovered in the Luobusa ophiolite is related to SiC formation needs further work.
5. To collect more samples of diamond, SiC, Fe-Si and Cr-C alloys from the chromitites, particularly those attached to other mineral phases or containing inclusions, is crucial for a better understanding of the origin of the Luobusa diamonds.
6. The finding of 1 mm size diamond fragments indicates that even bigger grains exist in the Luobusa ophiolite. Further effort should be made to seek bigger diamonds in ophiolitic rocks; this may aid in diamond deposit exploration.

APPENDIX I: ELECTRON MICROPROBE ANALYTICAL METHODS

All the mineral analyses were obtained on polished this sections using a JEOL 733 electron microprobe at the Dalhousie University Microprobe Laboratory. The beam operating conditions were set to 15 kV and 15 nA, and each spectrum was accumulated for 40 seconds. Geological standards were used for the instrumental calibration. Results were corrected by using the Link's ZAF matrix correction program.

Some of the mineral analyses were recalculated for their end-members. For Fo and Fa in olivine (Appendix II 1), total iron was assumed to be Fe^{2+}. The same assumption was applied in the calculation of end-members of the pyroxenes (Appendix II 5 and 6). For the calculation of cr numbers and mg numbers in the chromite (Appendix II 12), Fe^{2+} and Fe^{3+} were distributed on the basis of the stoichiometry of spinel $(Fe^{2+}, Mg)(Al, Cr, Fe^{3+})_2O_4$.

APPENDIX II - ELECTRON MICROPROBE ANALYSES OF THE MINERALS IN THE LUOBUSA CHROMITITES (IN WT%)

II 1 - Olivine

Grain	SiO2	TiO2	Al2O3	FeO	MnO	MgO	CaO	Na2O	K2O	Cr2O3	NiO	BaO	Total	Fo
		Euhedral grains												
IV-26	42.46	0.08	0.00	2.35	0.00	54.31	0.00	0.00	0.00	0.04	1.01	0.00	100.25	97.6
IV-27	42.07	0.00	0.00	2.29	0.00	54.25	0.00	0.00	0.00	0.05	0.89	0.02	99.63	97.7
IV-28	42.29	0.00	0.00	2.47	0.00	54.57	0.00	0.17	0.02	0.08	0.95	0.20	100.78	97.7
IV-30	42.37	0.00	0.00	2.16	0.01	54.28	0.02	0.00	0.02	0.00	0.99	0.18	100.03	97.8
IV-31	42.37	0.07	0.00	1.91	0.07	54.36	0.04	0.00	0.00	0.01	1.10	0.00	99.94	98.1
V-1	42.07	0.00	0.00	2.21	0.01	54.90	0.02	0.04	0.00	0.03	1.11	0.09	100.48	97.8
V-2	41.54	0.00	0.00	2.42	0.00	54.12	0.00	0.07	0.00	0.00	1.15	0.06	99.38	97.6
V-3	41.99	0.09	0.01	2.50	0.08	54.71	0.01	0.01	0.01	0.00	0.95	0.00	100.41	97.6
V-4	41.72	0.08	0.02	2.40	0.04	54.88	0.00	0.09	0.00	0.00	1.08	0.00	100.31	97.6
V-5	42.05	0.02	0.11	2.53	0.00	54.85	0.00	0.10	0.02	0.11	0.73	0.04	100.57	97.4
V-7	41.75	0.08	0.02	2.15	0.03	54.86	0.01	0.00	0.01	0.00	0.92	0.00	99.92	97.8
V-8	41.99	0.01	0.04	2.34	0.03	54.63	0.01	0.03	0.00	0.00	1.15	0.07	100.45	97.6
V-9	41.64	0.13	0.00	2.40	0.03	54.79	0.00	0.07	0.02	0.09	1.21	0.00	100.38	97.6
V-10	41.61	0.05	0.00	2.48	0.06	54.47	0.00	0.00	0.00	0.00	1.31	0.00	100.04	97.6
V-11	41.81	0.08	0.04	2.32	0.00	54.65	0.03	0.00	0.00	0.03	1.04	0.00	100.00	97.6
V-12	41.88	0.00	0.06	2.44	0.00	55.17	0.04	0.12	0.00	0.18	0.79	0.07	100.74	97.6
V-13	41.70	0.06	0.00	1.80	0.10	54.75	0.00	0.12	0.00	0.02	1.25	0.09	99.88	98.2
V-14	41.49	0.00	0.01	2.71	0.07	54.97	0.01	0.01	0.01	0.00	0.93	0.04	100.24	97.4
V-15	41.69	0.00	0.00	2.42	0.13	55.27	0.00	0.23	0.00	0.00	0.79	0.14	100.69	97.6

Grain	SiO2	TiO2	Al2O3	FeO	MnO	MgO	CaO	Na2O	K2O	Cr2O3	NiO	BaO	Total	Fo
V-16	41.69	0.15	0.00	2.62	0.07	54.52	0.00	0.00	0.02	0.00	1.35	0.00	100.53	97.4
V-17	42.08	0.00	0.06	2.22	0.02	55.49	0.01	0.15	0.00	0.10	1.07	0.00	101.25	97.8
V-18	41.78	0.00	0.03	1.98	0.00	55.02	0.04	0.00	0.00	0.02	1.27	0.00	100.12	98
V-19	41.51	0.00	0.05	2.80	0.02	54.89	0.00	0.01	0.00	0.03	1.05	0.13	100.49	97.2
V-21	41.78	0.00	0.00	1.96	0.03	54.91	0.03	0.00	0.00	0.00	1.28	0.00	100.00	98
V-22	41.92	0.04	0.00	2.02	0.00	55.02	0.04	0.09	0.00	0.00	1.11	0.00	100.26	98
V-23	41.77	0.12	0.00	2.01	0.00	55.13	0.00	0.06	0.02	0.00	1.06	0.03	100.27	98
V-24	42.01	0.05	0.00	2.42	0.00	54.91	0.00	0.02	0.00	0.02	1.12	0.00	100.56	97.6
V-25	42.02	0.00	0.00	2.28	0.07	54.83	0.12	0.12	0.00	0.00	1.09	0.09	100.68	97.8
V-26	41.88	0.00	0.00	1.74	0.00	55.34	0.00	0.05	0.00	0.06	1.12	0.04	100.28	98.2
V-27	41.73	0.00	0.01	2.56	0.03	54.24	0.00	0.00	0.00	0.00	0.75	0.05	99.36	97.4
V-28	41.65	0.00	0.00	3.18	0.12	54.21	0.03	0.00	0.01	0.00	0.77	0.00	99.97	96.8
V-29	42.16	0.03	0.01	2.25	0.00	54.82	0.00	0.00	0.00	0.10	1.07	0.00	100.44	97.8
V-30	42.24	0.02	0.05	2.22	0.00	55.35	0.05	0.04	0.03	0.03	1.08	0.00	101.12	97.8
V-32	41.69	0.02	0.00	2.43	0.00	54.72	0.05	0.13	0.00	0.07	0.96	0.00	100.11	97.6
V-33	41.76	0.04	0.00	2.42	0.10	54.42	0.07	0.07	0.00	0.05	1.07	0.01	100.02	97.6
V-34	41.38	0.00	0.05	2.30	0.02	54.41	0.00	0.00	0.01	0.05	0.74	0.00	98.96	97.6
V-35	41.82	0.05	0.00	1.62	0.06	55.07	0.02	0.04	0.00	0.00	1.11	0.00	99.80	98.4
V-36	42.00	0.00	0.00	2.46	0.03	55.05	0.01	0.01	0.03	0.00	1.04	0.00	100.63	97.6
V-37	41.67	0.00	0.00	3.14	0.00	54.69	0.00	0.01	0.04	0.00	0.75	0.16	100.49	96.8
		Anhedral grains												
II-8	42.09	0.00	0.00	3.13	0.01	54.05	0.00	0.01	0.01	0.03	1.11	0.00	100.44	96.9
III-30	42.02	0.00	0.00	3.63	0.01	53.89	0.00	0.07	0.00	0.00	0.71	0.12	100.54	96.4
IV-60	41.16	0.00	0.01	8.58	0.15	49.58	0.00	0.19	0.00	0.00	0.48	0.03	100.31	91.2

Grain	SiO2	TiO2	Al2O3	FeO	MnO	MgO	CaO	Na2O	K2O	Cr2O3	NiO	BaO	Total	Fo
IV-61	40.92	0.00	0.00	8.86	0.08	49.60	0.00	0.02	0.05	0.00	0.42	0.10	100.13	90.9
VII-a2	42.56	0.00	0.00	2.77	0.00	53.58	0.04	0.06	0.01	0.08	0.75	0.26	100.10	97.1
VII-a1	41.58	0.09	0.00	7.20	0.23	50.44	0.11	0.04	0.00	0.00	0.27	0.00	99.97	92.5
VII-a8	42.84	0.00	0.06	3.61	0.05	53.94	0.02	0.01	0.04	0.00	0.69	0.02	101.26	96.3
B1-82	41.12	0.00	0.00	5.77	0.05	51.29	0.00	0.09	0.02	0.09	0.51	0.07	99.04	94.1
B2-1'	42.02	0.00	0.06	3.42	0.05	53.92	0.00	0.24	0.02	0.00	0.80	0.16	100.72	96.6
B2-2'	42.20	0.00	0.00	3.13	0.00	54.04	0.00	0.00	0.00	0.04	0.81	0.00	100.22	96.8
B2-1	41.49	0.00	0.01	5.69	0.00	52.15	0.01	0.07	0.03	0.08	0.66	0.00	100.19	94.2
B2-2	42.03	0.00	0.03	2.99	0.07	53.66	0.00	0.01	0.00	0.00	0.70	0.00	99.65	97
B2-3	40.42	0.00	0.00	8.38	0.00	48.82	0.00	0.09	0.00	0.00	0.44	0.01	98.31	91.1
B2-5	41.22	0.00	0.00	8.31	0.18	49.96	0.05	0.17	0.05	0.01	0.23	0.04	100.27	91.5
B2-6	40.74	0.09	0.00	8.11	0.15	49.95	0.00	0.08	0.01	0.05	0.28	0.00	99.55	91.6
B2-7	42.37	0.01	0.08	3.16	0.02	53.90	0.00	0.00	0.00	0.03	0.83	0.00	100.42	96.8
B2-10	42.04	0.00	0.01	3.28	0.01	53.74	0.02	0.00	0.03	0.00	0.81	0.00	99.99	96.8
B2-11	42.20	0.08	0.02	2.72	0.07	54.11	0.00	0.00	0.03	0.03	0.81	0.03	100.11	97.2
B2-13	41.67	0.11	0.00	3.52	0.00	53.56	0.00	0.14	0.00	0.00	0.60	0.00	99.71	96.4
B2-14	41.47	0.00	0.00	3.36	0.09	53.04	0.04	0.04	0.00	0.04	0.65	0.10	98.93	96.6
B2-17	42.14	0.00	0.00	3.19	0.00	54.05	0.00	0.10	0.04	0.00	0.84	0.10	100.49	96.8
B2-20	42.05	0.01	0.00	3.29	0.09	53.97	0.00	0.13	0.00	0.00	0.65	0.00	100.20	96.8
B2-21	42.33	0.02	0.18	2.91	0.05	54.28	0.07	0.10	0.00	0.03	0.59	0.00	100.63	97.2
B2-22	42.06	0.15	0.00	3.01	0.00	54.11	0.00	0.21	0.00	0.00	0.63	0.00	100.18	97
B2-28	41.39	0.00	0.00	4.67	0.11	52.21	0.03	0.00	0.01	0.00	0.45	0.00	98.90	95.2
B2-30	42.30	0.01	0.00	3.09	0.14	54.30	0.03	0.08	0.00	0.00	0.74	0.05	100.76	97
B2-33	42.18	0.00	0.00	3.01	0.03	54.08	0.03	0.07	0.03	0.05	0.70	0.00	100.19	97
B2-37	40.87	0.00	0.00	7.81	0.09	50.48	0.06	0.26	0.00	0.03	0.23	0.19	100.14	92

Grain	SiO2	TiO2	Al2O3	FeO	MnO	MgO	CaO	Na2O	K2O	Cr2O3	NiO	BaO	Total	Fo
B2-41	42.05	0.00	0.00	3.27	0.00	54.12	0.09	0.00	0.00	0.00	0.77	0.28	100.59	96.8
B11-10	41.26	0.00	0.00	7.07	0.11	51.03	0.03	0.04	0.00	0.00	0.45	0.03	100.06	92.8
B11-11	42.21	0.00	0.03	2.80	0.06	54.42	0.00	0.14	0.00	0.02	0.79	0.03	100.51	97.2
		Anhedral grains, containing high-Cr chromite inclusions												
II-61	42.16	0.07	0.05	2.50	0.00	54.46	0.01	0.08	0.06	0.09	0.91	0.00	100.41	97.5
III-14	42.26	0.00	0.00	2.95	0.03	53.88	0.00	0.08	0.05	0.00	0.79	0.00	100.05	97
III-15	42.00	0.12	0.08	3.24	0.02	54.19	0.00	0.13	0.01	0.08	0.94	0.00	100.81	96.8
III-18	42.01	0.00	0.00	2.99	0.13	54.21	0.00	0.08	0.01	0.13	0.77	0.10	100.44	97
		Anhedral grains, containing low-Cr chromite inclusions												
III-19	41.16	0.00	0.00	7.20	0.02	51.16	0.03	0.00	0.00	0.37	0.39	0.00	100.36	92.7
III-20	41.08	0.09	0.00	8.52	0.25	49.98	0.06	0.05	0.00	0.00	0.20	0.00	100.23	91.3
		Anhedral grains, intergrown with Opx												
III-3	41.06	0.00	0.00	9.36	0.22	49.62	0.02	0.13	0.04	0.00	0.42	0.01	100.87	90.4
III-4	41.23	0.00	0.03	8.63	0.06	50.78	0.00	0.00	0.05	0.06	0.38	0.18	101.39	91.2
III-6	41.25	0.04	0.00	7.82	0.09	50.79	0.00	0.10	0.00	0.00	0.41	0.00	100.50	92
III-11	41.11	0.02	0.00	8.97	0.19	50.83	0.12	0.20	0.02	0.00	0.32	0.01	101.79	91.1

II 2 - Zircon

Grain	ZrO2	SiO2	TiO2	Al2O3	FeO	MgO	HfO2	ThO2	Y2O3	La2O3	UO3	Nb2O5	SrO	Ce2O3	Ta2O5	Total
IV-36	65.91	33.20	0.00	0.04	0.03	0.07	0.33	0.02	0.81	0.00	0.00	0.55	0.00	0.16	0.00	101.13
IV-37	66.10	32.47	0.00	0.03	0.00	0.04	0.29	0.00	1.13	0.00	0.00	0.00	0.00	0.17	0.85	101.09
IV-38	66.78	32.71	0.00	0.05	0.00	0.05	0.36	0.00	0.73	0.03	0.00	0.07	0.00	0.03	0.47	101.29
IV-39	66.93	31.96	0.00	0.09	0.00	0.02	0.11	0.11	1.06	0.00	0.00	0.00	0.22	0.00	1.62	102.13
IV-40	67.18	32.24	0.00	0.00	0.00	0.00	0.00	0.00	0.70	0.00	0.04	0.03	0.32	0.00	0.68	101.19
IV-41	66.48	32.86	0.14	0.00	0.05	0.07	0.07	0.00	0.66	0.14	0.00	0.28	0.00	0.21	0.00	100.97
IV-42	65.90	31.94	0.05	0.00	0.00	0.04	0.41	0.00	0.74	0.00	0.00	0.11	0.00	0.00	1.66	100.85
IV-43	67.07	33.01	0.09	0.00	0.07	0.00	0.06	0.00	0.43	0.00	0.20	0.17	0.00	0.00	0.30	101.40
IV-44	66.37	32.14	0.12	0.00	0.00	0.08	0.65	0.09	0.55	0.11	0.00	0.32	0.00	0.28	1.25	101.96
IV-45z	66.44	31.74	0.07	0.00	0.00	0.04	0.73	0.00	0.57	0.05	0.06	0.35	0.10	0.00	2.41	102.55
IV-45z	66.47	31.80	0.04	0.00	0.02	0.00	0.58	0.00	0.64	0.11	0.00	0.00	0.17	0.19	1.76	101.77
IV-45za	65.74	32.18	0.03	0.00	0.04	0.11	0.82	0.00	0.61	0.00	0.00	0.00	0.00	0.00	1.35	100.87
IV-45zb	66.36	31.78	0.06	0.00	0.03	0.04	0.82	0.30	1.58	0.00	0.00	0.40	0.10	0.00	2.14	103.60
IV-45zc	66.32	31.64	0.00	0.00	0.00	0.03	0.85	0.12	0.79	0.00	0.00	0.00	0.00	0.00	2.14	101.89
IV-45zd	66.35	31.86	0.00	0.01	0.00	0.14	0.82	0.14	0.96	0.00	0.33	0.00	0.05	0.00	2.17	102.82
IV-45ze	66.17	31.76	0.07	0.00	0.00	0.07	0.99	0.05	0.85	0.12	0.12	0.28	0.15	0.27	2.26	103.16

III 3 - **Sillimanite and Sphene**

Grain	SiO2	TiO2	Al2O3	FeO	MnO	MgO	CaO	Na2O	K2O	Cr2O3	NiO	P2O5	Total
Sillimanite													
VII-a7	37.37	0.05	62.91	0.10	0.06	0.00	0.02	0.02	0.00	0.00	0.00	0.00	100.53
VII-a21	39.46	0.06	58.73	0.18	0.00	0.00	0.71	0.63	0.02	0.00	0.00	0.04	99.86
VII-b8	36.91	0.12	62.87	0.03	0.00	0.00	0.03	0.00	0.00	0.00	0.12	0.03	100.12
VII-b11	37.12	0.00	60.90	0.64	0.00	0.45	0.00	0.16	0.31	0.09	0.00	0.05	99.89
VII-b12	36.79	0.00	60.49	0.91	0.00	0.70	0.00	0.05	0.47	0.00	0.00	0.00	99.40
VII-b13	36.89	0.03	63.35	0.07	0.03	0.06	0.06	0.07	0.00	0.04	0.00	0.00	100.67
VII-b14	37.07	0.04	59.46	1.29	0.00	0.88	0.01	0.03	0.62	0.01	0.00	0.06	99.59
VII-b15	37.03	0.00	62.75	0.05	0.00	0.05	0.07	0.13	0.00	0.10	0.01	0.07	100.26
VII-b16	37.12	0.01	63.07	0.12	0.08	0.10	0.00	0.01	0.02	0.00	0.19	0.00	100.80
VII-b17	37.08	0.10	62.38	0.08	0.01	0.04	0.00	0.00	0.04	0.00	0.01	0.00	99.75
VII-b18	37.25	0.13	63.30	0.02	0.03	0.09	0.01	0.05	0.00	0.06	0.00	0.05	101.00
B5-1	36.92	0.07	63.42	0.11	0.07	0.00	0.06	0.00	0.01	0.00	0.00	0.01	100.67
B5-2	40.39	0.00	60.21	0.14	0.00	0.12	0.05	0.02	0.00	0.00	0.00	0.12	101.19
B5-3	37.68	0.05	63.43	0.17	0.00	0.11	0.06	0.00	0.04	0.09	0.00	0.10	101.72
B5-4	37.06	0.03	62.94	0.16	0.07	0.00	0.04	0.00	0.03	0.00	0.14	0.07	100.56
B5-5	36.86	0.01	62.64	0.23	0.07	0.06	0.00	0.10	0.03	0.03	0.05	0.06	100.15
B5-6	37.26	0.00	62.70	0.06	0.00	0.01	0.05	0.05	0.04	0.06	0.00	0.13	100.46
B5-7	37.45	0.11	63.27	0.20	0.03	0.05	0.03	0.01	0.00	0.00	0.00	0.02	101.17
B5-8	36.74	0.20	62.75	0.04	0.15	0.07	0.03	0.00	0.01	0.00	0.00	0.00	100.00
B5-9	38.02	0.00	62.82	0.09	0.00	0.03	0.05	0.13	0.04	0.07	0.00	0.08	101.35
B5-10	37.73	0.00	63.63	0.19	0.00	0.10	0.04	0.08	0.00	0.00	0.00	0.07	101.84
B5-11	37.47	0.00	63.57	0.22	0.00	0.04	0.00	0.00	0.00	0.08	0.06	0.08	101.73
B5-12	37.07	0.05	60.76	0.69	0.10	0.53	0.05	0.00	0.43	0.00	0.09	0.00	99.82
Sphene													
IV-48	29.88	33.81	1.38	1.53	0.13	0.00	27.24	0.00	0.00	0.00	0.16	0.07	95.68
IV-49	29.92	34.80	1.54	1.61	0.23	0.01	28.43	0.05	0.00	0.00	0.00	0.07	96.58

II 4 - Garnet

Grain	SiO2	TiO2	Al2O3	FeO	MnO	MgO	CaO	Na2O	K2O	Cr2O3	NiO	Total	Gro	Py	Alm	Spe
Almandine																
IV-53	36.40	0.01	20.95	39.50	0.47	2.24	0.86	0.06	0.02	0.00	0.06	100.58	0.8	9.1	87.4	1.2
IV-54	36.55	0.00	20.68	38.23	0.48	2.46	1.10	0.00	0.03	0.00	0.00	99.55	2.2	9.9	85.7	1.2
IV-50	37.14	0.00	20.98	38.25	0.50	2.24	1.50	0.10	0.00	0.01	0.04	100.76	4.0	8.8	85.6	1.2
IV-57	36.74	0.00	20.73	39.35	0.41	2.36	0.91	0.05	0.04	0.00	0.06	100.65	0.8	9.5	86.9	0.8
IV-59	36.89	0.01	20.94	38.72	0.18	2.56	1.09	0.00	0.00	0.05	0.11	100.56	2.8	10.3	86.5	0.0
IV-62	36.67	0.01	20.84	39.82	0.36	2.22	0.74	0.00	0.06	0.00	0.14	100.86	0.4	8.8	88.5	0.8
B3-6	37.49	0.06	21.13	27.92	1.02	3.93	8.50	0.02	0.00	0.04	0.02	100.13	20.3	15.4	58.6	2.4
B3-9	37.09	0.00	20.97	33.83	3.19	3.62	1.67	0.03	0.01	0.01	0.03	100.45	2.6	14.3	73.7	7.2
Fe-Mn garnet																
B3-12	37.02	0.06	20.99	26.80	13.20	2.12	1.23	0.08	0.00	0.00	0.00	101.51	2.0	8.3	58.4	29.7
VI-2	36.73	0.00	20.57	21.86	15.81	3.30	1.43			0.02	0.02	99.75	1.1	13.0	47.1	35.9
VI-2	37.04	0.03	20.59	21.13	15.58	3.35	1.38			0.00	0.00	99.10	2.2	13.6	46.8	35.6
Uvarovite																
Va-20	35.11	0.68	0.55	1.15	0.00	0.12	33.80	0.01	0.00	27.84	0.00	99.26				

II 5 - **Orthopyroxene**

Grain	SiO2	TiO2	Al2O3	FeO	MnO	MgO	CaO	Na2O	K2O	Cr2O3	NiO	BaO	P2O5	Total	En	Fs	Wo
II-12	55.99	0.03	2.37	5.82	0.13	33.58	0.70	0.09	0.00	0.80	0.04	0.00	0.02	99.58	89.91	8.77	1.32
II-14	55.55	0.07	3.11	5.78	0.07	33.35	0.70	0.00	0.00	0.90	0.10	0.02	0.09	99.74	89.91	8.76	1.33
II-15	55.93	0.00	2.44	5.20	0.15	32.57	2.42	0.04	0.00	0.76	0.16	0.14	0.20	100.02	87.48	7.85	4.67
II-16	56.58	0.00	2.40	5.56	0.08	33.98	0.44	0.00	0.02	0.78	0.14	0.07	0.00	100.06	90.8	8.35	0.85
II-17	56.17	0.06	2.19	5.87	0.15	34.00	0.51	0.02	0.00	0.77	0.22	0.00	0.00	100.03	90.28	8.72	1
III-38	58.81	0.07	0.52	3.05	0.01	36.94	0.62	0.00	0.00	0.33	0.33	0.00	0.02	100.69	94.45	4.41	1.14
III-39	58.54	0.00	0.62	3.15	0.07	35.99	1.38	0.04	0.04	0.34	0.12	0.23	0.00	100.55	92.83	4.58	2.59
VII-a3	57.66	0.07	1.33	5.27	0.16	34.62	0.53	0.10	0.01	0.60	0.09	0.00	0.00	100.46	91.3	7.7	1
VII-a4	57.62	0.04	1.91	4.91	0.15	34.62	0.41	0.02	0.00	0.70	0.00	0.00	0.19	100.57	91.9	7.2	0.9
VII-a6	57.25	0.00	2.67	5.28	0.10	34.02	0.55	0.15	0.02	0.78	0.23	0.11	0.16	101.33	91.1	7.9	1
B2-16	55.48	0.14	3.54	5.46	0.21	33.58	0.47	0.07	0.00	0.75	0.05	0.00	0.00	99.78	90.9	8.2	0.9
B6-7	56.98	0.00	2.39	5.38	0.04	34.08	0.36	0.22	0.00	0.75	0.27	0.21	0.04	100.73			
B7-11	58.15	0.11	2.04	4.88	0.17	34.94	0.69	0.10	0.00	0.76	0.21	0.00	0.01	102.07			
B7-19	53.82	0.00	4.90	5.07	0.08	31.06	4.22	0.14	0.02	2.03	0.00	0.00	0.00	101.41			
B8-1	57.44	0.00	2.28	5.43	0.12	33.71	1.20	0.05	0.00	0.84	0.07	0.13	0.10	101.49			
B8-2	57.25	0.07	2.77	5.33	0.16	34.02	0.63	0.12	0.00	0.68	0.06	0.00	0.08	101.16			
B8-3	56.54	0.05	3.16	5.92	0.21	33.50	0.53	0.11	0.00	0.77	0.14	0.00	0.05	100.97			
B8-4	58.08	0.00	2.42	5.20	0.11	34.57	0.97	0.17	0.00	0.56	0.05	0.06	0.09	102.29			
B8-6	57.40	0.06	1.51	5.21	0.20	34.22	0.67	0.03	0.00	0.53	0.00	0.08	0.02	99.94			
B8-7	57.55	0.03	2.93	5.31	0.01	34.29	0.51	0.11	0.00	0.86	0.11	0.06	0.00	101.85			
B8-9	56.96	0.09	3.04	5.52	0.24	33.93	0.60	0.09	0.00	0.91	0.00	0.00	0.00	101.38			
B8-12	56.93	0.00	3.25	5.81	0.03	33.97	0.52	0.18	0.00	0.92	0.18	0.28	0.09	102.20			

Grain	SiO2	TiO2	Al2O3	FeO	MnO	MgO	CaO	Na2O	K2O	Cr2O3	NiO	BaO	P2O5	Total	En	Fs	Wo
B8-13	58.82	0.10	1.13	4.24	0.06	34.92	1.38	0.17	0.00	0.50	0.07	0.00	0.14	101.53			
B8-14	56.61	0.03	3.19	5.71	0.15	33.53	0.58	0.04	0.00	0.89	0.23	0.01	0.00	100.98			
B11-12	55.53	0.21	3.85	5.48	0.12	33.43	0.54	0.18	0.05	0.74	0.13	0.00	0.07	100.43	90.8	8.2	1
B11-15	55.70	0.01	3.13	5.53	0.09	33.81	0.53	0.19	0.00	0.74	0.02	0.09	0.00	99.84	90.7	8.4	0.9
B11-1	55.28	0.05	3.48	5.55	0.00	33.34	0.75	0.06	0.00	0.70	0.16	0.00	0.17	99.55	90	8.4	1.6
B11-3	56.13	0.04	1.32	5.15	0.16	34.14	0.61	0.08	0.00	0.69	0.05	0.00	0.27	98.64	91.1	7.7	1.2
B11-4	55.86	0.00	3.34	5.64	0.15	33.92	0.43	0.21	0.00	0.73	0.13	0.03	0.24	100.69	90.6	8.4	0.94
B11-5	55.40	0.08	2.22	3.96	0.15	29.68	7.13	0.20	0.00	0.68	0.08	0.00	0.10	99.68	80.2	5.9	13.9
B11-6	55.97	0.06	2.70	5.24	0.12	33.16	1.54	0.18	0.00	0.58	0.19	0.06	0.16	99.97	89.1	7.8	3.1
B11-7	55.16	0.18	3.38	5.57	0.20	33.47	0.40	0.15	0.00	0.75	0.00	0.00	0.00	99.29	90.6	8.4	1
B11-8	55.97	0.08	2.52	5.05	0.24	33.88	1.02	0.05	0.02	0.74	0.00	0.17	0.04	99.78	90.7	7.5	1.8
B11-9	56.08	0.11	2.20	5.35	0.10	33.89	0.50	0.16	0.00	0.78	0.18	0.00	0.02	99.38	91	8.1	0.9
B11-13	55.58	0.09	3.09	5.61	0.16	33.57	0.57	0.04	0.00	0.67	0.16	0.07	0.04	99.65	90.3	8.4	1.3
B11-14	57.48	0.00	0.59	5.07	0.13	34.60	0.83	0.06	0.00	0.58	0.00	0.11	0.19	99.64	91.1	7.4	1.5
B11-14	57.15	0.07	0.67	4.94	0.15	34.55	0.94	0.08	0.00	0.49	0.00	0.03	0.00	99.07	90.9	7.3	1.8
Intergrown with diopside (B11-2')																	
B11-2	55.14	0.00	3.14	5.54	0.07	33.23	0.45	0.14	0.00	0.96	0.03	0.00	0.00	98.71	90.6	8.5	0.9
B11-2"	54.82	0.04	3.33	5.48	0.09	33.08	0.53	0.20	0.00	0.83	0.07	0.03	0.06	98.55	90.6	8.5	0.9
B11-2"'	55.35	0.04	3.21	5.34	0.23	33.41	0.64	0.09	0.00	0.84	0.08	0.00	0.14	99.39	90.6	8.2	1.2
Intergrown with olivine and diopside																	
III-2	57.29	0.06	2.41	6.37	0.14	34.38	0.22	0.19	0.01	0.15	0.03	0.00	0.04	101.32	90.26	9.36	0.38
III-8	56.58	0.00	2.29	5.67	0.18	34.48	1.17	0.07	0.00	0.74	0.03	0.04	0.08	101.23	89.6	8.26	2.14
III-10	56.88	0.00	2.18	5.87	0.20	34.98	0.72	0.11	0.00	0.56	0.15	0.05	0.00	101.69	90.24	8.54	1.22
III-14	56.89	0.00	2.18	5.69	0.16	34.78	0.71	0.26	0.00	0.68	0.15	0.00	0.03	101.51	90.49	8.28	1.23
III-15	55.95	0.00	2.46	5.70	0.06	33.75	0.76	0.03	0.00	0.63	0.16	0.02	0.04	99.58	90.02	8.51	1.47

II 6 - **Clinopyroxene**

Grain	SiO2	TiO2	Al2O3	FeO	MnO	MgO	CaO	Na2O	K2O	Cr2O3	NiO	Total	En	Fs	Wo	Ac
Green, containing chromite inclusions																
II-A	54.20	0.01	1.04	1.06	0.13	16.97	24.63	0.73	0.00	1.45	0.08	100.31	46.9	1.6	48.9	2.6
III-13	54.81	0.01	0.92	0.57	0.18	17.22	24.95	0.63	0.00	1.57	0.07	100.94	47.5	0.9	49.5	2.2
III-16	54.66	0.01	0.73	0.72	0.00	17.58	25.26	0.52	0.00	1.16	0.31	100.96	47.8	1.1	49.4	1.8
III-17	54.48	0.11	1.32	1.12	0.01	17.04	24.49	0.90	0.00	1.47	0.16	101.11	46.7	1.8	48.2	3.2
Colorless, intergrown with chromite																
II-75	54.64	0.07	0.61	0.63	0.05	17.58	25.26	0.64	0.00	1.45	0.11	101.04	47.6	1.0	49.1	2.3
Colorless to pale green, intergrown with olivine or enstatite																
III-1	53.14	0.16	2.94	1.92	0.00	16.71	24.64	0.10	0.00	0.94	0.24	100.80	47.1	3.1	49.9	0.0
III-5	53.56	0.00	2.54	2.05	0.13	16.95	24.80	0.35	0.00	1.10	0.10	101.57	46.6	3.2	49.0	1.3
III-7	53.49	0.12	2.58	2.02	0.07	17.36	24.22	0.27	0.00	1.05	0.05	101.23	47.8	3.1	48.2	0.9
III-12	53.51	0.00	2.22	2.18	0.00	17.74	24.68	0.16	0.00	0.99	0.14	101.61	48.2	3.4	48.5	0.0
III-13	53.29	0.16	2.25	1.90	0.07	17.04	24.65	0.32	0.00	1.21	0.13	101.02	46.9	3.1	48.8	1.2
III-16	52.65	0.02	3.00	2.17	0.03	16.45	24.39	0.03	0.00	1.11	0.12	99.96	46.8	3.5	49.8	0.0
B11-2'	52.50	0.17	3.40	1.86	0.00	16.28	24.17	0.48	0.01	1.22	0.05	100.13	46.1	2.8	49.2	1.9
Green, anhedral grains																
II-1	54.43	0.08	1.00	0.91	0.05	16.95	24.73	0.65	0.00	1.50	0.12	100.42	47.0	1.4	49.3	2.3
II-2	54.65	0.12	0.76	0.70	0.00	17.41	25.31	0.53	0.02	1.34	0.23	101.08	47.5	1.1	49.6	1.9
II-4	54.62	0.11	1.08	0.81	0.00	17.23	24.81	0.76	0.00	1.47	0.23	101.11	47.2	1.2	48.9	2.7
B1-80	53.72	0.10	1.04	0.82	0.00	16.81	24.41	0.48	0.03	1.57	0.06	99.05	47.4	1.3	49.5	1.8
B1-83	52.95	0.12	1.27	0.90	0.02	16.43	24.04	0.73	0.00	1.58	0.00	98.03	46.7	1.5	49.1	2.7
B1-84	53.34	0.14	1.30	1.02	0.00	16.54	23.42	0.85	0.00	1.85	0.14	98.58	47.2	1.6	48.1	3.1
B1-85	53.66	0.01	1.14	0.79	0.00	17.04	24.20	0.77	0.00	1.76	0.18	99.56	47.5	1.2	48.5	2.8
B1-86	53.77	0.08	1.22	0.98	0.01	16.23	23.94	0.72	0.00	1.60	0.02	98.57	46.5	1.6	49.3	2.7
B1-87	53.91	0.14	1.20	0.80	0.00	17.12	24.10	0.57	0.00	1.87	0.17	99.89	48.1	1.2	48.6	2.1

Grain	SiO2	TiO2	Al2O3	FeO	MnO	MgO	CaO	Na2O	K2O	Cr2O3	NiO	Total	En	Fs	Wo	Ac
B1-88	53.52	0.07	1.05	0.73	0.00	16.57	24.16	0.78	0.00	1.66	0.25	98.78	46.9	1.2	49.1	2.9
VI-89	54.44	0.10	1.18	0.73	0.00	16.90	24.92	0.59	0.00	1.79	0.11	100.75	46.9	1.2	49.8	2.2
VI-90	54.15	0.00	1.18	1.12	0.04	17.04	23.76	0.75	0.00	1.50	0.00	99.55	47.7	1.8	47.8	2.7
VI-91	54.64	0.00	1.06	0.72	0.00	17.15	24.82	0.69	0.00	1.70	0.14	100.92	47.3	1.1	49.2	2.5
VI-92	54.77	0.00	1.21	0.96	0.08	17.08	24.82	0.68	0.00	1.51	0.00	101.12	47.0	1.5	49.1	2.5
VII-a25	55.25	0.13	1.03	0.80	0.01	17.05	24.71	0.65	0.00	1.32	0.19	101.14	47.4	1.2	49.2	2.2
VII-a22	54.85	0.06	1.02	0.88	0.01	17.23	24.05	0.68	0.00	1.29	0.11	100.17	48.1	1.2	48.1	2.5
VII-a23	55.29	0.16	0.87	0.70	0.01	17.02	24.80	0.59	0.00	1.48	0.00	100.93	47.2	1.2	49.4	2.2
VII-a25	54.26	0.04	1.13	1.07	0.00	17.60	23.63	0.58	0.00	1.51	0.11	99.93	49.2	1.5	47.4	2.2
Colorless, euhedral grains																
IV-1	54.30	0.00	1.23	0.91	0.12	17.10	24.19	1.02	0.01	1.56	0.11	100.53	47.1	1.4	47.8	3.7
IV-4	54.64	0.00	0.89	0.94	0.00	17.30	24.64	0.69	0.00	1.51	0.15	100.76	47.5	1.4	48.6	2.5
IV-6	54.62	0.14	0.68	0.75	0.04	17.50	24.58	0.48	0.00	1.04	0.04	99.89	48.3	1.2	48.8	1.7
IV-7	54.21	0.00	1.06	0.99	0.00	17.04	23.64	0.94	0.01	1.59	0.08	99.57	47.6	1.5	47.5	3.4
IV-9	54.47	0.12	1.13	1.03	0.13	17.12	24.17	0.85	0.00	1.49	0.12	100.63	47.3	1.6	48.0	3.1
IV-10	54.84	0.06	1.10	0.91	0.14	17.19	24.27	0.85	0.01	1.50	0.10	100.99	47.5	1.4	48.1	3.0
IV-11	54.41	0.09	1.05	1.23	0.00	16.92	24.08	0.93	0.00	1.74	0.10	100.53	46.8	1.9	47.9	3.3
IV-12	54.67	0.08	0.92	0.94	0.00	17.18	24.60	0.91	0.00	1.68	0.05	101.01	47.0	1.4	48.4	3.2
IV-13	54.58	0.10	1.18	1.27	0.01	17.06	24.05	0.78	0.00	1.51	0.00	100.54	47.3	2.0	47.9	2.8
IV-14	54.58	0.18	1.22	0.90	0.00	17.17	24.40	0.84	0.01	1.65	0.18	101.15	47.3	1.4	48.3	3.0
IV-15	54.43	0.02	1.12	0.92	0.00	17.28	24.22	0.73	0.00	1.56	0.14	100.41	47.8	1.4	48.2	2.6
IV-16	54.26	0.07	1.17	1.24	0.00	17.08	24.04	0.81	0.02	1.48	0.24	100.41	47.3	1.9	47.9	2.9
Green, euhedral grains																
V-3	53.69	0.00	1.20	1.33	0.09	16.88	24.41	0.90	0.00	1.59	0.03	100.13	46.4	2.1	48.2	3.3
V-4	53.96	0.11	1.14	1.08	0.00	16.89	24.51	1.02	0.00	1.74	0.08	100.54	46.3	1.5	48.5	3.7
V-5	53.46	0.04	1.17	1.00	0.03	16.94	24.15	0.76	0.02	1.40	0.16	99.12	47.4	1.5	48.3	2.8
V-6	53.83	0.01	1.00	1.10	0.07	17.07	24.79	0.80	0.00	1.45	0.02	100.13	46.7	1.8	48.8	2.7
V-7	53.90	0.11	0.94	0.89	0.00	17.30	25.07	0.65	0.00	1.38	0.05	100.30	47.0	1.5	49.1	2.4

Grain	SiO2	TiO2	Al2O3	FeO	MnO	MgO	CaO	Na2O	K2O	Cr2O3	NiO	Total	En	Fs	Wo	Ac
V-8	53.66	0.00	1.01	1.08	0.07	17.08	24.85	0.78	0.01	1.47	0.07	100.07	46.8	1.5	48.9	2.7
V-9	53.80	0.14	1.38	1.17	0.00	17.19	24.50	0.95	0.00	1.76	0.04	100.94	46.8	1.8	48.0	3.3
V-10	54.10	0.05	0.49	0.88	0.05	17.90	25.31	0.57	0.00	0.99	0.00	100.35	47.9	1.2	48.8	2.1
V-11	53.66	0.08	1.15	1.18	0.09	17.31	24.31	0.95	0.00	1.44	0.05	100.21	47.3	1.8	47.6	3.3
V-12	53.75	0.00	1.06	0.94	0.00	17.21	24.56	1.01	0.00	1.52	0.40	100.44	46.9	1.5	48.1	3.6
V-13	53.66	0.04	0.80	0.95	0.00	17.61	25.02	0.55	0.00	1.34	0.11	100.09	47.8	1.5	49.0	1.8
V-14	53.88	0.19	1.15	0.96	0.00	17.31	24.85	0.78	0.00	1.57	0.06	100.76	47.1	1.5	48.6	2.7
V-15	54.02	0.00	0.85	1.01	0.01	17.44	25.11	0.70	0.00	1.30	0.14	100.58	47.2	1.5	49.0	2.4
V-16	53.53	0.02	1.25	1.27	0.00	17.21	24.32	1.00	0.00	1.75	0.15	100.50	46.8	1.8	47.7	3.6
V-17	54.13	0.09	1.02	1.13	0.15	17.31	24.60	0.90	0.00	1.38	0.06	100.75	47.1	1.8	48.0	3.0
V-18	53.82	0.00	1.29	1.03	0.05	17.08	24.57	0.88	0.00	1.45	0.23	100.39	47.0	1.5	48.5	3.1
V-19	54.04	0.06	1.12	1.07	0.00	17.40	24.42	0.93	0.00	1.46	0.25	100.75	47.4	1.5	47.7	3.3
V-20	54.13	0.00	0.85	0.71	0.01	17.35	25.04	0.61	0.05	1.44	0.06	100.25	47.4	1.2	49.2	2.1
V-21	54.24	0.03	1.11	0.88	0.19	17.49	24.89	0.73	0.00	1.36	0.00	100.91	47.7	1.2	48.6	2.4
V-22	53.98	0.13	1.32	1.15	0.00	17.11	24.71	0.94	0.00	1.51	0.04	100.89	46.5	1.8	48.3	3.3
Slight green, anhedral grains																
B3-6	54.66	0.35	0.57	3.32	0.10	16.85	24.69	0.73	0.00	0.13	0.00	101.40	45.1	5.1	47.5	2.4
B3-6'	52.71	0.42	0.61	3.84	0.08	15.67	24.12	0.64	0.00	0.15	0.10	98.35				
B3-16	52.42	0.73	1.44	4.27	0.07	15.21	24.33	0.58	0.02	0.13	0.00	99.20	42.4	6.7	48.8	2.1
Dark green grain																
III-21	52.88	0.04	2.89	2.30	0.00	16.18	24.95	0.22	0.00	1.29	0.00	100.76	45.7	3.7	50.6	0.0
Augite, yellow brown, hexagon																
B3-8	53.29	0.00	0.28	7.14	0.36	13.74	25.35	0.26	0.00	0.07	0.01	100.49	37.9	11.0	50.2	0.9
Augite, colorless, prism																
B10-1	53.27	0.03	0.71	6.75	0.27	13.60	25.28	0.20	0.00	0.07	0.00	100.17	38.3	10.6	51.1	

II 7 - Amphibole, Biotite and Phlogopite

Grains	B3-1'	B3-21	B3-38	B3-24	B3-1	B3-28	B3-29	B3-30	B3-32
	Amph	**Amph**	**Amph**	**Biotite**	**Phlog**	**Phlog**	**Phlog**	**Phlog**	**Phlog**
SiO2	43.17	42.28	41.99	37.65	38.55	38.80	37.65	38.50	35.75
TiO2	2.88	2.89	2.93	1.27	2.22	2.15	1.88	2.55	1.70
Al2O3	10.60	10.36	10.42	19.68	13.03	13.60	12.50	13.66	11.79
FeO	8.27	8.14	8.84	15.71	7.74	7.64	6.79	8.25	6.88
MnO	0.00	0.02		0.12	0.14	0.17	0.06	0.00	0.09
MgO	16.41	15.49	15.63	11.35	21.40	21.44	20.18	20.43	21.10
CaO	11.71	11.80	11.52	0.01	0.14	0.00	0.58	0.01	0.13
Na2O	3.09	2.70	2.93	0.45	1.39	1.36	2.13	1.72	2.04
K2O	1.33	1.34	1.38	7.77	4.86	7.48	3.50	6.84	6.11
Cr2O3	0.24	0.19		0.05	0.04	0.00	0.00	0.03	0.02
NiO	0.00	0.00		0.00	0.11	0.00	0.12	0.07	0.08
BaO	0.14	0.07		0.17	0.18	0.58	0.00	0.32	2.15
P2O5	0.17	0.05		0.03	0.00	0.17	0.07	0.03	0.16
Total	98.00	95.33	95.65	94.27	89.94	93.39	85.46	92.42	87.99
Si	6.58	6.62	6.56	6.12	6.34	6.22	6.40	6.22	6.20
Al	1.90	1.92	1.92	3.76	2.52	2.56	2.52	2.60	2.40
Ti	0.34	0.34	0.34	0.14	0.26	0.26	0.24	0.32	0.22
Fe	1.06	1.06	1.16	2.14	1.06	1.04	0.96	1.10	0.98
Mg	3.72	3.62	3.64	2.76	5.23	5.14	5.14	4.92	5.44
Ca	1.92	1.99	1.93						
Na	0.91	0.82	0.89	0.14	0.43	0.44	0.70	0.56	0.68
K	0.26	0.26	0.28	1.61	1.01	1.54	0.76	1.42	1.34
Mg/ Mg+Fe	0.78	0.77	0.76	0.56	0.83	0.84	0.84	0.82	0.85

II 8 - Chlorite

Grain	SiO2	TiO2	Al2O3	FeO	MnO	MgO	CaO	Na2O	K2O	Cr2O3	NiO	BaO	P2O5	Total
VII-b1	32.56	0.08	13.13	0.56	0.00	33.25	0.00	0.00	0.00	4.62	0.62	0.00	0.00	84.81
VII-b2	34.31	0.00	13.65	0.18	0.15	33.99	0.07	0.00	0.00	1.45	0.59	0.09	0.00	84.47
B2-19	34.13	0.01	12.10	1.47	0.00	34.52	0.00	0.17	0.00	0.66	0.00	0.00	0.07	83.14
B3-1	38.55	2.22	13.03	7.74	0.14	21.40	0.14	1.39	4.86	0.04	0.11	0.18	0.00	89.94
B4-1	33.60	0.16	15.42	0.97	0.00	32.22	0.26	0.05	0.15	2.21	0.43	0.17	0.00	85.66
B4-3	33.80	0.11	14.23	0.85	0.03	34.16	0.01	0.04	0.02	3.40	0.77	0.00	0.11	87.42
B4-4	32.42	0.10	16.27	0.84	0.00	33.80	0.05	0.18	0.00	2.45	0.49	0.07	0.24	86.69
B4-5	32.22	0.04	14.58	0.68	0.00	32.12	0.09	0.00	0.00	3.12	0.62	0.10	0.05	83.58
B4-6	35.12	0.13	14.06	0.94	0.00	33.81	0.14	0.00	0.17	2.02	0.74	0.12	0.12	87.27
B4-7	31.61	0.14	15.23	1.11	0.16	32.88	0.01	0.15	0.00	2.48	0.52	0.00	0.09	84.32
B4-8	33.90	0.01	13.86	0.80	0.05	34.37	0.00	0.02	0.01	4.34	0.75	0.07	0.07	88.18
B6-12	33.27	0.24	14.18	0.77	0.06	32.23	0.02	0.04	0.07	2.72	0.74	0.00	0.12	84.34
B6-17	34.35	0.06	10.98	0.93	0.00	33.95	0.00	0.08	0.04	4.25	0.72	0.08	0.05	85.45
B8-11	33.53	0.11	14.55	0.55	0.06	33.11	0.03	0.03	0.00	2.43	0.59	0.00	0.17	85.00
B9-14	35.72	0.00	12.59	0.63	0.00	35.91	0.00	0.37	0.02	0.08	0.00	0.09	0.00	85.42
B11-1	33.40	0.03	12.07	0.64	0.02	33.75	0.04	0.05	0.00	4.45	0.54	0.08	0.07	85.05

Grain	SiO2	TiO2	Al2O3	FeO	MnO	MgO	CaO	Na2O	K2O	Cr2O3	NiO	BaO	P2O5	Total
B11-2	31.46	0.16	16.34	0.87	0.01	32.83	0.00	0.06	0.00	3.19	0.70	0.00	0.00	85.63
B11-3	33.46	0.18	10.08	0.70	0.00	33.93	0.02	0.02	0.00	5.73	0.56	0.00	0.05	84.69
B11-9	33.33	0.24	15.86	0.84	0.00	33.38	0.28	0.06	0.08	2.48	0.57	0.07	0.00	87.18
B11-7	32.74	0.00	12.83	0.61	0.09	32.78	0.00	0.02	0.00	4.04	0.44	0.03	0.03	83.59
B11-8	34.98	0.10	9.69	0.89	0.00	34.64	0.02	0.11	0.00	5.06	0.66	0.00	0.02	86.15
B11-10	33.24	0.17	15.06	0.59	0.05	32.99	0.01	0.08	0.02	2.08	0.51	0.00	0.00	84.82
III-12	32.58	0.14	13.75	0.71	0.00	33.67	0.02	0.05	0.00	2.91	0.51	0.07	0.05	84.44
I-64	34.13	0.03	12.19	0.35	0.12	35.97	0.00	0.22	0.02	2.66	0.05	0.02	0.02	85.75
I-66	33.83	0.12	10.09	0.42	0.00	35.17	0.07	0.00	0.04	6.71	0.65	0.00	0.04	87.09
II-76	36.14	0.00	7.80	0.46	0.00	37.88	0.00	0.14	0.00	4.19	0.01	0.08	0.08	86.83
II-81	36.59	0.02	6.73	0.39	0.00	36.94	0.03	0.24	0.03	5.51	0.00	0.01	0.00	86.49
III-3	33.94	0.10	11.99	1.00	0.11	35.07	0.08	0.02	0.00	1.71	1.72	0.00	0.11	85.73
III-11	34.88	0.01	12.52	0.39	0.05	35.44	0.00	0.03	0.02	1.16	0.61	0.00	0.06	85.12
Icr31-A-1	31.69		13.50	0.45		35.57				4.22				85.42
Icr31-A-2	32.21		12.71	0.52		35.45				3.03				83.91
Icr31-A-3	32.76		12.40	0.29		36.41				3.13				84.98
Icr31-A-4	32.23		12.57	0.44		35.64				4.51	0.75			86.14
Icr31-A-5	32.75		10.31	0.29		36.20				6.27				85.81
Icr31-A-6	33.16		10.83			36.66		0.26		4.65				85.55

II 9 - Serpentine

Grain	SiO2	TiO2	Al2O3	FeO	MnO	MgO	CaO	Na2O	K2O	Cr2O3	NiO	P2O5	BaO	Total
I-27	42.05	0.02	1.39	1.12	0.03	41.70	0.09	0.13	0.00	1.71	0.25	0.00	0.00	88.51
I-63	42.28	0.00	1.56	1.01	0.06	41.11	0.06	0.33	0.00	1.72	0.17	0.06	0.05	88.41
II-B	43.28	0.00	0.00	0.95	0.01	37.63	0.09	0.04	0.02	0.21	0.56	0.05	0.07	82.98
II-C	40.65	0.11	3.07	1.36	0.00	37.33	0.20	0.12	0.00	2.50	0.47	0.09	0.00	85.96
II-D	42.18	0.00	0.07	2.11	0.07	35.07	0.24	0.00	0.00	0.44	0.92	0.18	0.21	81.55
II-74	42.19	0.02	1.11	1.84	0.03	39.11	0.19	0.16	0.00	1.12	0.00	0.00	0.00	85.78
II-77	43.18	0.00	0.70	0.85	0.00	39.95	0.03	0.15	0.00	0.67	0.23	0.06	0.00	85.87
II-78	43.15	0.00	0.09	1.78	0.11	38.07	0.15	0.05	0.00	0.52	0.69	0.00	0.05	84.69
II-79	42.70	0.05	1.06	1.01	0.09	39.67	0.05	0.07	0.00	0.72	0.46	0.04	0.00	85.95
II-82	42.45	0.10	1.62	0.63	0.14	38.27	0.11	0.17	0.02	0.69	0.35	0.12	0.00	84.70
II-84	41.34	0.00	2.44	0.59	0.00	39.40	0.07	0.19	0.00	2.22	0.35	0.08	0.00	86.68
II-83	41.49	0.20	2.80	0.69	0.00	39.25	0.10	0.11	0.00	2.39	0.25	0.13	0.00	87.46
III-2	40.87	0.06	2.38	1.04	0.01	39.37	0.03	0.27	0.00	1.55	0.02	0.20	0.03	85.81
III-4	42.21	0.13	0.76	1.65	0.00	37.67	0.08	0.07	0.00	0.77	0.32	0.15	0.00	83.83
III-5	41.93	0.00	0.89	2.19	0.02	36.83	0.14	0.00	0.05	0.22	0.54	0.07	0.00	82.89
III-6	38.70	0.04	0.79	2.53	0.14	29.91	0.24	0.00	0.02	0.77	0.38	0.12	0.00	73.75
III-7	42.82	0.00	0.91	2.43	0.09	36.11	0.14	0.07	0.00	1.77	0.52	0.08	0.00	85.02
III-8	40.76	0.00	1.32	2.42	0.00	33.81	0.07	0.04	0.01	0.75	0.40	0.17	0.23	80.06
III-9	40.75	0.00	1.06	2.24	0.06	33.22	0.17	0.01	0.03	0.86	0.53	0.12	0.00	79.13
III-10	39.71	0.09	0.78	2.81	0.09	28.00	0.12	0.00	0.05	1.14	2.13	0.10	0.00	75.09
B6-2	43.93	0.07	0.63	3.05	0.07	39.05	0.11	0.12	0.00	0.00	0.08	0.12	0.00	87.23
B6-9	34.92	0.04	0.05	7.30	0.11	41.17	0.67	0.19	0.05	0.01	0.47	0.08	0.00	85.07

II 10 - Plagioclase and K-feldspar

Grain	SiO2	TiO2	Al2O3	FeO	MnO	MgO	CaO	Na2O	K2O	Cr2O3	NiO	BaO	Total	An	Ab	Or
Plagioclase																
B2-3'	59.39	0.00	24.65	0.00	0.00	0.03	7.02	7.40	0.10	0.05	0.00	0.04	98.67	33.9	65.3	0.8
B2-9	61.35	0.00	23.24	0.11	0.00	0.08	5.49	7.29	0.70	0.03	0.00	0.26	98.54	28.0	67.8	4.2
B2-18	60.40	0.00	24.11	0.16	0.06	0.02	6.01	7.48	0.31	0.00	0.05	0.03	98.64	30.0	68.3	1.7
B2-25	61.68	0.03	23.44	0.00	0.00	0.00	5.46	7.77	0.08	0.00	0.05	0.00	98.51	28.0	72.0	
B2-31	59.36	0.04	24.48	0.02	0.07	0.06	6.82	7.47	0.09	0.01	0.00	0.02	98.43	33.3	66.7	
B2-34	61.20	0.08	24.04	0.03	0.07	0.00	5.77	8.25	0.01	0.08	0.12	0.00	99.66	28.2	71.8	
B2-55	62.25	0.05	24.36	0.00	0.00	0.10	5.95	8.22	0.09	0.00	0.07	0.00	101.09	28.5	71.5	
B2-57	60.53	0.01	25.45	0.02	0.14	0.06	7.36	7.45	0.18	0.00	0.02	0.02	101.24	35.2	64.0	0.8
B6-16	60.94	0.00	25.06	0.00	0.07	0.08	6.86	7.87	0.01	0.00	0.03	0.00	100.92	32.8	67.2	
B6-3	60.79	0.00	25.37	0.00	0.03	0.14	6.97	7.38	0.03	0.00	0.02	0.00	100.75	34.2	65.8	
B6-4	62.37	0.00	24.07	0.00	0.00	0.00	5.70	7.57	0.05	0.00	0.00	0.20	99.96	29.6	70.4	
B6-10	62.08	0.00	24.42	0.00	0.05	0.06	5.95	8.37	0.11	0.05	0.00	0.03	101.11	28.2	71.8	
B6-11	62.82	0.00	24.34	0.05	0.07	0.08	5.77	6.70	0.07	0.01	0.00	0.12	100.03	32.1	67.9	
B7-9	60.59	0.00	25.57	0.01	0.10	0.04	7.50	7.17	0.02	0.00	0.03	0.00	101.03	36.4	63.6	
B9-6	62.97	0.02	25.93	0.03	0.00	0.06	6.71	7.87	0.04	0.11	0.12	0.00	103.86	32.2	67.8	
B9-9	57.51	0.09	27.78	0.17	0.07	0.02	10.00	5.45	0.21	0.09	0.18	0.00	101.57	49.6	49.6	0.8
K-feldspar																
B2-15	63.71	0.06	18.54	0.04	0.00	0.06	0.12	1.23	14.47	0.02	0.15	1.39	99.81		11.5	88.5
B2-32	63.12	0.00	18.15	0.00	0.01	0.00	0.05	1.19	14.18	0.07	0.00	1.23	98.01		11.6	88.4
B2-35	64.73	0.08	18.48	0.00	0.04	0.10	0.03	2.21	11.25	0.00	0.01	0.56	97.50		22.9	77.1
B2-54	65.70	0.00	18.66	0.00	0.00	0.00	0.01	1.41	14.04	0.00	0.01	0.72	100.54		13.6	86.4

II 11 - Alloys

Grain	Zn	Cu	Fe	As	S	Ni	Mn	Co	Ag	Au	Sn	Pb	Sb	W	Bi	Cr	Ti	Si	Al	Total
Fe-Si alloy																				
4	0.00	0.00	45.37	0.16	0.09	0.00	0.02	0.17	0.11	0.40	0.07	0.25	0.00	0.00	0.00	0.00	0.03	56.16	0.15	102.98
7	0.00	0.00	45.05	0.24	0.17	0.04	0.03	0.16	0.00	0.51	0.16	0.00	0.00	0.00	0.39	0.09	0.00	56.02	0.21	103.08
5	0.01	0.00	44.73	0.25	0.11	0.00	0.18	0.00	0.02	0.51	0.29	0.08	0.01	0.00	0.27	0.00	0.00	55.94	0.05	102.44
75	0.18	0.00	44.62	0.11	0.09	0.00	0.11	0.09	0.12	0.43	0.10	0.19	0.00	0.00	0.07	0.00	0.03	55.81	0.10	102.06
76	0.17	0.00	44.43	0.21	0.15	0.00	0.05	0.12	0.10	0.25	0.10	0.00	0.00	0.00	0.31	0.03	0.10	55.52	0.18	101.73
Fe-Si alloy (two sections from one grain)																				
8	0.23	0.14	44.57	0.13	0.19	0.00	0.19	0.02	0.00	0.44	0.18	0.00	0.00	0.00	0.67	0.07	0.08	56.04	0.05	102.99
9	0.12	0.00	44.82	0.19	0.12	0.00	0.21	0.31	0.00	0.45	0.18	0.05	0.03	0.00	0.32	0.23	0.00	56.10	0.07	103.21
12	0.00	0.16	44.62	0.14	0.13	0.06	0.24	0.13	0.02	0.58	0.28	0.01	0.04	0.00	0.35	0.11	0.00	55.68	0.05	102.61
14	0.05	0.00	45.06	0.14	0.07	0.04	0.33	0.34	0.06	0.28	0.11	0.18	0.00	0.00	0.17	0.23	0.00	55.92	0.02	103.00
1_1	0.24	0.00	44.83	0.28	0.17	0.00	0.15	0.00	0.00	0.44	0.15	0.00	0.00	0.00	0.48	0.13	0.02	55.11	0.11	102.11
1_2	0.00	0.15	44.50	0.18	0.20	0.03	0.23	0.06	0.06	0.50	0.35	0.00	0.08	0.00	0.56	0.19	0.05	55.77	0.11	103.00
1_3	0.00	0.03	44.66	0.17	0.13	0.00	0.22	0.39	0.16	0.28	0.28	0.00	0.08	0.00	0.07	0.17	0.06	55.76	0.00	102.46
4,	0.00	0.15	44.52	0.20	0.17	0.04	0.33	0.29	0.00	0.50	0.03	0.00	0.00	0.00	0.44	0.38	0.00	54.99	0.14	102.18
5,	0.00	0.11	44.87	0.23	0.20	0.00	0.31	0.11	0.00	0.66	0.16	0.00	0.00	0.00	0.57	0.14	0.00	55.94	0.10	103.40
6,	0.00	0.00	44.30	0.15	0.19	0.00	0.18	0.18	0.17	0.49	0.14	0.00	0.00	0.00	0.42	0.08	0.00	55.83	0.02	102.14
7,	0.00	0.00	44.77	0.30	0.24	0.00	0.10	0.16	0.00	0.53	0.25	0.00	0.00	0.00	0.73	0.10	0.00	55.72	0.08	102.97

Grain	Zn	Cu	Fe	As	S	Ni	Mn	Co	Ag	Au	Sn	Pb	Sb	W	Bi	Cr	Ti	Si	Al	Total
8,	0.00	0.12	44.60	0.20	0.09	0.11	0.31	0.00	0.01	0.40	0.05	0.19	0.00	0.00	0.10	0.00	0.01	55.80	0.00	101.99
9,	0.00	0.00	44.80	0.23	0.15	0.06	0.33	0.12	0.00	0.58	0.20	0.04	0.00	0.00	0.26	0.15	0.00	55.92	0.06	102.90
10,	0.02	0.00	44.74	0.15	0.09	0.04	0.20	0.15	0.15	0.46	0.00	0.13	0.00	0.00	0.09	0.15	0.00	56.14	0.09	102.60
11,	0.07	0.00	44.36	0.19	0.10	0.01	0.25	0.14	0.02	0.43	0.00	0.09	0.00	0.00	0.18	0.06	0.00	55.88	0.04	101.82
12,	0.00	0.08	44.49	0.13	0.11	0.01	0.10	0.07	0.08	0.52	0.20	0.23	0.00	0.00	0.10	0.08	0.00	56.00	0.00	102.20
13,	0.09	0.00	44.64	0.06	0.19	0.07	0.12	0.19	0.00	0.65	0.18	0.00	0.00	0.00	0.32	0.08	0.01	56.09	0.00	102.70
14,	0.16	0.00	45.02	0.16	0.15	0.00	0.22	0.00	0.00	0.68	0.11	0.23	0.00	0.00	0.16	0.12	0.00	55.73	0.00	102.75
15,	0.23	0.08	44.81	0.22	0.17	0.00	0.40	0.00	0.00	0.46	0.27	0.00	0.07	0.00	0.25	0.00	0.01	55.81	0.11	102.89
Fe-Ni alloy (in pentlandite)																				
66	0.41	0.02	27.35	0.00	0.14	70.08	0.01	0.73	0.00	0.16	0.00	0.00	0.00	0.16	0.11	0.00	0.02	0.00	0.00	99.20
68	0.22	0.71	24.69	0.17	0.05	74.00	0.03	0.15	0.12	0.14	0.11	0.00	0.03	0.08	0.13	0.00	0.00	0.00	0.05	100.68

SiC (carbon was not measured but was assumed to be the missing element, i.e. by difference)

	Si	Ti	Al	Fe	Mn	Mg	Ca	Cr	Ni	Ba	C	**Total**		
B10-1	69.78	0.00	0.00	0.04	0.03	0.02	0.00	0.02	0.00	0.00	30.12	99.90		
B10-2	69.80										30.01	99.80		
B10-3	69.76										30.14	99.90		

II 12 - Chromite

Grain	SiO2	TiO2	Al2O3	FeO	MnO	MgO	CaO	Na2O	K2O	Cr2O3	NiO	Total	Mg#	Cr#	Fe#
		Euhedral grains													
I-1	0.19	0.27	10.44	15.45	0.32	14.38	0.00	0.17	0.00	59.18	0.06	100.47	68.8	79.1	5.1
I-2	0.15	0.23	10.36	14.95	0.17	14.36	0.07	0.10	0.02	59.77	0.17	100.36	68.6	79.5	4.4
I-3	0.10	0.26	10.41	14.19	0.43	14.68	0.00	0.16	0.00	59.89	0.04	100.17	70.4	79.3	4.2
I-4	0.09	0.21	10.42	14.15	0.33	14.76	0.06	0.09	0.00	59.52	0.00	99.62	70.8	79.3	4.4
I-5	0.13	0.32	10.25	12.93	0.24	15.68	0.00	0.17	0.01	60.78	0.07	100.59	74	79.9	4.2
I-6	0.23	0.12	10.18	16.32	0.36	13.56	0.06	0.06	0.00	59.18	0.28	100.34	65.5	79.6	4.8
I-7	0.21	0.30	9.87	14.30	0.04	14.93	0.06	0.16	0.03	60.11	0.18	100.18	71.3	80.3	4.9
I-8	0.36	0.31	10.26	14.20	0.23	14.82	0.06	0.10	0.02	59.76	0.09	100.22	70.8	78.9	4.5
I-9	0.14	0.28	10.62	14.87	0.19	14.61	0.04	0.03	0.06	60.27	0.23	101.33	68.9	79.3	4.2
I-10	0.18	0.33	10.30	14.70	0.22	14.79	0.04	0.19	0.01	60.21	0.26	101.23	70.1	79.6	4.7
I-11	0.19	0.22	10.43	14.66	0.45	14.78	0.05	0.12	0.00	59.72	0.23	100.86	70.4	79.4	4.8
I-12	0.22	0.19	10.10	15.64	0.45	13.90	0.08	0.19	0.00	59.70	0.01	100.49	67.1	79.8	4.6
I-13	0.11	0.27	9.58	14.38	0.00	14.68	0.06	0.13	0.03	60.12	0.20	99.55	71	80.9	4.9
I-14	0.23	0.15	10.23	14.09	0.15	15.41	0.04	0.17	0.01	59.92	0.22	100.62	73.2	79.7	5.4
I-16	0.13	0.13	10.16	14.11	0.15	15.51	0.05	0.17	0.00	59.59	0.03	100.04	73.7	79.7	5.8
I-17	0.16	0.20	9.98	14.35	0.30	14.86	0.02	0.05	0.00	59.85	0.09	99.85	71.1	80	4.9
I-18	0.13	0.20	9.88	14.05	0.35	15.32	0.01	0.22	0.00	60.17	0.07	100.41	73.3	80.4	5.5
I-19	0.09	0.29	10.22	15.63	0.40	14.16	0.03	0.12	0.01	59.56	0.11	100.63	67.6	79.6	4.8
I-20	0.15	0.27	10.33	14.30	0.40	15.20	0.00	0.11	0.04	60.42	0.00	101.20	71.7	79.7	4.7
II-1	0.12	0.07	10.10	15.04	0.43	14.63	0.02	0.17	0.00	59.73	0.20	100.50	69.9	79.8	5.1

Grain	SiO2	TiO2	Al2O3	FeO	MnO	MgO	CaO	Na2O	K2O	Cr2O3	NiO	Total	Mg#	Cr#	Fe#
II-2	0.12	0.28	10.40	16.62	0.13	13.55	0.05	0.07	0.04	58.73	0.10	100.08	65.4	79.1	5.1
II-3	0.14	0.19	10.20	14.70	0.24	14.44	0.06	0.17	0.03	60.10	0.05	100.32	69	79.8	4.2
II-4	0.10	0.19	10.14	16.34	0.35	13.69	0.07	0.13	0.00	58.57	0.07	99.65	66.6	79.5	5.5
II-6	0.25	0.23	10.45	14.27	0.00	15.14	0.08	0.05	0.00	60.47	0.29	101.25	71.7	79.6	4.8
II-7	0.19	0.19	10.80	13.35	0.33	15.48	0.02	0.07	0.00	59.93	0.07	100.44	73.2	78.9	4.4
II-8	0.15	0.28	10.24	14.26	0.63	14.89	0.02	0.03	0.00	60.87	0.00	101.39	70.8	80	4.8
II-10	0.18	0.21	10.25	16.15	0.37	13.81	0.06	0.11	0.00	59.62	0.08	100.85	66	79.7	4.7
VI-4	0.20	0.23	10.51	14.25	0.07	14.08	0.00			59.53	0.05	98.91	68.1	79.2	3.38
VI-6	0.17	0.27	10.01	15.68	0.23	13.41	0.00			59.20	0.11	99.07	65.1	79.9	3.9
I-21	0.20	0.25	13.94	23.29	0.20	10.21	0.01	0.28	0.00	51.96	0.00	100.33	49.4	71.4	6.3
I-22	0.09	0.24	13.45	22.83	0.17	10.78	0.00	0.11	0.03	52.85	0.04	100.60	51.9	71.1	6.8
IV-23	0.12	0.23	15.28	20.76	0.32	11.16	0.06	0.09	0.03	52.80	0.00	100.85	53.2	69.8	4.2
		Euhedral chromite with high Fe													
IV-62	0.28	0.17	10.16	26.24	0.44	8.97	0.00	0.06	0.00	54.67	0.07	101.05	44.3	78.3	8.4
IV-63	0.17	0.25	8.04	28.42	0.64	7.44	0.04	0.16	0.01	55.11	0.04	100.33	37.5	82.2	10.1
IV-64	0.18	0.29	10.19	25.67	0.34	8.74	0.02	0.13	0.03	55.36	0.08	101.03	43.3	78.5	7.2
IV-61	0.24	0.32	7.97	27.32	0.28	7.67	0.00	0.22	0.00	57.06	0.18	101.26	38.5	82.8	7.6
IV-54	0.16	0.32	9.08	24.83	0.23	8.88	0.08	0.07	0.04	57.10	0.00	100.80	44.1	80.9	6.7
IV-59	0.18	0.37	8.95	27.65	0.22	9.69	0.01	0.10	0.00	52.50	0.19	99.86	48.2	79.7	12.8
IV-60	0.17	0.22	10.39	22.60	0.18	9.89	0.00	0.12	0.14	57.94	0.06	101.71	48.3	79	5
VI-10	0.27	0.08	10.28	22.55	0.19	9.40	0.08			56.16	0.17	99.17	47	78.6	5.2
		Anhedral grains													
VI-14	0.15	0.16	10.77	13.45	0.40	14.45	0.01			60.87	0.12	100.39	69.1	79.2	2.65
VI-15	0.17	0.12	10.37	13.92	0.27	14.75	0.06			60.34	0.03	100.03	70.6	79.6	3.9
VI-16	0.07	0.11	10.54	13.61	0.46	14.47	0.08			60.65	0.20	100.19	69.4	79.4	3.1
VI-17	0.15	0.13	11.38	15.26	0.26	13.55	0.02			59.13	0.23	100.12	65.1	77.7	3.2
VI-18	0.17	0.09	8.19	15.96	0.44	13.01	0.04			62.90	0.00	100.79	63.1	83.8	3.4

Grain	SiO2	TiO2	Al2O3	FeO	MnO	MgO	CaO	Na2O	K2O	Cr2O3	NiO	Total	Mg#	Cr#	Fe#
VI-19	0.12	0.21	10.67	13.15	0.12	14.68	0.00			60.25	0.00	99.20	70.6	79.1	3
VI-28	0.18	0.22	9.93	13.82	0.18	14.81	0.00			60.99	0.05	100.17	71.2	80.5	4.2
		Intergrown with serpentine													
I-23	0.12	0.33	9.93	13.81	0.42	14.99	0.00	0.04	0.01	60.47	0.41	100.53	71.8	80.3	4.4
I-24	0.18	0.16	9.46	14.06	0.21	14.96	0.08	0.09	0.00	61.12	0.00	100.31	71.8	80.5	4.7
I-26	0.20	0.18	10.35	13.06	0.17	15.37	0.04	0.02	0.00	61.20	0.19	100.78	72.6	79.8	3.7
II-1	0.16	0.29	10.49	13.38	0.08	14.93	0.00	0.02	0.05	60.69	0.09	100.19	71.2	79.6	3.5
II-8	0.15	0.22	10.06	14.50	0.34	15.27	0.05	0.26	0.02	60.06	0.19	101.12	72.5	80	5.6
II-11	0.16	0.20	10.33	13.76	0.13	15.07	0.07	0.13	0.00	60.65	0.29	100.80	71.6	79.8	4.2
II-14	0.22	0.22	10.04	13.45	0.04	15.68	0.08	0.13	0.00	60.48	0.13	100.48	74.5	80.2	5.1
II-23	0.13	0.29	10.16	13.88	0.34	15.67	0.11	0.13	0.00	59.65	0.17	100.52	74.2	79.7	5.5
II-25	0.19	0.15	10.86	13.32	0.29	15.55	0.01	0.12	0.00	60.19	0.18	100.86	73.6	78.9	4.4
II-4	0.16	0.11	10.43	13.97	0.32	14.54	0.00	0.06	0.00	60.46	0.13	100.17	69.5	79.5	3.5
II-7	0.09	0.28	10.46	13.43	0.22	15.45	0.00	0.15	0.03	60.90	0.07	101.07	72.8	79.7	4.2
II-9	0.16	0.16	10.71	14.47	0.52	14.95	0.04	0.06	0.04	59.82	0.00	100.93	71.8	79	5.3
II-12	0.10	0.43	10.22	12.83	0.19	16.15	0.00	0.10	0.00	60.47	0.26	100.74	76	79.9	5
II-15	0.15	0.22	10.72	13.44	0.11	15.48	0.00	0.02	0.00	59.38	0.17	99.70	73.6	78.8	4.7
II-16	0.08	0.33	11.33	13.43	0.26	15.56	0.03	0.11	0.00	58.53	0.26	99.90	74.2	77.7	5
II-17	0.13	0.34	10.61	13.72	0.21	15.03	0.02	0.00	0.00	58.95	0.03	99.03	72.2	78.8	4.6
II-18	0.18	0.21	11.17	12.67	0.25	15.97	0.00	0.15	0.04	59.83	0.06	100.54	75.2	78.3	4.4
II-19	0.19	0.27	11.26	12.76	0.10	16.15	0.05	0.18	0.00	60.26	0.08	101.30	75.4	78.2	4.4
II-24	0.16	0.23	9.95	14.28	0.19	15.58	0.03	0.08	0.02	60.41	0.26	101.20	73.7	80.3	5.8
II-26	0.21	0.26	10.32	13.21	0.51	15.05	0.09	0.00	0.04	60.05	0.12	99.87	71.8	79.5	3.7
III-10	0.11	0.23	10.50	13.80	0.07	15.36	0.07	0.17	0.01	60.07	0.05	100.42	72.7	79.3	4.7
III-11	0.09	0.25	10.63	14.01	0.09	14.89	0.00	0.14	0.00	60.24	0.00	100.34	70.8	79.2	4
III-12	0.15	0.27	10.15	14.04	0.31	15.23	0.02	0.00	0.00	60.39	0.23	100.78	72	79.9	4.7
III-13	0.15	0.12	10.34	13.36	0.04	15.36	0.00	0.12	0.01	60.75	0.13	100.38	72.8	79.8	4.2

Grain	SiO2	TiO2	Al2O3	FeO	MnO	MgO	CaO	Na2O	K2O	Cr2O3	NiO	Total	Mg#	Cr#	Fe#
VII-a10	0.22	0.17	10.98	11.77	0.34	14.93	0.01	0.16	0.05	61.65	0.00	100.29	70.9	78.9	1.2
		Intergrown with chlorite													
I-28	0.15	0.18	9.98	12.92	0.18	15.72	0.00	0.12	0.00	61.10	0.00	100.35	74.1	80.4	4.2
I-29	0.14	0.26	10.03	12.85	0.43	15.83	0.00	0.08	0.00	60.51	0.14	100.26	75.5	80.2	4.9
II-2	0.14	0.13	9.70	13.96	0.10	15.18	0.05	0.20	0.00	60.97	0.08	100.51	72.3	80.9	4.7
II-5	0.19	0.25	10.48	13.80	0.29	15.74	0.08	0.16	0.01	60.37	0.21	101.57	74.2	79.4	5.3
II-6	0.18	0.18	9.99	13.91	0.22	15.32	0.04	0.12	0.00	60.33	0.09	100.37	73	80.2	5.1
II-21	0.20	0.20	10.25	13.78	0.25	15.09	0.01	0.13	0.01	59.65	0.19	99.76	72.3	79.7	4.7
II-22	0.15	0.29	9.80	13.71	0.13	15.37	0.05	0.13	0.00	61.48	0.00	101.11	72.4	80.9	4.4
		Intergrown with diopside													
I-30	0.16	0.24	10.96	12.93	0.12	15.24	0.07	0.03	0.02	60.42	0.13	100.30	72.2	78.6	3.4
I-32	0.09	0.23	10.84	13.42	0.20	15.48	0.04	0.12	0.00	60.06	0.04	100.52	73.3	78.9	4.4
I-34	0.15	0.14	11.41	13.42	0.21	15.49	0.05	0.12	0.01	59.69	0.25	100.94	72.8	77.9	4.2
II-13	0.20	0.18	9.50	14.05	0.04	15.11	0.06	0.09	0.00	61.07	0.25	100.54	71.9	81.1	4.7
		Chromite inclusions in silicate minerals													
		in olivine													
II-23	0.20	0.21	10.14	14.55	0.39	14.43	0.04	0.08	0.00	60.87	0.21	101.14	68.7	80	3.7
II-24	0.15	0.31	10.07	14.28	0.17	14.51	0.05	0.14	0.00	61.45	0.14	101.26	68.7	80.4	3.4
III-16	0.15	0.30	10.64	13.77	0.41	14.72	0.05	0.04	0.01	60.30	0.16	100.56	70	79.2	3.4
III-18	0.17	0.21	10.32	14.05	0.00	14.90	0.00	0.15	0.00	61.73	0.09	101.62	70.1	80	3.7
III-22	0.10	0.35	10.78	15.21	0.17	14.53	0.00	0.02	0.00	58.68	0.06	99.91	69.4	78.5	5.1
III-15	0.10	0.03	32.21	18.28	0.37	14.49	0.00	0.13	0.02	34.75	0.11	100.48	63.6	41.9	4.2
III-19	0.05	0.14	33.13	18.35	0.23	14.55	0.00	0.23	0.00	33.59	0.19	100.46	63.6	40.5	4.2
III-20	0.15	0.11	34.63	19.58	0.26	14.73	0.06	0.17	0.00	30.02	0.34	100.05	63.9	36.8	5.8
III-21	0.10	0.08	34.94	18.99	0.44	14.91	0.06	0.18	0.03	30.31	0.05	100.07	64.2	36.6	5.8
		in diopside													
II-25	0.18	0.22	11.51	13.23	0.25	14.94	0.22	0.08	0.00	59.23	0.01	99.85	71.2	77.6	3.7

Grain	SiO2	TiO2	Al2O3	FeO	MnO	MgO	CaO	Na2O	K2O	Cr2O3	NiO	Total	Mg#	Cr#	Fe#
II-26	0.27	0.11	10.45	13.71	0.41	14.69	0.28	0.05	0.02	60.06	0.02	100.08	70.4	79.5	4.1
III-14	0.21	0.24	11.21	12.00	0.00	15.84	0.02	0.08	0.01	61.60	0.23	101.44	74.3	78.7	2.8
III-17	0.19	0.21	10.91	13.29	0.26	15.05	0.01	0.11	0.05	61.01	0.20	101.30	71	78.9	3.2
		Chromitę (very high chromium)													
IV-34	0.53	0.33	4.28	13.29	0.42	12.82	0.06	0.02	0.03	68.72	0.05	100.56	63.7	91.5	0.4

II 13 - Sulphides

Grain	Zn	Cu	Fe	As	S	Ni	Mn	Co	Ag	Au	Sn	Pb	Sb	W	Bi	Cr	Ti	Si	Al	Total
		Pyrite (fragments, larger)																		
3'	0.29	0.00	47.06	0.13	54.27	0.00	0.01	0.45	0.02	0.04	0.00	0.00	0.00	0.15	0.00	0.00	0.00	0.04	0.06	102.52
4'	0.02	0.10	46.78	0.25	54.42	0.01	0.00	0.13	0.00	0.43	0.03	0.00	0.00	0.19	0.00	0.02	0.00	0.05	0.02	102.45
7'	0.08	0.00	46.92	0.27	54.18	0.00	0.00	0.25	0.00	0.25	0.00	0.00	0.00	0.14	0.00	0.00	0.00	0.01	0.03	102.14
8'	0.12	0.00	47.08	0.18	54.30	0.00	0.00	0.05	0.00	0.16	0.03	0.00	0.00	0.11	0.00	0.05	0.00	0.05	0.03	102.16
9'	0.00	0.13	46.72	0.26	54.09	0.12	0.04	0.19	0.00	0.31	0.07	0.00	0.16	0.02	0.00	0.06	0.00	0.09	0.08	102.31
1	0.22	0.00	45.90	0.31	54.17	0.06	0.00	0.16	0.00	0.02	0.06	0.00	0.02	0.21	0.00	0.03	0.00	0.02	0.05	101.23
2	0.56	0.00	46.20	0.32	54.39	0.00	0.08	0.20	0.16	0.00	0.04	0.00	0.00	0.18	0.18	0.00	0.00	0.09	0.04	102.44
3	0.44	0.00	46.22	0.31	53.97	0.07	0.00	0.21	0.00	0.25	0.01	0.00	0.04	0.11	0.00	0.03	0.00	0.09	0.06	101.83
6	0.21	0.00	46.85	0.26	54.26	0.03	0.08	0.19	0.01	0.40	0.00	0.00	0.00	0.18	0.00	0.06	0.00	0.06	0.01	102.60
11	0.13	0.00	46.89	0.41	54.16	0.02	0.00	0.07	0.04	0.48	0.15	0.00	0.10	0.10	0.00	0.02	0.00	0.07	0.01	102.62
15	0.11	0.00	46.62	0.10	54.13	0.05	0.04	0.18	0.00	0.14	0.00	0.00	0.08	0.03	0.00	0.00	0.00	0.07	0.03	101.58
16	0.24	0.00	46.68	0.25	53.88	0.15	0.06	0.00	0.00	0.02	0.00	0.00	0.00	0.08	0.00	0.00	0.00	0.01	0.02	101.38
17	0.20	0.00	46.80	0.20	53.76	0.00	0.00	0.15	0.07	0.28	0.01	0.00	0.00	0.15	0.00	0.00	0.00	0.09	0.04	101.74
18	0.11	0.00	47.37	0.15	54.54	0.08	0.01	0.00	0.03	0.25	0.03	0.00	0.08	0.04	0.00	0.02	0.00	0.03	0.01	102.75
19	0.07	0.00	47.16	0.16	54.56	0.00	0.09	0.19	0.00	0.36	0.14	0.00	0.08	0.12	0.00	0.00	0.00	0.08	0.05	103.07
20	0.12	0.00	46.79	0.20	54.08	0.00	0.00	0.21	0.00	0.04	0.00	0.00	0.00	0.21	0.00	0.02	0.01	0.03	0.03	101.74
21	0.35	0.00	46.78	0.23	54.46	0.05	0.00	0.22	0.06	0.09	0.12	0.00	0.02	0.26	0.00	0.05	0.00	0.00	0.08	102.78
22	0.05	0.16	47.53	0.23	54.54	0.00	0.00	0.23	0.00	0.38	0.00	0.00	0.07	0.13	0.00	0.00	0.00	0.05	0.03	103.39

Grain	Zn	Cu	Fe	As	S	Ni	Mn	Co	Ag	Au	Sn	Pb	Sb	W	Bi	Cr	Ti	Si	Al	Total
69	0.25	0.11	45.64	2.40	51.77	0.04	0.00	0.02	0.00	0.33	0.00	0.00	0.00	0.05	0.00	0.03	1.22	0.04	0.05	101.95
70	0.34	0.01	46.63	1.15	53.67	0.03	0.00	0.21	0.08	0.30	0.17	0.00	0.07	0.07	0.00	0.00	0.00	0.03	0.04	102.81
71	0.31	0.03	46.69	0.20	54.38	0.04	0.01	0.28	0.06	0.40	0.00	0.00	0.06	0.24	0.00	0.00	0.00	0.03	0.03	102.76
72	0.39	0.00	46.35	0.15	54.37	0.00	0.00	0.24	0.00	0.09	0.00	0.00	0.12	0.25	0.00	0.00	0.00	0.07	0.03	102.05
73	0.69	0.00	45.53	1.07	53.27	0.10	0.09	0.10	0.02	0.01	0.03	0.00	0.05	0.13	0.00	0.00	0.00	0.05	0.04	101.18
74	0.44	0.00	46.67	2.31	52.67	0.04	0.03	0.21	0.00	0.11	0.15	0.00	0.14	0.00	0.00	0.03	0.00	0.07	0.05	102.92
		One pyrite grain (intergrowing with silicate mineral)																		
52	1.00	0.01	45.91	0.27	54.42	0.09	0.03	0.18	0.01	0.30	0.00	0.00	0.00	0.11	0.00	0.03	0.00	0.07	0.03	102.45
53	0.40	0.00	46.67	0.22	54.18	0.00	0.00	0.93	0.00	0.00	0.08	0.00	0.08	0.08	0.00	0.02	0.00	0.10	0.04	102.81
55	0.42	0.00	45.19	0.25	52.28	0.00	0.00	0.14	0.00	0.22	0.21	0.00	0.09	0.02	0.00	0.00	0.01	0.03	0.01	98.86
56	0.46	0.01	46.72	0.24	54.24	0.00	0.00	0.00	0.00	0.19	0.00	0.00	0.00	0.20	0.00	0.00	0.00	0.06	0.08	102.21
57	0.82	0.00	46.89	0.18	54.30	0.00	0.06	0.07	0.00	0.01	0.00	0.00	0.16	0.27	0.00	0.02	0.00	0.01	0.03	102.82
58	0.22	0.00	46.02	0.23	54.39	0.00	0.00	0.21	0.00	0.32	0.02	0.00	0.04	0.14	0.00	0.00	0.00	0.00	0.08	101.66
		Pyrite (euhedral, bigger)																		
10	0.13	0.18	46.67	1.43	53.54	0.00	0.00	0.04	0.00	0.19	0.09	0.00	0.07	0.00	0.00	0.00	0.00	0.13	0.08	102.56
13	0.00	0.00	45.96	1.93	53.10	0.19	0.05	0.00	0.00	0.41	0.14	0.00	0.02	0.00	0.00	0.00	0.00	0.07	0.03	101.90
		Pyrite (euhedral, smaller)																		
79	0.28	0.00	47.11	1.23	53.81	0.03	0.00	0.02	0.00	0.15	0.00	0.00	0.00	0.26	0.00	0.00	0.00	0.05	0.04	102.99
80	0.39	0.00	46.56	1.31	53.15	0.11	0.00	0.14	0.01	0.20	0.00	0.00	0.00	0.19	0.00	0.06	0.00	0.03	0.00	102.17
81	0.37	0.00	46.46	2.37	52.65	0.01	0.00	0.16	0.00	0.24	0.11	0.00	0.02	0.00	0.00	0.01	0.00	0.09	0.00	102.48

Grain	Zn	Cu	Fe	As	S	Ni	Mn	Co	Ag	Au	Sn	Pb	Sb	W	Bi	Cr	Ti	Si	Al	Total
82	0.43	0.00	45.89	1.15	53.28	0.00	0.00	0.08	0.00	0.17	0.20	0.00	0.05	0.04	0.00	0.00	0.00	0.06	0.08	101.44
83	0.18	0.05	45.67	2.01	52.99	0.44	0.07	0.50	0.00	0.19	0.00	0.00	0.01	0.09	0.00	0.06	0.07	0.03	0.09	102.44
84	0.05	0.00	45.76	4.28	51.19	0.04	0.00	0.21	0.03	0.20	0.09	0.00	0.12	0.18	0.00	0.02	0.00	0.05	0.03	102.24
85	0.47	0.00	46.88	0.39	53.99	0.00	0.04	0.15	0.00	0.00	0.00	0.00	0.00	0.03	0.00	0.00	0.00	0.07	0.04	102.06
		Arsenopyrite (euhedral, bigger)																		
5'	0.00	0.05	35.01	44.65	20.98	0.00	0.02	0.24	0.00	0.00	0.00	0.00	0.00	0.14	0.00	0.00	0.01	0.04	0.00	101.15
6'	0.06	0.00	35.04	44.54	20.91	0.00	0.00	0.00	0.14	0.01	0.00	0.00	0.00	0.27	0.33	0.01	0.01	0.00	0.00	101.31
		Arsenopyrite (euhedral, smaller)																		
35	0.33	0.00	35.80	43.26	21.97	0.00	0.07	0.02	0.13	0.08	0.08	0.00	0.07	0.28	0.05	0.03	0.02	0.02	0.01	102.22
36	0.19	0.01	36.05	42.71	22.37	0.07	0.06	0.00	0.00	0.25	0.00	0.00	0.18	0.24	0.21	0.00	0.00	0.00	0.00	102.36
37	0.35	0.00	35.27	44.09	21.67	0.00	0.00	0.00	0.16	0.04	0.00	0.00	0.21	0.14	0.31	0.05	0.01	0.00	0.00	102.28
38	0.21	0.00	35.23	45.38	20.57	0.00	0.00	0.24	0.00	0.00	0.03	0.00	0.08	0.31	0.35	0.00	0.00	0.04	0.00	102.43
39	0.39	0.06	35.08	45.04	21.00	0.00	0.00	0.18	0.03	0.01	0.00	0.00	0.12	0.16	0.25	0.00	0.01	0.04	0.00	102.37
40	0.31	0.00	35.75	42.21	23.04	0.00	0.00	0.04	0.00	0.13	0.18	0.00	0.21	0.20	0.27	0.00	0.09	0.01	0.00	102.43
41	0.56	0.18	35.47	42.85	22.44	0.12	0.00	0.25	0.00	0.04	0.00	0.00	0.00	0.15	0.08	0.00	0.00	0.02	0.01	102.17
42	0.65	0.12	35.14	44.91	20.66	0.00	0.04	0.12	0.00	0.29	0.00	0.00	0.04	0.04	0.00	0.01	0.00	0.08	0.00	102.11
43	0.23	0.18	35.57	40.73	22.79	0.00	0.01	0.01	0.02	0.28	0.15	0.00	0.14	0.25	0.24	0.00	0.00	0.00	0.00	100.61
44	0.76	0.07	34.92	45.61	20.96	0.08	0.08	0.07	0.01	0.20	0.17	0.00	0.18	0.00	0.14	0.00	0.03	0.05	0.03	103.33
45	0.41	0.05	35.53	43.11	21.82	0.00	0.05	0.19	0.00	0.00	0.00	0.00	0.00	0.17	0.22	0.05	0.00	0.05	0.01	101.66
46	0.65	0.08	35.81	42.42	22.77	0.09	0.00	0.10	0.00	0.23	0.00	0.00	0.00	0.21	0.07	0.07	0.00	0.03	0.00	102.52

Grain	Zn	Cu	Fe	As	S	Ni	Mn	Co	Ag	Au	Sn	Pb	Sb	W	Bi	Cr	Ti	Si	Al	Total
47	0.71	0.07	35.31	43.10	22.14	0.15	0.00	0.18	0.00	0.00	0.12	0.00	0.31	0.15	0.23	0.00	0.01	0.06	0.00	102.56
48	0.22	0.00	35.55	41.98	22.40	0.00	0.00	0.17	0.00	0.00	0.00	0.00	0.03	0.10	0.00	0.00	0.18	0.04	0.00	100.66
49	0.21	0.16	35.15	44.34	21.11	0.01	0.00	0.10	0.00	0.00	0.00	0.00	0.02	0.13	0.60	0.00	0.00	0.07	0.00	101.89
50	0.71	0.00	35.15	44.59	22.31	0.11	0.00	0.00	0.00	0.12	0.15	0.00	0.10	0.20	0.18	0.10	0.00	0.00	0.00	103.72
51	1.11	0.19	35.11	42.78	22.61	0.00	0.03	0.00	0.00	0.00	0.07	0.00	0.13	0.03	0.21	0.03	0.12	0.07	0.00	102.51
		Pentlandite (FeNiS, with Fe-Ni alloys)																		
65	0.80	0.00	40.39	0.16	33.70	23.63	0.00	0.48	0.05	0.11	0.00	0.00	0.00	0.29	0.00	0.05	0.00	0.00	0.01	99.67
67	0.33	0.09	40.75	0.27	33.68	23.92	0.00	0.83	0.00	0.11	0.09	0.00	0.08	0.13	0.00	0.00	0.00	0.03	0.03	100.34
		Galena (PbS)																		
1'	0.22	0.26	0.13	0.00	12.73	0.00	0.05	0.00	0.08	0.16	0.09	86.07	0.42	0.04	0.12	0.00	0.00	0.05	0.02	100.44
2'	0.00	0.00	0.13	0.00	12.54	0.03	0.00	0.00	0.33	0.17	0.00	86.08	0.06	0.11	0.00	0.00	0.00	0.04	0.02	99.51
77	0.71	0.00	0.07	0.02	12.54	0.21	0.00	0.01	0.03	0.06	0.00	86.46	0.00	0.09	0.00	0.09	0.00	0.02	0.04	100.35
78	0.19	0.00	0.01	0.08	12.58	0.09	0.00	0.03	0.16	0.26	0.00	86.45	0.22	0.09	0.00	0.08	0.00	0.02	0.05	100.30
		Galena (PbS) (intergrownwith ZnS and dolomite)																		
26	0.15	0.16	0.00	0.00	12.81	0.07	0.00	0.00	0.00	0.20	0.00	85.99	0.00	0.13	0.00	0.07	0.00	0.01	0.00	99.59
27	0.00	0.03	0.01	0.02	12.78	0.07	0.07	0.07	0.00	0.14	0.00	86.24	0.00	0.20	0.00	0.13	0.00	0.01	0.02	99.81
		Sphalerite (ZnS)																		
28	67.04	0.00	0.71	0.28	32.63	0.11	0.00	0.00	0.01	0.01	0.00	0.00	0.05	0.00	0.21	0.00	0.00	0.12	0.03	101.19
29	66.74	0.00	0.58	0.30	33.23	0.00	0.00	0.01	0.00	0.00	0.00	0.00	0.00	0.19	0.62	0.00	0.00	0.05	0.02	101.74
32	66.81	0.08	0.59	0.22	32.31	0.00	0.00	0.00	0.00	0.00	0.00	0.00	0.00	0.22	0.00	0.11	0.02	0.00	0.03	100.39

II 14 - Apatite, calcite, dolomite and celestite

Grains	SiO2	TiO2	Al2O3	FeO	MnO	MgO	CaO	Na2O	K2O	Cr2O3	NiO	P2O5	BaO	Total
		Apatite												
II-6	0.00	0.00	0.00	0.03	0.00	0.09	56.41	0.18	0.01	0.13	0.00	42.09	0.13	99.06
IV-32	0.00	0.00	0.00	0.04	0.08	0.04	56.44	0.13	0.01	0.08	0.00	41.89	0.19	98.90
IV-34	0.00	0.00	0.00	0.10	0.00	0.02	56.28	0.08	0.00	0.05	0.04	42.17	0.18	98.92
B3-2	0.24	0.01	0.09	0.00	0.00	0.25	53.82	0.20	0.00	0.00	0.00	39.83	0.00	94.44
		Calcite												
B3-2'	0.25	0.00	0.07	0.25	0.10	0.10	57.71	0.00	0.03	0.02	0.00	0.00	0.06	58.57
B3-3	0.11	0.00	0.07	0.21	0.07	0.11	58.65	0.08	0.02	0.00	0.07	0.00	0.05	59.44
		Dolomite in galena												
IV-1	0.03	0.01	0.00	0.04	0.00	22.53	28.93	0.13	0.00	0.00	0.00	0.04	0.12	51.83
IV-2	0.05	0.00	0.02	0.25	0.00	21.92	29.07	0.01	0.00	0.08	0.20	0.00	0.00	51.58
IV-3	0.10	0.01	0.00	0.25	0.10	21.77	31.48	0.07	0.00	0.01	0.00	0.06	0.15	54.01
		Celestite (O was analysed, but by assumption)												
	Si	**Ca**	**Na**	**Ba**	**Sr**	**S**	**O**	**Total (ATOM%)**						
B3-7	0.42	0.15		0.59	18.84	18.02	61.97	100.00						
	0.45	0.11	0.34	2.09	17.52	18.08	61.41	100.00						

II 15 - **Minerals in the granite sample**

Grain	SiO2	TiO2	Al2O3	FeO	MnO	MgO	CaO	Na2O	K2O	Cr2O3	NiO	P2O5	Total	An	Ab	Or
		K-feldspar														
G-7	65.71	0.08	18.61	0.06	0.00	0.08	0.00	0.81	15.19	0.00	0.00	0.22	100.76		7.5	92.5
G-13	65.69	0.10	18.62	0.08	0.00	0.05	0.00	1.23	14.55	0.04	0.00	0.00	100.37		11.7	88.3
G-14	64.97	0.00	18.20	0.00	0.00	0.00	0.04	0.40	14.73	0.01	0.19	0.12	98.88		3.5	96.5
		Plagioclase														
G-8	68.00	0.00	20.85	0.16	0.00	0.00	1.49	9.65	0.06	0.07	0.05	0.11	100.57	8.1	91.9	
G-9	67.09	0.04	21.53	0.05	0.07	0.00	2.36	8.88	0.03	0.06	0.00	0.18	100.29	13	87	
G-5	61.96	0.00	24.22	0.05	0.10	0.00	5.90	7.81	0.19	0.04	0.16	0.02	100.62	29.2	70	0.8
G-10	64.92	0.05	22.54	0.04	0.00	0.00	4.01	8.38	0.16	0.09	0.00	0.03	100.20	21.1	78.1	0.8
G-12	61.96	0.00	24.17	0.04	0.01	0.07	5.74	7.91	0.12	0.06	0.00	0.00	100.08	28.3	70.8	0.8
		Quartz														
G-1	100.29	0.00	0.00	0.09	0.02	0.05	0.00	0.04	0.00	0.00	0.00	0.15	100.64			
G-3	100.20	0.11	0.00	0.02	0.05	0.00	0.00	0.00	0.00	0.00	0.02	0.23	100.62			
		Garnet														
G-19	36.58	0.07	20.15	25.36	16.52	1.21	0.50	0.14	0.00	0.00	0.18	0.24	100.96			
G-21	36.44	0.07	20.06	24.52	17.60	0.90	0.13	0.01	0.05	0.00	0.09	0.23	100.11			

REFERENCES

Akio, S., Eiji, O. and Takumi, K, 1995. Flotation of diamond in mantle melt at high pressure. Science, 269: 216-218.

Allegre, C.J., Courtillot, V., Mattauer, M., Tapponnier, P., et al., 1984. Structure and evolution of the Himalaya-Tibet orogenic belt. Nature (London), 307: 17-22.

Anthony, J.W., Bideaux, R.A, Bladh, K.W. and Nicols, M.C., 1990. Handbook of Mineralogy. Mineral Data Publishing, Tucson, Arizona.

Arai, S., Matsukage, K., Isobe, E. and Vysotskiy, S., 1997. Concentration of incompatible elements in oceanic mantle: Effect of melt/wall interaction in stagnant or failed melt conduits within peridotite. Geochimica et Cosmochimica Acta, 61: 671-675.

Arculus, R.J., 1985. Oxidation status of the mantle: past and present. Ann. Rev. Earth Planet. Sci., 13: 75-95.

Arima, M., Nakayama, K., Akaishi, M., Yamaoka, S. and Kanda, H., 1993. Crystallization of diamond from a silicate melt of kimberlite composition in high-pressure and high-temperature experiments. Geology, 21: 968-970.

Auge, T., 1987. Chromite deposits in the northern Oman ophiolite: mineralogical constraints. Mineralium Deposita, 22: 1-10.

Badziag, P., Verwoerd, W.S., Ellis, W.P. and Greiner, N.R., 1990. Nanometre-sized diamonds are more stable than graphite. Nature, 343: 244-245.

Bai, W.-J., Hu, X.-F., Yang, J.-S. and Zhou, M.-F., 1993. No relationship between mountain-building and collision for plate tectonics. Geological Review (Chinese), 39: 111-117.

Bai, W.-J., Hu, X.-F., Yang, J.-S. and Zhou, M.-F., 1994. An analysis about geological history of the Yarlung Zangbo Plate Suture zone and the Himalayas and the Qinghai-Tibet plateau. Tibetan Geology, No. 1: 93-102.

Bai, W.-J. and Yang, J.-S., 1985. The basin-mountain system of Asia and its tectonic stress field. Journal of Geology of Jilin, No. 4: 33-40.

Bai, W.-J. and Yang, J.-S., 1987. A model for the uplifting of the Qinghaai-Tibet plateau: evidence from basin-mountain collision in continent. Bulletin of the Changchun University of Geological Sciences, 17: 131-142.

Bai, W.-J. and Yang, J.-S., 1988. On the collision of the Indian plate and Eurasian plate and the uplift of the Tibetan plateau. Regional Geology of China, No. 4: 362-368.

Bai, W.-J., Zhou, M.-F., Cai, Y. and Hu, X.-F., 1989. The types and characteristics of basic and ultrabasic rocks from China. Bulletin of the Institute of Geology, Chinese Academy of Geological Sciences (in Chinese), No. 20: 51-74.

Bai, W.-J., Zhou, M.-F. and Robinson, P.T., 1993. Possibly diamond-bearing mantle peridotites and podiform chromitites in the Luobusa and Donqiao ophiolites, Tibet. Canadian Journal of Earth Sciences, 30: 1650-1659.

Ballhaus, C. and Frost, B.R., 1994. The generation of oxidized CO_2-bearing basaltic melts from reduced CH_4-bearing upper mantle sources. Geochimica et Cosmochimica Acta, 58: 4931-4940.

Barazangi, M. and Ni, J., 1982. Velocities and propagation characteristics of Pn and Sn beneath the Himalayan arc and Tibetan plateau: Possible evidence for underthrusting of India continental lithosphere beneath Tibet. Geology, 10: 179-185.

Bird, J.M. and Weathers, M.S., 1975. Josephinite: specimens from the earth's core? Earth and Planetary Science Letters, 28: 51-64.

Boyd, F.R. and Finnerty, A.A., 1980. Conditions of origin of natural diamonds of peridotite affinity. Journal of Geophysical Research, 85: 6911-6918.

Boyd, F.R. and Gurney, J.J., 1986. Diamonds and the African lithosphere. Science, 232: 472-477.

Boyd, F.R., Gurney, J.J. and Richardson, S.H., 1985. Evidence for a 150-200 km thick Archean lithosphere form diamond inclusion thermobarometry. Nature, 315: 387-389.

Boyd, S.R., Mattey, D.P., Pillinger, C.T., Milledge, H.J., Mendelssohn, M. and Seal, M., 1987. Multiple growth events during diamond genesis: an integrated study of carbon and nitrogen isotopes and nitrogen aggregation state in coated stones. Earth and Planetary Science Letters, 86: 341-358.

Boyd, S.R., Pineau, F. and Javoy, M., 1994. Modelling the growth of natural diamonds. Chemical Geology, 116: 29-42.

Brey, G.P., Kogarko, L.N. and Ryabchikov, I.D., 1991. Carbon dioxide in kimberlitic melts. Neues Jahrbuch Fuer Mineralogie, 4: 159-168.

Bulanova, G.P., 1995. The formation of diamond. Journal of Geochemical Exploration, 53: 1-23.

Bulanova, G.P. and Spetsius, Z.V., 1990. Inclusions in diamond and minerals of mantle xenoliths from kimberlites as a source of information on the upper mantle composition. In: International Mineralogical Association Meeting, 1990, Beijing, Vol. 2, Extended Abstracts. Pp. 784-785.

Bunch, T.E. and Olsen, E., 1975. Distribution and significance of chromium in meteorites. Geochimica et Cosmochimica Acta, 39: 911-927.

Cartigny, P., Boyd, S.R., Harris, J.W. and Javoy, M., 1997. Nitrogen isotopes in peridotitc diamonds from Fuxian, China: the mantle signature. Terra Nova, 9: 175-179.

Chan, C.-L., 1993. A moissanite-like phase. Geological Society of America, Abstracts and Programs, 25: A-383.

Chen, Y.-D., Suzanne-Y, O.R., Kinny, P.D. and Griffin, W.L., 1994. Dating lower crust and upper mantle events: an iron microprobe study of xenoliths from kimberlitic pipes, South Australia. Lithos, 32: 77-94.

Claoue-Long, J.C., Sobolev, N.V., Shatsky, V.S. and Sobolev, A.V., 1991. Zircon response to diamond-pressure metamorphism in the Kokchetav massif, USSR. Geology, 19: 710-713.

Davies, G.R., Nixon, P.H., Pearson, D.G. and Obata, M., 1993. Tectonic implications of graphitised diamonds in the Ronda peridotite, S. Spain. Geology, 21: 471-474.

Deer, W.A., Howie, R.A. and Zussman, J., 1995. An introduction to the rock-forming minerals, 2nd edition, 1992. Longman House, England. Pp. 696.

Deines, P., 1980. The carbon isotopic composition of diamond: relationship to diamond shape, color, occurrence and vapor composition. Geochimica et Cosmochimica Acta, 44: 943-961.

DeVries, R.C., 1997. Diamonds from warm water. Nature, 385: 485.

Dewey, J.F. and Burke, K.C.A., 1973. Tibetan, Variscan and Precambrian basement reactivation: products of continental collision. Journal of Geology, 81: 683-692.

Dewey, J.F., Shackleton, R.M., Chang, C.-F. and Yiyin, S., 1988. The tectonic evolution

of the Tibetan Plateau. Philosphical Transactions of the Royal Society of London, series, A: Mathematical and Physical Sciences, 327: 379-413.

Dick, H.J.B. and Bullen, T., 1984. Chromian spinel as a petrogenetic indicator in abyssal and Alpine-type peridotites and spatially associated lavas. Contributions to Mineralogy and Petrology, 86: 54-76.

Dobrzhinetskaya, L.F., Braun, T.V., Sheshkel, G.G. and Podkuiko, Y.A., 1994, Geology and structure of diamond-bearing rocks of the Kokchetav massif (Kazakhstan). Tectonophysics, 233: 293-313.

Dobrzhinetskaya, L.F., Eide, E.A., Larsen, R.B., Sturt, B.A., tronnes, R.G., Smith, D.C., Taylor, W.R. and Posukhova, T.V., 1995. Microdiamond in high-grade metamorphic rocks of the Western Gnesis region, Norway. Geology, 23 (7): 597-600.

Dresser, J.A., 1913. Preliminary report on the serpentine and associated rock of Southern Quebec. Memoir - Geological Survey of Canada, No. 22: 1-103.

Eggler, D.H., 1989. Kimberlites: how do they form? In: J. Ross (Editor), Kimberlites and Related Rocks, Geological Society of Australia, Special Publication, Blackwell, Oxford. Vol. 1, pp. 489-504.

England, P. and Houseman, G., 1986. Finite strain calculations of continental deformation, 2. Comparison with the India-Asia collision zone. Journal of Geophysical Research B, 91: 3664-3676.

England, P. and Houseman, G., 1988. The mechanics of the Tibetan Plateau. Philosphical Transactions of the Royal Society of London, series, A: Mathematical and Physical Sciences, 326: 301-320.

England, P. and McKenzie, D., 1982. A thin viscous sheet model for continental deformation. Geophysical Journal of the Royal Astranomical Society, 70: 295-321.

Essene, E.J. and Fisher, D.C., 1986. Lightning strike fusion: extreme reduction and metal-silicate liquid immiscibility. Science, 234: 189-193.

Evans, T. and Harris, J.W., 1989. Nitrogen aggregation, inclusion equilibrium temperatures and the age of diamonds. In: J. Ross et al. (Editors), Kimberlites and Related Rocks, Geological Society of Australia, Special Publication, No. 14, V. 2: 1001-1006.

Evstigneeva, T. and Tarkian, M., 1996. Synthesis of platinum-group minerals under

hydrothermal conditions. European Journal of Mineralogy, 8: 549-564.

Falloon, T.J. and Green, D.H., 1989. The solidus of carbonated, fertile peridotite. Earth and Planetary Science Letters, 94: 364-370.

Fang, Q. and Bai, W.-J., 1981. The discovery of Alpine-type diamond-bearing ultrabasic intrusions in Tibet. Geological Review (Beijing), 27: 455-457.

Ferrario, A. and Garutti, G., 1990. Platinum-group mineral inclusions in chromitites of the Finero mafic-ultramafic complex (Ivrea Zone, Italy). Mineralogy and Petrology, 41: 125-143.

Fielding, E.J., Isacks, B.L., Barazangi, M. and Duncan, C.C., 1994. How flat is Tibet? Geology, 22:163-167.

Frost, B.R., 1985. On the stability of sulfides, oxides, and native metals in serpentinite. Journal of Petrology, 26: 31-63.

Garanin, V.K. and Kudryavtseva, G.P., 1990. Morphology, physical properties of inclusion-bearing diamonds from Yakutian kimberlites. Lithos, 25: 211-217.

Girardeau, J., Marcoux, J., Fourcade, E., Bassoullet, J.P. and Tang, Y., 1985. Xaixa ultramafic rocks, centre Tibet, China: tectonic environment and geodynamic significance. Geology, 13: 330-333.

Girardeau, J. and Mercier, J.C.C., 1988. Petrology and texture of the ultramafic rocks of the Xigaze ophiolite (Tibet): constraints for mantle structure beneath slow-spreading ridges. Tectonophysis, 147: 33-58.

Griffin, W.L., Gurney, J.J. and Ryan, C.G., 1992. Variations in trapping temperatures and trace elements in peridotite-suite inclusions from African diamonds: evidence for two inclusion suites and implications for lithossphere stratigraphy. Contributions to Minerology and Petrology, 110: 1-15.

Griffin, W.L., Jaques, A.L., Sie, S.H., Ryan, C.G., Cousens, D.R. and Suter, G.F., 1988. Conditions of diamond growth: a proton microprobe study of inclusions in West Australian diamonds. Contributions to Mineralogy and Petrology, 99: 143-158.

Griffin, W.L. and Ryan, C.G., 1995. Trace elements in indicator minerals: area selection and target evaluation in diamond exploration. Journal of Geochemical Exploration, 53: 311-337.

Gurney, J.J., 1986. Diamonds. The FourthInternational Kimberlite Conference, Abstracts

- Geological Society of Australia, pp. 363-367.

Gurney, J.J., 1989. Diamonds. In: J.Ross et al. (Editors), Kimberlites and Related Rocks, Geological Society of Australia, Special Publication, No. 14, V. 2: 935-965.

Gurney, J.J., Harris, J.W., Rickard, R.S. and Cardoso, P., 1986. Mineral inclusions in diamonds from Koffiefontein mine. Extended Abstracts, the FourthInternational Kimberlite Conference, pp. 389-391.

Guthrie, G.D., Veblen, D.R., Navon, O. and Rossman, G.R., 1991. Submicrometer fluid inclusions in turbid-diamond coats. Earth and Planetary Science Letters, 105: 1-12.

Haggerty, S.E., 1986. Diamond genesis in a multiply-constrained model. Nature, 320: 34-37.

Haggerty, S.E., 1994. Superkimberlites: A geodynamic diamond window to the Earth's core. Earth and Planetary Science letters, 122: 57-69.

Harris, J., Hutchison, M.T., Hursthouse, M., Light, M. and Harte, B., 1997. A new tetragonal silicate mineral occurring as inclusions in lower-mantle diamonds. Nature, 387: 486-488.

He, G., 1987. Mantle xenoliths from kimberlites in China. In: P.H. Nixon (Editor), Mantle Xenoliths. Wiley, New York. pp. 181-185.

Helmstaedt, H.H., 1994. Natural diamond occurrences and tectonic setting of "primary" diamond deposits. Course Notes for Cordilleran Section of GAC Short Course 18 on Kimberlites and Diamond Indicator Minerals. Vancouver, p. 1-79.

Hervig, R.L., Smith, J.V., Steele, I.M., Gurney, J.J., Meyer, H.O.H. and harris, J.W., 1980. Diamonds: minor elements in silicate inclusions: pressure-temperature implications. Journal of Geophysical Research, 85: 6919-6929.

Hirn, A., 1988. Features of the crust-mantle structure of the Himalayas-Tibet: A comparison with seismic traverses of the Alpine, Pyrenean and Variscan orogenic belts. Philosphical Transactions of the Royal Society of London, series, A: Mathematical and Physical Sciences, 326: 17-32.

Hirn, A., Lepine, J.-C. and 11 others, 1984. Crustal structure and variability of the Himalayan bordor of Tibet. Nature, 307: 23-25.

Hough, R.M., Gilmour, I., Pillinger, C.T., Arden, J.W., Gilkes, K.W.R., Yuan, J. and Milledge, H.J., 1995. Diamond and silicon carbide in impact melt rock from the

Ries impact crater. Nature, 378: 41-43.

Houseman, G.A., McKenzie, D.P. and Molnar, P., 1981. Convective instability of a thickened boundary layer and its relevance for the thermal evolution of continental convergent belts. Journal of Geophysical Research B, 86: 6115-6132.

Irifune, T., Koizumi, T. and Ando, J-I., 1996. An experimental study of the garnet-perovskite transformation in the system $MgSiO_3$-$Mg_3Al_2Si_3O_{12}$. Physics of Earth and Planetary Interiors, 96: 147-157.

Janse, A.J.A., 1994. Review of supposedly non-kimberlitic and non-lamproitic diamond host rocks. In: H.O.A. Meyer and O.H. Leonardos (Editors), Proceedings of the Fifth International Kimberlite Conference 2, Diamonds: Characterization, Genesis and Exploration. Departmento Nacional da Producao Mineral, Brasilia, CPRM special publication 1B, Jan/94. pp. 144-159.

Jaques, A.L. and 7 others, 1989. Composition of crystalline inclusions and C-isotopic composition of Argyle and Ellendale diamonds. In: J. Ross et al. (Editors), Kimberlites and Related Rocks, Geological Society of Australia, Special Publication, No. 14, V. 2: 966-989.

Javoy, M., Pineau, F. and Demaiffe, D., 1984. Nitrogen and carbon isotopic composition in diamonds from Mbuji Mayi (Zaire). Earth and Planetary Science Letters, 68: 399-412.

Johan, Z., 1984. Genesis of chromite deposits in the 'Massif du Sud' ophiolitic complex, New Caledonia: example of a high-temperature, fluid-rich, one-forming system. The twenty-seventh international geological congress, Abstracts, 6: 146-147.

Johan, Z., 1986. Chromite deposits of New Caledonian ophiolite nappes. In: W. Petrascheck et al. (Editors), Chromites, Theophrastus Publ. S. A., Athens, Greece. pp. 311-338.

Kesson, S.E. and Ringwood, A.E., 1989. Slab-mantle interactions 2: The formation of diamonds. Chemical Geology, 78: 97-119.

Kerr, R.A., 1993. Bits of the lower mantle found in Brazilian diamonds. Science, 261: 1391.

Kinny, P.D. and Meyer, H.O.A., 1994. Zircon from the mantle: A new way to date old diamonds. The Journal of Geology. 102: 475-481.

Kirkley, M.B., Gurney, J.J. and Levinson, A.A., 1991. Age, origin and emplacement of

diamonds: scientific advancess in the last decade. Gems and Gemology, 27: 2-25.

Kirkley, M.B., Gurney, J.J., Otter, M.L., Hill, S.J. and Daniers, L.R., 1991. The application of the sources of C isotope measurements to the identification of the sources of C in diamonds: a review. Applied Geochemistry, 6: 477-494.

Klingenberg, B.M.E.T. and Kushiro, I., 1996. Melting of a chromite-bearing harzburgite and generation of boninitic melts at low pressures under controlled oxygen fugacity. Lithos, 37: 1-14.

Knittle, E. and Jeanloz, R., 1986. High-pressure metallization of FeO and implications for the Earth's core. Geophysical Research Letters, 13: 1541-1544.

Knittle, E. and Jeanloz, R., 1991. Earth's core-mantle boundary: results of experiments at high pressures and temperatures. Science, 251: 1438-1443.

Koeberl, C., 1995. Diamonds everywhere. Nature, 378: 17-18.

Kunz, G.F., 1905. Moissanite, a natural silicon carbide. American Journal of Science, 19: 396-397.

Lane, J.E., Carter, C.H. and Davis, R.F., 1988. Kinetics and mechanisms of high-temperature creep in silicon carbide: III, Sintered a-silicon carbide. Jour. Amer. Ceram. Soc., 71: 281-295.

Leblanc, M., 1995. Chromitite and ultramafic rock compositional zoning through a paleotranssform fault, Poum, New Caledonia. Economic Geology and the Bulletin of the Society of Economic Geologists, 90: 2028-2039.

Leblanc, M. and Violette, J.F., 1983. Distribution of aluminium-rich and chromium-rich chromite pods in ophiolitic peridotites. Economic Geology, 78: 293-301.

Lehmann, J., 1983. Diffusion between olivine and spinel: application to geothermometry. Earth and Planetary Science Letters, 64: 123-138.

Leung, I.S., 1990. Silicon carbide cluster entrapped in a diamond from Fuxian, China. American Mineralogist, 75: 1110-1119.

Leung, I.S., Guo, W., Friedman, I. and Gleason, J., 1990. Natural occurrence of silicon carbide in a diamondiferous kimberlite from Fuxian. Nature (London), 346: 352-354.

Leung, I.S., Taylor, L.A., Tsao, C.S. and Han, Z., 1996. SiC in diamond and kimberlites:

implications for nucleation and growth of diamond. International Geology Review, 38: 595-606.

Lipschutz, M.E. and Anders, E., 1961. On the mechanism of diamond formation. Science, 134: 2095-2099.

Lorand, J.P. and Ceulener, G., 1989. Silicate and base-metal sulfide inclusions in chromites from the Magsad area (Oman ophiolite, Gulf of Oman): a model for entrapment. Lithos, 22: 173-190.

Lukyanova, L.L., Smirnov, Yu. D., Zil-berman, A.M. and Chernyshova, Ye.M., 1980. A diamond find in picrites from the Urals. International Geology Review, 22: 1189-1193.

Lyakhovich, V.V., 1980. Origin of accessory moissanite. International Geology Review, 22: 961-969.

Mange, M.A. and Maurer, H.Z.F., 1989. Heavy minerals in color. Chapman & Hall.

Mason B. and Berry, L.G., 1968. Elements of Mineralogy. W.H. Freeman and Company, San Francisco and London, 550 pp.

Mathez, E.A., Fogel, F.A., Hutcheon, I.D. and Marshintsev, V.K., 1995. Carbon isotopic composition and origin of SiC from kimberlites of Yakutia, Russia. Geochimica et Cosmochimica Acta, 59: 781-791.

McCallum, M.E., 1976. Diamonds in an upper mantle peridotite nodule from kimberlite in Southern Wyoming. Science, 192: 253-256.

McCammon, C., Hutchison, M. and Harris, J., 1997. Ferric iron content of mineral inclusions in diamonds from Sao Luiz: a view into the lower mantle. Science, 278: 434-436.

McElduff, B., 1989. Inclusions in chromite from Troodos (Cyprus) and their petrological significance. Ph.D. thesis, Moutan-Universitat Leoben, Austria, pp. 143.

McElduff, B. and Stumpfl, E.F., 1991. The chromite deposits of the Troodos Complex, Cyprus - evidence for the role of a fluid phase accompanying chromite formation. Mineralium Deposita, 26: 307-318.

Melcher, F., Grum, W., Simon, G., Thalhammer, T.V. and Stumpfl, E, 1997. Petrogenesis of the ophiolitic giant chromite deposit of Kempirsai, Kazakhstan: a study of solid and fluid inclusions in chromite. Journal of Petrology, 38: 1419-1458.

Menzies, M.A. and Hawkesworth, C.J., 1987. Upper mantle processes and composition. In: P.H. Nixon (Editor), Mantle Xenoliths, Wiley, pp. 725-738.

Menzies, M., Rogers, N., Tindle, A. and Hawkesworth, C., 1987. Metasomatic and enrichment processes in lithospheric peridotites, an effect of asthenosphere-lithosphere interraction. In: M.A. Menzies and C.J. Hawkesworth (Editors), Mantle Metasomatism, Academic Press, pp. 313-364.

Meyer, H.O.A., 1975. Chromium and genesis of diamonds. Geochimica et Cosmochimica Acta, 39: 929-936.

Meyer, H.O.A., 1985. Genesis of diamond: a mantle saga. American Mineralogist, 70: 344-355.

Meyer, H.O.A., 1987. Inclusions in diamond. In: P.H. Nixon (Editor), Mantle Xenoliths. John Wiley & Sons Ltd, Wiley. pp. 501-522.

Meyer, H.O.A. and McCallum, M.E., 1986. Mineral inclusions in diamonds from the Sloan kimberlites, Colorado. The Journal of Geology, 94: 600-612.

Milledge, H.J., Mendelssohn, M.J., Seal, M., Rouse, J.E., Swart, P.K. and Pillinger, C.T., 1983. Carbon isotopic variations in spectral type II diamonds. Nature, 303: 791-792.

Milton, C. and Vitaliano, D., 1985. Moissanite SiC, a geological aberration. Abstracts with Programs - Geological Society of America, 17: 665.

Mitchell, R.H., 1991. Kimberlites and lamproites: primary sources of diamond. Geoscience Canada, 18: 1-18.

Modern Crystallography, 1979. Modern Crystallography, Vol. 3. Nauka, Moscow, 480 pp.

Molnar, P., 1988. A review of geophysical constraints on the deep structure of the Tibetan Plateau, the Himalaya and the Karakoram, and their tectonic implications. Philosphical Transactions of the Royal Society of London, series, A: Mathematical and Physical Sciences, 326: 33-88.

Monastersky, R., 1995. Microscopic diamonds crack geologic mold. Science, 148: 22.

Moody, J.B., 1976. Serpentinization: a review. Lithos, 9: 125-138.

Moore, R.O. and Gurney, J.J., 1985. Pyroxene solid solution in garnets included in diamonds. Nature, 318: 553-555.

Moore, R.O. and Gurney, J.J., 1989. Mineral inclusions in diamond from the Monastery kimberlite, South Africa, In: J. Ross et al. (Editors), Kimerlite and Related Rocks, Geological Society of Australia, Special Publication, No. 14, V. 2: 1029-1041.

Moore, R.O., Otter, M.L., Rickard, R.S., Harris, J.W. and Gurney, J.J., 1986. The occurrence of moissanite and ferro-periclase as inclusions in diamond. Fourth International Kimberlite Conference, Extended Abstracts, Geological Society of Australia, 16: 409-411.

Murck, B.W. and Campbell, I.H., 1986. The effects of temperature, oxygen fugacity and melt composition on the behaviour of chromium in basic and ultrabasic melts. Geochimica et Cosmochimica Acta, 50: 1871-1887.

Murphy, M.A., Yin, A., and 7 others, 1997. Did the Indo-Asia collision alone create the Tibetan Plateau. Geology, 25: 719-722.

Navon, O., 1991. Infrared determination of high internal pressures in diamond fluid inclusions. Nature, 353: 746-748.

Navon, O., Hutcheon, I.D., Rossman, G.R. and Wasserburg, G.J., 1988. Mantle-derived fluids in diamond micro-inclusions. Nature, 335: 784-789.

Nelson, K.D., Zhao, W. and 24 others, 1996. Partially molten middle crust beneath Southern Tibet: synthesis of project INDEPTH results. Science, 274: 1684-1688.

Nicolas, A., Girardeau, J., and 6 others, 1981. The Xigaze ophiolite (Tibet): a peculiar oceanic lithosphere. Nature (London), 294: 414-417.

Nisbet, E.G., 1982. The tectonic setting and petrogenesis of komatiites, In: N.T. Arndt and E.G. Nisbet (editors), Komatiites, George Allen and Unwin (publishers) Ltd., London, p 501-520.

Nixon, P.H., 1995. The morphology and nature of primary diamondiferous occurrences. Journal of Geochemical Exploration, 53: 41-71.

Novgorodova, M.I., Yusupov, R.G. and dmitrieva, M.T., 1984. Cubic SiC intergrown with graphite and diamond from the mineral pitch. Dokl. Akad. Nauk SSSR, 227: 1222-1227.

Orberger, B., Lorand, J.P., Girardeau, J., Mercier, J.C.C. and Pitragool, S., 1995.

Petrogenesis of ultramafic rocks and associated chromitites in the Nan Uttaradit ophiolite, Northern Thailand. Lithos, 35: 153-182.

Otter, M.L. and Gurney, J.J., 1989. Mineral inclusions in diamonds from the Sloan diatreme, Colorado-Wyoming State Line kimberlite district, North America. In: Kimberlites and Related Rocks, Geological Society of Australia, Special Publication, No. 14, V. 2: 1042-1053.

Pattisson, D.R. and Levinson, A.A, 1995. Are euhedral microdiamonds formed during ascent and decompression of kimberlite magma? Implications for use of microdiamonds in diamond grade estimation. Applied Geochemistry, 10: 725-738.

Peacock, S.M., 1993. Large-scale hydration of the lithosphere above subducting slabs. Chemical Geology, 108: 49-59.

Pearson, D.G., Davies, G.R., Nixon, P.H. and Milledge, H.J., 1989. Graphitised diamonds from a peridotite massif in Morocco and implications for anomalous diamond occurrences. Nature (London), 338: 60-62.

Powell, C., 1986. Continental underplating model for the rise of the Tibetan Plateau. Earth and Planetary Science Letters, 81: 79-94.

Ratschbacher, L., Frisch, W., Liu, G. and Chen, C., 1994. Distributed deformation in southern and western Tibet during and after the India-Asia collision. Journal of Geophysical Research, 99: 19917-19945.

Richardson, S.H., 1986. Latter day origin of diamonds of eclogitic paragenesis. Nature, 322: 623-626.

Richardson, S.H., Gurney, J.J. and Cardoso, P., 1989. Mineral inclusions in diamonds from Koffiefontein Mine, In: J. Ross et al. (Editors), Kimberlites and Related Rocks, Geological Society of Australia, Special Publication, No. 14, V. 2: Blackwell Scientific Publications, Melbourne.

Richardson, S.H., Gurney, J.J., Erlank, A.J. and Harris, J.W., 1984. Origin of diamond in old enriched mantle. Nature, 310: 198-202.

Richardson, S.H., Harris, J.W. and Gurney, J.J., 1993. Three generations of diamonds from old continental mantle. Nature, 366: 256-258.

Ringwood, A.E., 1990. Slab-mantle interactions: 3, petrogenesis of intraplate magmas and structure of the upper mantle. Chemical Geology, 82: 187-207.

Roberts, S., 1992. Influence of the partial melting regime on the formation of ophiolitic chromitite. In: L.M. Parsons et al. (eds.), Ophiolites and Their Modern Oceanic Analogues. Geological Society Special Publications, 60: 203-217.

Robinson, P.T., Melson, W.G., O'Hearn, T. and Schmincke, H.V., 1983. Volcanic glass composition of the Troodos ophiolite, Cyprus. Geology, 11: 400-404.

Roeder, P.L. and Reynolds, I., 1991. Crystallization of chromite and chromium stability in basaltic melts. Journal of Petrology, 32: 909-934.

Ross, N.L., Akaogi, M., Navrotsky, A., Susaki, J. and McMillan, P., 1986. Phase transitions among the $CaSiO_3$ polymorphs (wollastonite, garnet and perovskite structure): studies by high-pressure synthesis, high-temperature calorimetry, and vibrational spectroscopy and calculation. Journal of Geophysical Research, 91: 4685-4696.

Sato, Y. and Kamo, M., 1992. Synthesis of diamond from the vapour phase. In: J.E. Field (eds.), The Properties of Natural and Synthetic Diamond, 2nd edition, pp. 423-469. Academic Press, London.

Sautter, V., Haggerty, S.E. and Field, S., 1991. Ultra-deep (>300 km) ultramafic xenoliths: new petrologic evidence from the transition zone. Science, 252: 827-830.

Schiano, P. and Clocchiatti, R., 1994. Worldwide occurrence of silica-rich melts in subcontinental and suboceanic mantle minerals. Nature (London), 368: 621-624.

Schrauder, M., Koeberl, C. and Navon, O., 1996. Trace element analyses of fluid-bearing diamonds from Jwaneng, Botswana. Geochimica et Cosmochimica Acta, 60: 4711-4724.

Schrauder, M. and Navon, O., 1993. Solid carbon dioxide in a natural diamond. Nature, 365: 42-44.

Scott-Smith, B.H., Danchin, J.W., Harris, J.W. and Stracke, K.J., 1984. Kimberlites near Orrorroo, South Australia, In: J. Kornprobst (Editor), Kimberlites and Related Rocks, Elsevier, Amsterdam, pp. 121-141,.

Searle, M.P., Windley, B.F., and 9 others, 1987. The closing of the Tethys and the tectonics of the Himalaya. Geological Society of America Bulletin, 98: 678-701.

Sellschop, J.P.F., 1979. Nuclear probes in physical and geochemical studies of natural diamonds. In: J.E. Field (Editor), The Properties of Diamond, Academic Press,

New York, pp. 107-1163.

Shimizu, N. and Richardson, S.H., 1987. Trace element abundance patterns of garnet inclusions in peridotite-suite diamonds. Geochimica et Cosmochimica Acta, 51: 755-758.

Slodkevich, V.V., 1983. Graphite pseudomorphs after diamond. International Geological Review; 25: 497-514.

Sobolev, N.V., 1974. Deep-seated inclusions in kimberlites and the problem of the composition of the upper mantle. (Translated by American Geophysical Union, Washington, D.C., 1977).

Sobolev, N.V., Kaminsky, F.V., Griffin, W.L., Yefimova, E.S., Win, T.T., Ryan, C.G. and Botkunov, A.I., 1997. Mineral inclusions in diamonds from the Sputnik kimberlite pipe, Yakutia. Lithos, 39: 135-157.

Sobolev, N.V. and Shatsky, V.S., 1990. Diamond inclusions in garnets from metamorphic rocks: a new environment for diamond formation. Nature, 343: 742-745.

Sobolev, V.S., Sobolev, N.V. and Lavrent'yev, Yu.G, 1972. Inclusions in diamond extracted from a diamonderous eclogite (in Russian). Doklady akademia Nauk SSSR, 207: 164-167.

Sobolev, V.S., Sobolev, N.V. and Lavrent'yev, Yu.G, 1975. Chrome-rich clinopyroxenes from the kimberlites of Yakutia. Neues Jahrbuch fuer Mineralogie, 123: 213-218.

Stachel, T. and Harris, J.W., 1997. Syngenetic inclusions in diamond from the Birim field (Ghana) - a deep peridotitc profile with a history of depletion and re-enrichment. Contributions to Mineralogy and Petrology, 127: 336-352.

Stachel, T., Harris, J.W. and Brey, G.P., 1998. Rare and unusual mineral inclusions in diamonds from Mwadui, Tanzaniz. Contributions to Mineralogy and Petrology, 132: 34-47.

Stockman, H.W. and Hlava, P.F., 1984. Platinum-group minerals in Alpine chromitites from Southwestern Oregon. Economic Geology, 79: 491-508.

Sunagawa, I., 1982. Gem materials, natural and artificial. Current Topics in Materials Science, 10: 353-497.

Taylor, W.R. and Green, D.H., 1989. The role of reduced C-O-H fluids in mantle partial melting. In: J. Ross et al. (Editors), Kimberlites and Related Rocks, Geological Society of Australia, Special Publications, No. 14, V. 2: 595-602.

Taylor, W.R., Jaques, A.L. and Ridd, M., 1990. Nitrogen-defect aggregation characteristics of some Australasian diamonds: Time-temperature constraits on the source regions of pipe and alluvial diamonds. American Mineralogist, 75: 1290-1310.

Taylor, W.R., Milledge, H.J., Griffin, B.J., Nixon, P.H., Kamperman, M. and Mattey, D.P., 1995. Characteristics of microdiamonds from ultramafic massifs in Tibet: authentic ophiolitic diamonds or contamination. Extended Abstracts, the sixth international kimberlites conference, Russia, 623-624.

Trautman, R.L., Griffin, B.J., Taylor, W.R., Spetsius, Z.V., Smith, O.B. and Lee, D.C., 1997. A comparison of the microdiamonds from kimberlite and lamproite of Yakutia and Australia. Russian Geology and Geophysics, 38: 341-355.

Von Quadt, A., Ferrario, A., Diella, V., Hansmann, W., Vavra, G. and Keppel, V., 1992. U-Pb ages of zircons from chromitites of the phlogopite peridotite of Finero, Ivrea zone, northern Italy. In: J.E. Quick and S. Sinigoi (Editors), Ivrea-Verbano zone workshop, pp. 20.

Walmsley, J.C. and Lang, A.R., 1992. Oriented biotite in natural diamond coat. Mineral Magazine, 56: 108-111.

Wang, A., Pasteris, J.D., Meyer, H.O.A. and Dele-Duboi, M.L., 1994. Msanesite-bearing inclusion assemblage in natural diamond. Earth and Planetary Science Letters, 141: 293-306.

Wang, X., Bao, P., Deng, W. and Wang, F., 1987. Xizang ophiolite (in Chinese). Geological Memoirs, 8: 215-288.

Wilson, M., 1989. Igneous Petrogenesis. London, Unwin Hyman.

Wyllie, P.J., 1987. Metasomatism and fluid generation in mantle xenoliths. In: P.H. Nixon (Editor), Mantle Xenoliths, Wiley, pp. 609-623.

Xu, Shutong, A.I. Okay, Ji Shouyuan, A.M.C. Sengor, Su Wen, Liu Yican, jiang Laili, 1992. Diamond from the Dabie Shan metamorphic rocks and its implication for tectonic setting. Science, 256: 80-82.

Yan, B., Liang, R., Fang, Q., Yang, F. and Wan, C., 1986. Characteristic of diamond and associated minerals in Qiaoxi and Hongqu, Xizang. Bulletin of Institute of Geology, CAGS (in Chinese), 14: 61-125.

Yan, B. and Sun, D., 1982. The character of diamonds in ultrabasic rocks in Xizang (Tibet). Bulletin of the Institute of Geology, Chinese Academy of Geological Sciences, 64.

Zhang, H.-Y. and Ba, D.-Z., and 5 others, 1996. Study of Luobusa typical chromite ore deposit, Qusong County, Tibet (Xizang). Xizang People Press, Lhasa, China, 181 pp.

Zhao, W., Mechie, J., and 10 others, 1997. Seismic mapping of crustal structure beneath the Indus-Yarlung suture, Tibet. Terra Nova, 9: 42-46.

Zhao, W. and Morgan, W.J., 1985. Uplift of Tibetan Plateau. Tectonics, 4: 359-369.

Zhao, W. and Morgan, W.J., 1987. Injection of Indian crust into Tibetan lower crust: a two-dimensional finite element model study. Tectonics, 6: 489-504.

Zhao, X.-Z., Roy, R., Cherlan, K.A. and Badzian, A., 1997. Hydrothermal growth of diamond in metal-C-H_2O systems. Nature, 383: 513-515.

Zhou, M.-F., 1995. Petrogenesis of the podiform chromitites in the Luobusa ophiolite, Southern Tibet. Ph.D. thesis, Dalhousie University.

Zhou, M.-F., Robinson, P.T., Malpas, J. and Li, Z.-J., 1996. Podiform chromitites in the Luobusa ophiolite (Southern Tibet): Implications for Melt-rock interaction and chromite segregation in the upper mantle. Journal of Petrology, 37: 3-21.

Zhou, M.-F. and Robinson, P.T., 1997. Origin and tectonic environment of podiform chromite deposits. Economic Geology, 92: 259-262.